Work in collaboration with:

Evaluation of the therapeutic potential of piezoelectric fibers-coated thin films for the treatment of myocardial infarction

Luís Miguel de Almeida Monteiro

Dissertação

Mestrado Integrado em Bioengenharia

Porto, 2016

U.PORTO

FEUP FACULDADE DE ENGENHARIA UNIVERSIDADE DO PORTO

INSTITUTO DE CIÊNCIAS BIOMÉDICAS ABEL SALAZAR UNIVERSIDADE DO PORTO

INSTITUTO DE INVESTIGAÇÃO E INOVAÇÃO EM SAÚDE UNIVERSIDADE DO PORTO

INEB Instituto de Engenharia Biomédica

Work in collaboration with:

CNC CENTER FOR NEUROSCIENCE AND CELL BIOLOGY UNIVERSITY OF COIMBRA, PORTUGAL

Evaluation of the therapeutic potential of piezoelectric fibers-coated thin films for the treatment of myocardial infarction

Luís Miguel de Almeida Monteiro

Orientadora: Drª. Diana Santos Nascimento (INEB/i3S)

Co-orientadores: Drª. Perpétua Pinto-do-Ó (INEB/i3S, ICBAS)

Dr. Lino Ferreira (CNC)

Porto, 2016

“In order to succeed, your desire for success should be greater than your fear of failure”

Bill Cosby

TABLE OF CONTENTS

ACKNOWLEDGEMENTS

I would like to thank Prof. Perpétua for receiving me on the Heart Team since the Curricular Internship and, as a professor and researcher, for instigating in me the interest on fundamental biology and how it can be beautifully combined with bioengineering concepts.

I hereby show my gratitude to Diana for accepting to be my supervisor in this work, having the patience to be the “pacemaker” of a “bradyarrhythmic” student, always believing more in his “proficiency” than himself. I thank her for her scientific guidance, admiring her scientific curiosity and love for science.

I thank the Stem Cell Microenvironments in Repair and Regeneration (a.k.a. Heart Team) for welcoming me so warmly right from the start, with their unique family-like behavior (and for introducing me to sushi). I thank Vasco and Sílvia for their herculean patience in teaching me how to work, right since by baby (or neonatal) steps on the laboratory and for their support on several occasions. I thank Tiago for his sharp sense of humor and its help and advice, especially concerning histology. I also thank Francisca for her support and advise, and Tatiana from their sympathy and support from the beginning and for making sure that we have regular Team Meetings. I want to acknowledge Francisco Nóvoa for his expertise and help in the electrocadiographic assessments of the herein work.

I acknowledge Dr. Lino Ferreira and Pedro Gouveia for allowing this collaborative work to be possible.

I would like acknowledge Cláudia Machado for her support in the histology. I also would like to thank Rúben for borrowing the biopsy punch to apply the patches. Additionally, I would like to thank the members of the Animal Facility, such as Dr. Sofia Lamas, D. Fátima e Nuno for its support, allowing us to work.

I want to acknowledge the INEB researchers, in general, for their supportive way of work.

Agradeço aos meus amigos e colegas de Bioengenharia (especialmente aos Biotecs i3Sianos) pela boa disposição e companhia às várias horas de almoço.

Agradeço aos meus amigos mais chegados e à minha família por todo o apoio que me têm dado.

For last but not least, I would like to acknowledge the funding for the herein work since, without it, it wouldn´t be possible.

This work was financed by MITP-TB/ECE/0013/2013, FEDER - Fundo Europeu de Desenvolvimento Regional funds through the COMPETE 2020 - Operacional Programme for Competitiveness and Internationalisation (POCI), Portugal 2020, and by Portuguese funds through FCT - Fundação para a Ciência e a Tecnologia/Ministério da Ciência, Tecnologia e Inovação in the framework of the project “Institute for Research and Innovation in Health Sciences”- POCI-01-0145- FEDER-007274.

LIST OF ABBREVIATIONS

µm	Micrometer
AII	Angiotensin II
ACE	Angiotensin-converting enzyme
AuNWs	Gold nanowires
AP	Action potential
AVN	Atrioventricular node
Cav1.2	Slow L-type calcium inward channel
Cav3.1	T-type calcium channel
CM	Cardiomyocyte
CNTs	Carbon nanotubes
CO	Cardiac output
CVDs	Cardiovascular diseases
Cx	Connexin
ECG	Electrocardiograms
ECM	Extracellular matrix
ESC	Embryonic stem cells
ESC-CM	Embryonic stem cells-derived cardiomyocytes
ET	Endothelin
FS	Fractional shortening
HE	Hematoxylin-Eosin
HR	Heart Rate
I_f	Pacemaker current
I_{Kr}	Rapidly activating delayed rectifying potassium channels
I_{Ks}	Slowly activating delayed rectifying potassium channels
I_{Na}	Sodium current
I_{to}	Transient outward potassium current
ip	Intraperitoneally
iPSCs	Induced pluripotent stem cells
Kv11.1	Voltage-activated potassium channels
Kv7.1	Voltage-gated potassium channels
LAD	Left Anterior Descending
LV	Left ventricle
LVAW	LV anterior wall thickness
$LVID_d$	LV internal diameter during diastole
$LVID_s$	LV internal diameter during systole
LVPW	LV posterior wall thickness
LVOT	LV outflow tract diameter
$LVVOL_d$	LV volume during diastole
$LVVOL_s$	LV volume during systole
mm	Millimeter
MI	Myocardial Infarction
M-mode	Motion mode
MMP	Matrix metalloproteinase
MSC	Mesenchymal Stromal Cells
MT	Masson's Trichrome

Nav1.5	Membrane voltage-gated fast Na^+ channels
NCD	Non-communicable disease
NE	Norepinephrine
Pa	Pascal
PANI	Polyaniline
PBS	Phosphate buffered saline
PCL	Polycaprolactone
PIPs phosphates	Phosphoinositide
PPy	Polypyrrole
PSLAX	Parasternal long-axis
PVA	Polyvinyl alcohol
PVDF	Polyvinylidene fluoride
PVDF-TrFE	Polyvinylidene fluoride–trifluoroethylene
PW Doppler	Pulsed Wave Doppler
QTc	QT corrected for the HR
RAAS	Renin-angiotensin-aldosterone system
RT	Room temperature
S	Siemens
SAN	Sinoatrial node
SAX	Short-axis
SEM	Standard error of the mean
SERCA2a	Sarcoplasmic reticulum Ca^{2+} ATPase 2a
SV	Stroke volume
TGF-β	Transforming growth factor beta
TIMP	tissue inhibitors of metalloproteinases
VSPs	Voltage-sensitive phosphatases
VTI	Velocity-time integral of the aortic flow

LIST OF FIGURES

LIST OF TABLES

1. ABSTRACT

Cardiovascular diseases (CVDs) are the leading cause of death worldwide. Moreover, ischemic heart diseases account for most CVDs-related deaths and, alone, are the leading cause of death worldwide. These conditions often lead to acute myocardial infarction (MI) that involves ischemia-induced cardiomyocyte (CM) death and the formation of a non-functional scar tissue at the infarcted site, greatly impairing cardiac function, often leading to heart failure. Moreover, this collagen-rich scar tissue lacks electrical conductivity which often promotes the occurrence of arrhythmias in a scenario of MI due to the disruption of electrical conduction. Hence, in heart failure ventricular tachyarrhythmia (increased heart rate) and fibrillations (disorganized action potential (AP) propagation in the myocardium) are common events. Attempting to surpass the shortcomings of current gold-standard therapies, novel therapies, involving gene and/or cell therapy or tissue engineering have been emerging. Most of these therapies focus on improving cardiac function, reducing cardiac remodeling and/or are dedicated to restore cardiac electrical integrity. However, *in vivo* studies assessing therapeutic alternatives that promote concurrent contractile and electrical functional repair are scarce.

Piezoelectric materials exhibit an electric polarization (and a resultant electrical activity) upon mechanical stress (direct effect) or vice-versa (converse effect). Since the heart exhibits robust cyclic movements, the implantation of these materials on an injured myocardium holds great potential as could be possible to obtain a sustainable electrical activity, induced by native mechanical stimuli, with a consequent improvement of electromechanical integration and cardiac function. *In vitro* experiments have shown that thin films of polycaprolactone (PCL) covered in polyvinylidene fluoride–trifluoroethylene (PVDF-TrFE) piezoelectric fibers, maintained contractility and viability of cardiomyocytes *in vitro*, inducing their alignment, improved intercellular coupling, increased ionic channel expression and calcium handling. In line with these experiments the herein work aims to test the

therapeutic potential of these materials for the treatment of MI. For that purpose, these films (herein referred as “Piezo patches”) were implanted in the hearts of mice subjected to MI. One month after implantation, functional and histological characterization were performed. The materials induced an exacerbated inflammatory reaction associated with multinuclear inflammatory cells, resembling a foreign body reaction. Furthermore, although no significant differences were observed concerning echocardiographic analysis and cardiac remodeling, a consistent tendency for improvement was observed in the Piezo patch-treated animals. Of note, electrocardiograms showed that the materials piezoelectric fibers resulted in enhanced myocardial conduction with evidences of having a reduced susceptibility to suffer ventricular arrhythmia events, when compared with films containing non-conductive, polycaprolactone (PCL) fibers. Thus, the herein work support the use piezoelectric materials as tissue engineering conductive scaffolds and/or to be used in combination with other therapies towards improvement of electrical integrity following MI.

2. SUMÁRIO

As doenças cardiovasculares são a principal causa de morte no mundo. Entre estas, o enfarte agudo do miocárdio caracteriza-se pela morte de tecido viável e subsequente remodelagem cardíaca, onde há deposição de tecido cicatricial que prejudica a função do miocárdio e pode originar falência cardíaca. Esta cicatriz, rica em colagénio, tem fracas propriedades condutoras, promovendo frequentemente a ocorrência de arritmias devido à disrupção elétrica no miocárdio. Assim, em contexto de falência cardíaca é comum ocorrerem taquiarritmias ventriculares (ritmo cardíaco aumentado) e fibrilações. Numa tentativa de ultrapassar as limitações das terapias convencionais, têm surgido novas abordagens terapêuticas que procuraram melhorar a função e reduzir a remodelagem cardíaca ou restaurar a integridade elétrica do coração. No entanto, presentemente existem muito poucos estudos que avaliem *in vivo* novas terapias para melhorar simultaneamente a função contráctil e eléctrica.

Os materiais piezoelétricos exibem uma polarização elétrica (e, consequentemente, atividade elétrica) aquando da deformação mecânica (efeito direto) ou vice-versa (efeito inverso). Uma vez que o coração apresenta movimentos cíclicos robustos, a implantação destes materiais num miocárdio com lesão constitui uma alternativa com elevado potencial uma vez que possibilitaria obter atividade elétrica sustentável, induzida pelo estímulo mecânico nativo, com uma subsequente melhoria na integração eletromecânica e função cardíaca.

Experiências *in vitro* mostraram que filmes finos de policaprolactona contendo fibras de fluoreto de polivinilideno – trifluoroetileno (polímero com propriedades piezoelétricas) depositadas no topo, mantiveram eficazmente a contractilidade e viabilidade de cardiomiócitos, promovendo o seu alinhamento, melhorando o acoplamento intercelular, aumentando a expressão de determinados canais iónicos e regularizando os níveis de cálcio.

No seguimento das experiências descritas, o trabalho efetuado no contexto da presente tese consistiu em avaliar o potencial terapêutico destes materiais no tratamento do enfarte do miocárdio. Para esse efeito, os materiais foram implantados em coração de murganhos que foram submetidos a indução cirúrgica de enfarte do miocárdio. Um mês após implantação, os animais foram caracterizados ao nível histológico e funcional. Os materiais piezoelétricos induziram uma reação inflamatória com abundantes células inflamatórias multinucleares, à semelhança do que ocorre nas reações de corpo estranho. Adicionalmente, apesar de não se terem observado diferenças estatisticamente significativas na função contrátil e na remodelagem cardíaca, os diferentes parâmetros indicam uma melhoria ligeira do grupo implantado com fibras piezoeléctrica. Por electrocardiograma mostrou-se que as fibras piezoelétricas depositadas no miocárdio promoveram uma melhoria significativa da condução do miocárdio em comparação com filmes contendo fibras (não-condutoras) de policaprolactona.

Em suma, o presente trabalho revela que os materiais piezoelétricos utilizados poderão ter potencial como uma alternativa na engenharia de tecido cardíaco e/ou serem usados em combinação com outras terapias para melhorar especificamente a condução eléctrica do miocárdio.

3. INTRODUCTION

3.1. Epidemiology of Cardiovascular Diseases

Cardiovascular diseases (CVDs) consist in a group of conditions that involve the heart and/or blood vessels (*e.g* ischemic heart diseases, cerebrovascular diseases). These diseases are the leading cause of mortality worldwide with a current estimation of 17,3 million deaths per year (with an expected increase up to 23,6 million deaths by the year 2030), representing 31% of all global deaths [1, 2] (**Figure 1**). Although genetic factors can influence the occurrence of CVDs, by far, the most relevant risk factors include age, gender, family history, physical inactivity, smoking habits, alcohol consumption, obesity, diabetes, hypocholesteremia and hypertension [2-4]. Moreover, ischemic heart diseases, *i.e.* conditions that involve reduced blood supply to the myocardium (cardiac muscle), account for 46% and 38% of CVD-related deaths for males and females, respectively, and represent, alone, the leading cause of death worldwide [2, 5] (Figure 2). Importantly, CVDs are frequently associated to electrical disruption and the onset of arrhythmias [6], which can be fatal. In line with this, ventricular arrhythmias account for approximately 50% of deaths associated with chronic heart failure [7].

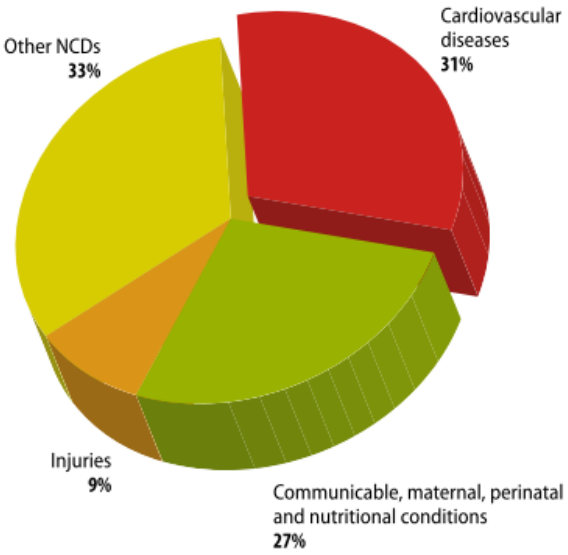

Figure 1 – Proportion of causes of death worldwide. (NCDs: non-communicable diseases; e.g. cancer). Source: ref [2].

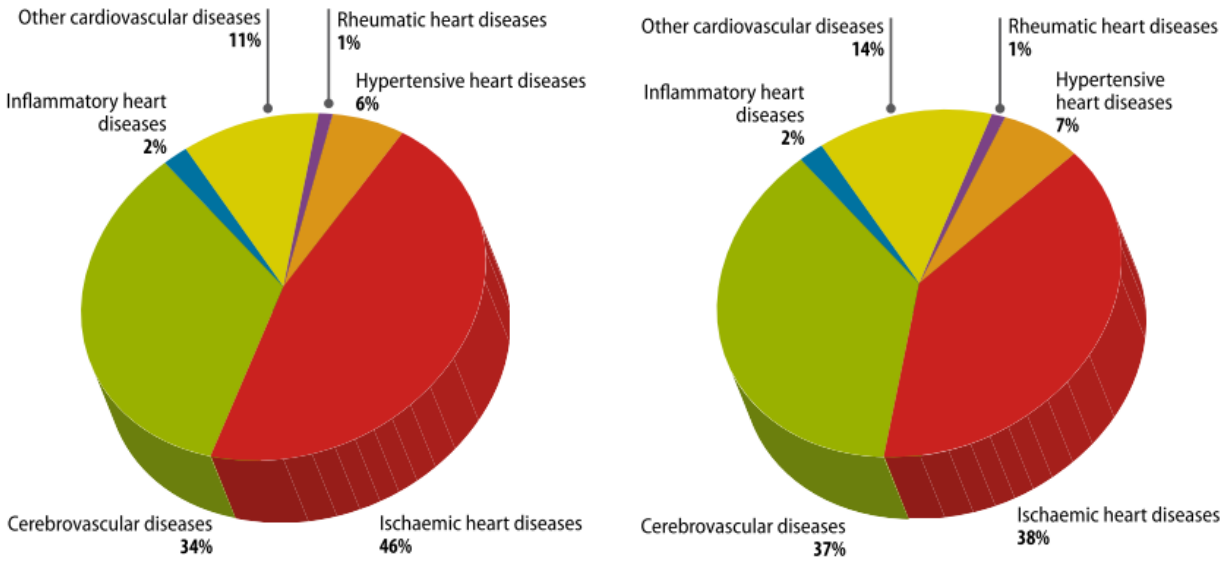

Figure 2 - Proportion of causes of CVD-related deaths worldwide, in males (left) and females (right). Source: ref. [2]

3.2. Myocardial Infarction: Etiology and Pathophysiology

As mentioned, ischemic heart diseases are the main cause of CVD-related deaths worldwide [2, 5]. One of the most common ischemic heart diseases is the acute myocardial infarction (MI). MI can be defined as myocardial cell death due to sustained ischemia at the myocardium level [8] and is frequently caused by the rupture of atherosclerotic plaques at the coronary arteries (which irrigate and supply oxygen to the myocardial tissue) ultimately leading to the rapid formation of a blood clot that results in their occlusion [8, 9]. However, MI can also be caused by secondary ischemic imbalances (e.g. coronary artery spasms) and stent-related thrombosis [8]. Moreover, MI frequently develops into heart failure [10, 11], which can be defined as a pathophysiological state in which the cardiac output is insufficient to assure enough blood organ perfusion to meet metabolic demands [12].

Owing to the often massive loss of viable myocardium by ischemia-induced cardiomyocyte (CM) necrosis, MI frequently results in a pathological remodeling *i.e.* alterations on the size, shape, structure and function of the left ventricle (LV) [13-15]. Initially, CM undergo

necrosis since these cells exhibit an high metabolic activity and, therefore, are sensitive to ischemia [16]. Then, an acute inflammatory reaction is initiated involving the recruitment of neutrophils (that, in mice, starts occurring at around 1-2 days after MI) and macrophages (at ~4 days, in mice [14]) that phagocyte necrotic CM debris at the infarcted site. The recruitment of inflammatory cells is stimulated by the release of, for instance, transforming growth factor beta (TGF-β) by necrotic CMs [14, 15]. Of note, neutrophils produce matrix metalloproteinases that cleave collagen and other extracellular matrix (ECM) constituents [14, 15, 17]. Consequently, these enzymes degrade the collagen-based intercellular struts that, in a healthy myocardium, preserve adjacent CMs together and assure proper fiber alignment and maintenance of normal CM morphology [17]. Then, due to cell loss and ECM degradation, the pressure that the blood on the LV cavity exerts on the infarcted LV wall, causes the CMs to slip (CM slippage), resulting in LV wall thinning and LV cavity dilation. At this point, the infarcted wall has very low mechanical resistance and the risk of rupture and/or aneurysm formation is elevated [14, 15]. Since adult mammalian CMs lack functionally relevant proliferative capacity [18], in order to improve mechanical integrity of the LV wall in these phase and equalize the forces exerted on LV wall (reducing wall stress), the mammalian heart resorts to a repair process, involving collagen deposition. In line with this, TGF-β stimulates fibroblast recruitment, massive proliferation and their differentiation to myofibroblasts [14, 15]. These cells then produce collagen type I and III resulting in the deposition of a collagen-rich scar tissue (fibrosis) at the infarcted zone and, frequently, interstitial fibrosis among viable CMs of the periphery [14, 15]. Fibrosis starts approximately at 7-14 days post MI and becomes completed at around 21 days, in a murine MI model [14]. Scar tissue, although conferring mechanical support to the infarcted wall at some extent, is non-contractile, thick, stiff and greatly impairs cardiac contractile function [16]. Moreover, collagen scarring is an electrically isolating tissue, which has a detrimental effect on cardiac conduction. Of note, increased wall stress and mechanical load as well as fibrosis triggers compensatory processes such as CM hypertrophy, where CMs increase their volume and further develop their contractile apparatus.

Due to functional impairment provoked by the exacerbated loss of CMs and subsequent formation of non-functional fibrotic tissue in a MI scenario and the fact that heart transplantation (the only effective long-term therapy for heart failure) has several shortcomings (*e.g.* organ donor shortage, immune rejection [14]) innovative therapeutic strategies have been emerging. Most of them focus on the improvement of heart function and cardiac remodeling (reviewed on [19, 20]). However, considering that arrhythmias are a main cause of sudden death in heart failure scenarios, a comprehensive understanding of the cardiac electrical system should not be disregarded and novel therapies to restore cardiac electrical integrity are necessary.

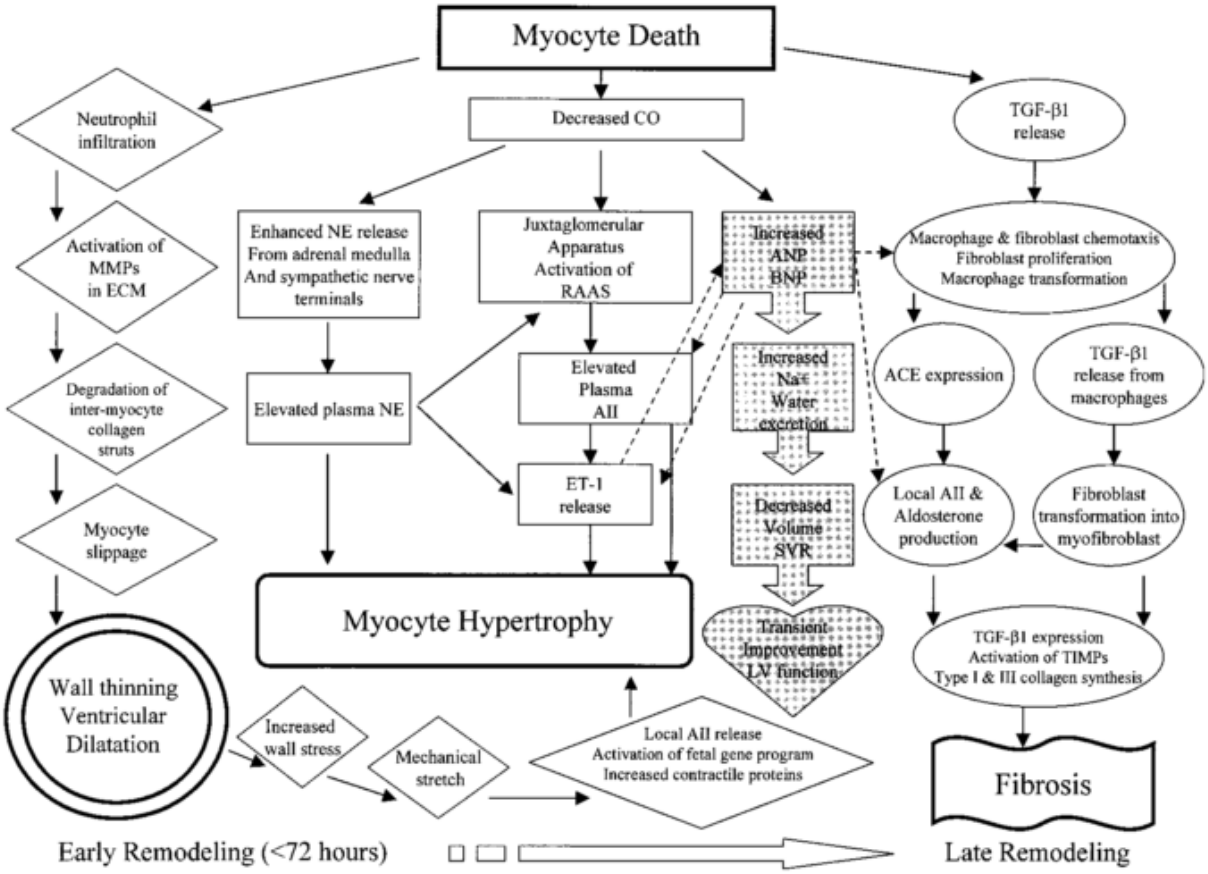

Figure 3 – Schematic representation of the several processes occurring during MI-related cardiac remodeling. AII – angiotensin II; ACE - angiotensin-converting enzyme; ECM – extracellular matrix; ET-1 – endothelin; CO – Cardiac Output; MMP – matrix metalloproteinase;; NE – norepinephrine; RAAS - renin-angiotensin-aldosterone system; TIMPs – tissue inhibitors of metalloproteinases. Source: ref. [15].

3.3. Cardiac Electrical System: the basics

A close interaction between specialized excitatory and conductive components and the working CMs (contractile component) is essential for the successive and rhythmic contractions and relaxations of the myocardium, which promote unidirectional blood flow at an adequate pressure [21, 22].

The main elements of the excitatory and conductive components are the sinoatrial node (SAN), the internodal pathways, the atrioventricular node (AVN), the bundle of His and the Purkinje fibers [22, 23] (Figure 4). This system is mainly composed of specialized CMs whose cytoarchitecture and electrophysiological properties vary according to their specific function and differ from working atrial and ventricular CMs [23-25].

Specialized CMs of the SAN, regulated by sympathetic and parasympathetic stimuli, spontaneously generate AP that directly propagates to: 1) the atrial myocardium leading to its contraction; 2) the internodal pathways; and, ultimately, to 3) the AVN. At the latter, the impulse propagation suffers an essential delay in order that blood from the atria fills the ventricles before ventricular contraction. Finally, the AP is propagated rapidly through the bundle of His and Purkinje fibers towards the ventricular working myocardium, which then contracts in syncytial manner [22, 26] (Figure 4).

At the cellular level, cardiac AP represents the variations of the CM membrane potential that follow an initial depolarization from a resting potential (-85 mV in working CMs) to a threshold potential (-40 mV), in a sequence of events mediated by ion channels. Essentially, in working CMs this AP can be divided in five phases (Figure 4): a) phase 0: upon stimulation from neighboring cells and depolarization to -40 mV, membrane voltage-gated fast Na^+ channels ($Na_V1.5$ channels) open which causes a rapid intake of Na^+ ions (I_{Na} currents) triggering a further depolarization to a peak of, approximately, +20 mV [21, 26-29]; b) phase 1: $Na_V1.5$ channels close and K^+ channels (*e.g.* $K_V4.2$, $K_V4.3$) open leading to a transient outward K^+ current (I_{to}) and, consequently, to a transient repolarization [21, 26, 28-30]; c) phase 2: opening of slow L-type calcium inward channels ($Ca_V1.2$) concomitant with the current

mediated by rapidly (I_{Kr} currents) and slowly (I_{Ks} currents) activating delayed outward rectifying K^+ channels (*e.g.* voltage-activated potassium channels (K_V11.1) and voltage-gated potassium channels (K_V7.1), respectively), maintain the AP in a relatively constant depolarized state (plateau) [21, 26, 28, 29, 31]; d) phase 3: Ca_V1.2 channels close and I_{Kr} and I_{Ks} cause a rapid repolarization to the resting potential [21, 26, 28, 29]; e) phase 4: the membrane potential is maintained at a resting level by K^+ inward rectifier channels (*e.g.* K_{IR}2.1) (I_{K1} currents) [21, 26, 28, 29]. Although working CMs need to be depolarized by neighboring cells, specialized CMs of the SANs and AVNs and Purkinje fibers, the so-called pacemaker cells, are able to spontaneously generate AP. This property is closely related to an unstable, and less negative resting potential (around -55 mV) comparing to working CMs. Such less negative resting potential is mainly due to an increased leakage of Na^+ resulting in an inward current of these ions (the pacemaker current, I_f) and that is mediated by the hyperpolarization-activated, cyclic-nucleotide-gated channels [32]. This I_f current, and the fact that most fast Na^+ channels are closed at potentials at -55 mV or higher, result on a slow diastolic depolarization of pacemaker cells (phase 4). When membrane potential reaches a threshold level, T-type (*e.g.* Ca_V3.1) and slow L-type Ca^{2+} channels open, depolarizing the cell up to +20mV (phase 0) (Figure 4) [22, 26, 29, 33].

The cardiac AP triggers the contraction of working CMs, allowing contraction of the atria and ventricles, through a process denominated excitation-contraction coupling. Depolarization of sarcolemma induces opening of L-type Ca^{2+} channels and, the subsequent increase in intracellular Ca^{2+} concentration, activates the ryanodine receptors (which are intracellular Ca^{2+} channels) in the sarcoplasmic reticulum's membrane, leading to release of this ion from the sarcoplasmic reticulum to the sarcoplasm, further increasing Ca^{2+} intracellular concentration [21, 34]. These ions bind to subunit C of troponin which causes a conformational change freeing the actin's myosin-binding sites from tropomyosin, leading to sarcomere contraction [21, 35].

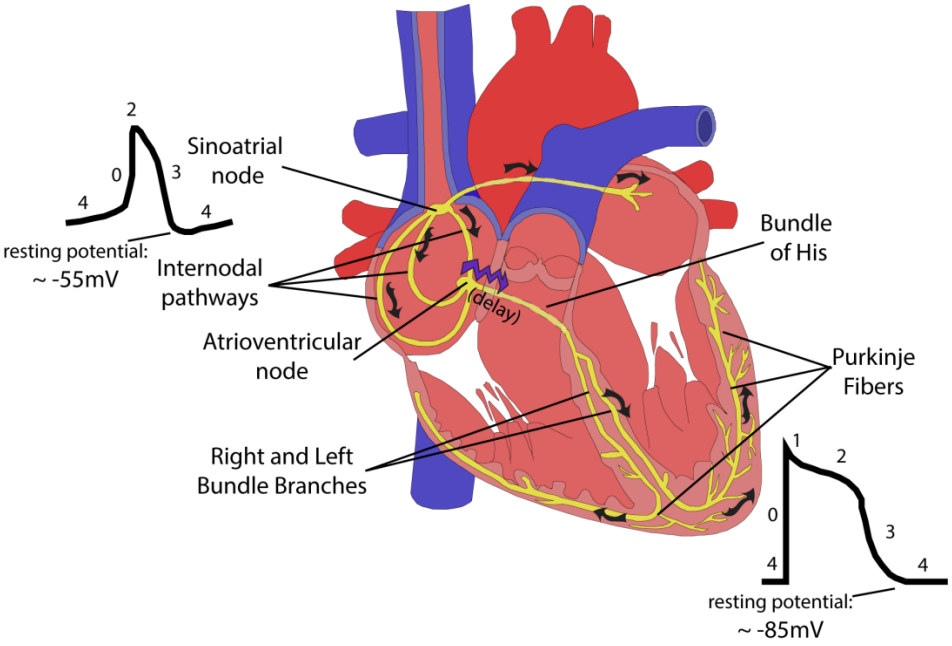

Figure 4 - Representation of the anatomy of the cardiac conduction system and the path of the action potential propagation throughout the structures (arrows) including the time delay observed at the AV junction (purple arrow). The shape of the action on SAN (Upper left) and working myocytes (Lower right) are represented along with the respective resting potentials and the different phases of the signal (numbers).

Finally, Ca^{2+} baseline intracellular levels are restored mainly being pumped back to the sarcoplasmic reticulum through the sarcoplasmic reticulum Ca^{2+} ATPase 2a (SERCA2a) or released from the cell via Na^{+}/Ca^{2+}-exchangers [21, 36]. There are evidences that, acting in late phase of the diastolic depolarization in pacemaker cells, this Ca^{2+} cycling also promotes spontaneous beating (the “calcium clock”), acting in combination with the membrane potential instability and I_f current [37, 38].

Impulse propagation between CMs is dependent on intercellular electrical coupling *i.e.* the ability of one cell to transport ions directly from its sarcoplasm to a neighboring one. This coupling is predominantly achieved through gap junctions which consist in two exactly aligned hemichannels, one from each coupling cell, composed of six subunits of connexin (Cx) proteins [39]. Cx45, Cx40 and Cx43 are the predominant isoforms expressed in CMs [40, 41]. Cx43 is the predominant isoform of adult working CMs [42-44] whereas Cx40 is expressed in His-Purkinje fibers and atrial working CMs (but not in ventricular working CMs) [43-46], and Cx45 expression is predominantly found at the AVN [44, 47, 48]. These three Cx isoforms

display different levels of conductance: Cx40 has the highest conductance and Cx45 the lowest [49-53]. Interestingly, these characteristics correlate with the velocity of impulse propagation characteristic of the different structures i.e. his-Purkinje fibers are fast-conducting structures, while the AVN is associated with a time delay in AP propagation, however this effect is also potentiated by smaller and less abundant gap junctions [47, 54]. Despite the widely and classical perception that impulse propagation between CMs is primarily through gap junctions (electrotonic model), there are evidences that intercalated discs may actively influence cell-cell impulse transmission, involving differential $Na_V1.5$ channel expression and extracellular space charge variations (ephaptic model) [reviewed on 55, 56]).

3.4. Disruption of Electrical Conduction after MI and Heart Failure

Cardiac electrical disruption often results in arrhythmias, which can comprise, for instance: altered heart rates (bradyarrhythmias and tachyarrhythmias corresponding to low and high heart rates, respectively); premature beats; atrial flutter; and fibrillations which comprises an unorganized AP propagation through the myocardial mass resulting in uncoordinated contractions and relaxations between different regions of the myocardium, which can be supraventricular (*e.g.* atrial fibrillation) or ventricular [57, 58].

Bradyarrhythmias are mainly caused by either SAN dysfunction (sick sinus syndrome) or disruption of the AVN conduction (AVN block or heart block). Considering that MI results in the deposition of a fibrotic tissue that it is not electrically conductive on myocardium rather than necessarily causing impaired of AP signal generation and/or AP propagation at a more central level of the specialized conductive system, this section focuses on tachyarrhythmias and fibrillations rather than bradyarrhythmias.

Tachyarrhythmias and fibrillations are frequently associated with CVDs, especially in heart failure scenario. The arrhythmogenic properties underlying heart failure are due to different factors, namely: ion channel remodeling; reduced excitability; impaired Ca^{2+} cycling; decreased intercellular electrical coupling; and formation of electrically isolating fibrotic tissue

[6, 59]. Concerning ion channel remodeling, evidences show that, upon heart failure, there is a reduction on the expression of ion channels related to repolarization currents (*e.g.* I_{to}, I_{Ks}) with concomitant increase in a delayed inward Na^+ current. These events result in prolonged AP duration, which promotes the occurrence of Ca^{2+}-mediated after-depolarizations. Reduced excitability, for instance during acute MI, usually occurs due to different factors such as increased K^+ extracellular concentration. The main effect of the latter is depolarization of cardiomyocytic resting potential, which induces a partial inactivation of the voltage-gated Na^+, reducing I_{Na} current and, consequently, excitability and conduction velocities. Reduced conduction velocities promote the onset of reentrant arrhythmias, as discussed below in this section. Calcium cycling is also commonly affected during heart failure, for instance, increased diastolic intracellular Ca^{2+} concentration, mainly due to higher leakage from the sarcoplasmic reticulum (related to impaired ryanodine receptor function) and/or a decrease reuptake of this ions from the sarcoplasmic reticulum (due to SERCA2a defective activity), are observed. This increase on the diastolic concentration also triggers after-depolarizations [59-62]. Concerning intercellular electrical coupling, Cx43 expression is reduced up to 50% in heart failure [63, 64]. Apart from causing conduction deceleration and discontinuity, defective intercellular coupling between the CMs also results in an increased subthreshold depolarization, which slowly inactivates the voltage-gated Na^+ channels, further reducing the I_{Na} current, and excitability [6, 59]. Furthermore, deposition of collagenous scar tissue, which is an electrical insulator, is common to a wide number of cardiovascular disorders and is particular evident after MI. Collagen deposition results on electrically isolated fibers of viable myocardium, discontinuing the conduction path and, globally, reducing the AP propagation velocity and, consequently, promoting the onset of reentrant arrhythmias [6, 59].

The most common phenomenon underlying the maintenance of ventricular and supraventricular (*e.g.* atrial fibrillation) tachyarrhythmia and fibrillations is the “reentry” mechanism. This can occur in a region of the myocardium in which AP encounters a path divided in two, a fast pathway (normal) and a slow pathway (for instance, a myocardial network

containing scar tissue), and which converge again in a downstream position of the path. This situation can lead to the creation of successive AP propagation cycles , in which AP propagates in circles, around the referred fast and slow pathways, and also backwards, increasing the frequency of excitation and, consequently, the heart rate. One pre-requisite for an anatomical reentry cycle to be sustained is the wavelength of the signal (defined as the product between the conduction velocity and the duration of refractory state) to be shorter than the physical, anatomical path in which the cycle occurs [6, 57, 59, 65].

The most common therapies that are available nowadays for tachyarrhythmias are: i) anti-arrhythmic drugs, which still have low efficacy and can, in specific circumstances, even aggravate the disorder [66, 67]; ii) implantable cardioverter defibrillators, which only act upon the onset of arrhythmias and have the issues shared with implantable devices [68]; and iii) surgeries such as AVN ablation on atrial fibrillation patients, which consists in permanently disrupting AVN (protecting the ventricles from the arrhythmic signal originated in the atria) and thus requiring the permanent use of an implantable pacemaker [69].

3.5. Novel Strategies To Restore Myocardial Electrical Conduction following MI

Functionally proficient cardiac electrical coupling highly depends on molecular players (*e.g.* ion channels, gap junctions) thus, gene-related therapies along with targeted delivery, hold high potential for restoring cardiac electrophysiology. In addition, the potential of cell therapies to modulate cardiac electrical integrity has also been under recent scrutiny (Figure 5).

Gene therapy approaches for treating or reducing the symptoms of ventricular or supraventricular tachyarrhythmias or fibrillations essentially involve: 1) direct repair of intercellular conduction – mainly by overexpressing connexins [6, 70-72]; 2) modulation of AP characteristics – such as increasing the AP upstroke velocity or altering AP duration or refractory period [73-75]; and 3) restoration of calcium cycling – predominantly by upregulating SERCA2a [76-78].

In most studies, animal models of MI and atrial fibrillation were used. In general, these strategies resulted in a reduced rate of occurrence of ventricular arrhythmias; reduced ventricular arrhythmia inducibility, assessed by programmed electrical stimulation of the myocardium and electrocardiograms (ECGs); and increased conduction velocities, observed through *ex vivo* optical mapping and *in vivo* invasive electrograms. Of note, the approach concerning the restoration of Ca^{2+} cycling through SERCA2a overexpression is not only being applied in several animal models, but also in humans, particularly in the Calcium-Up-Regulation by Percutaneous Administration of Gene Therapy In Cardiac Disease (CUPID) phase 1/2 clinical trial [79-81]. In this trial, recombinant adeno-associated viral vectors encoding for the human SERCA2a gene (AAV1/SERCA2a) were injected in patients with advanced heart failure which, during a 12-month follow-up, exhibited reduced symptoms and improved functional status, biomarker profile and LV function [80]. Additionally, patients presented less cardiovascular events and/or deaths following 3 years, when compared to placebo groups [81]. Curiously, although overexpression of SERCA2a in ischemia-reperfusion MI rat and porcine models decreased the number of life-threatening arrhythmias, that effect was not observed or even reversed in permanently occluded rat and porcine models of MI, probably to the fact that the Ca^{2+} cell overload and instability are more significant during reperfusion, rather than in a lasting ischemic state [82, 83]. This result underlines that the efficiency of a developed therapy may be highly dependent on the targeted condition and shows the importance of using different ischemic models for the treatment of a disease, as is the case of acute MI. Hence, the etiology of arrhythmias in that particular condition should be carefully considered for when developing novel therapeutic solutions. For instance, since AP propagation is dependent on the fast inward Na^+ currents, one would hypothesize that in heart failure scenarios, in which detrimental ionic channel remodeling occur, $Na_V1.5$ channel overexpression would have potential in restoring conduction and preventing the occurrence of reentrant arrhythmias. However, MI causes a general membrane depolarization, leading to $Na_V1.5$ channel inactivation which could hinder the usefulness of its overexpression. In that regard, a skeletal Na^+ channel isoform ($Na_V1.4$), which inactivates at a less negative voltage,

has been tested. This isoform results in a less extensive AP upstroke *in vitro* in CMs subjected to a depolarizing medium and has anti-arrhythmic effects *in vivo* [73-75]. Connexin-related strategies are an interesting example how one should not overlook the potential detrimental consequences of anti-arrhythmic strategies on the overall homeostasis of the myocardium, in the context of certain disease scenarios. Studies involving connexins overexpression had promising results [70, 71], however, it has also been shown that overexpressing Cx32 in a canine MI model causes an increase on the infarct size [72] by supporting the spread of inflammatory mediators throughout the myocardium [84]. Thus, although connexins could restore electrical integrity aspects of the myocardium, it could also negatively interfere with the myocardial repair and even have proarrhythmic effects due to increased scarring, reinforcing the notion that strategies should be thought in an integrative manner.

3.5.1. Role of cell therapies on cardiac electrical integrity

Considering the limitations of gold-standard therapies for CVDs and the often deleterious LV tissue remodeling characteristic of myocardial repair, novel strategies focusing on improving the latter process have been emerging. Cell therapies are one of the most extensively explored approaches, which involve different cell types (*e.g.* mesenchymal stromal cells (MSCs), skeletal myoblasts, embryonic stem cells (ESC)-derived CMs (ESC-CMs), cardiac progenitor cells) [reviewed on 20, 85]. In these studies, especially in animal models, the main assessed outcomes are LV tissue remodeling, neovascularization, and cardiac function. In addition, few studies also evaluate whether the aforementioned therapies have an effect on cardiac electrical integrity. In that sense, part of the studies in which this effect is assessed or that raise pertinent questions, are herein discussed.

Studies involving MSCs or bone marrow-derived cells have shown promising results, in both animal models and clinical trials, such as improved LV function, neovascularization, and reduced infarct size [86-91]. Nevertheless, these cells raised controversy concerning their influence on cardiac electrical integrity and arrhythmogenicity [92-102]. The authors that show evidence that MSCs or bone marrow-derived cells have a pro-arrhythmic potential *in vivo* [92,

93, 103] hypothesize that such effect could be a consequence of the electrical unexcitability of these cells, paracrine factors, or the accumulation of inflammatory mediators. Although MSCs are electrically unexcitable cells, *in vitro* studies showed that these cells are capable of repairing conduction block, in neonatal CMs cultures, through connexin-mediated coupling [104, 105]. Nevertheless, others showed that this heterocellular electrical coupling might cause reduced AP propagation velocities and gradients of duration of repolarization which could promote the occurrence of reentry circuits and, consequently, arrhythmias [99, 100]. This mechanism is similar to the effect of cardiac fibroblasts on cardiac conduction in a context of fibrosis, as these cells undergo direct electrical coupling with CMs via gap junctions [106], bridging distant unconnected CMs [107]. It is not yet understood whether this “intercellular bridges” are arrhythmogenic substrates or if the electrical bridging has also some beneficial effects by reducing conduction block through scar tissue. Furthermore, MSC-released paracrine factors can also promote disruption of the myocardial electrical integrity not only by altering AP characteristics, ion channel expression and increase re-entry inducibility of CMs (assessed by *in vitro* transwell experiments) [100]; but also by promoting cardiac nerve sprouting and sympathetic hyperinnervation [93, 103]. Oppositely, others studies point that MSCs can reduce the electrical disruption in a MI scenario or even exert an anti-arrhythmic effect [97, 98, 101]. Overall, MSCs were shown to decrease ventricular arrhythmia inducibility, reduce the disruption of gap junction organization in CMs of the infarct border zone and ameliorate the electrical activity. Although mechanistic insights are lacking, the authors speculated that gap junction-mediated coupling between MSCs and CMs support AP propagation into the infarcted region, reducing the length of the anatomical conduction path and reducing the incidence of reentry arrhythmias. Additionally, it was suggested that the lack of electrical excitability in combination with the intercellular coupling could not have a significant pro-arrhythmic effect because the number of surviving MSCs in the myocardium decreases in few days, being the proportion MSCs:CMs much lower than in *in vitro* experiments where arrhythmogenicity was shown. Furthermore, the beneficial effect of MSCs on cardiac conduction can also be associated with the decrease in infarct size and increase in

the number of surviving CMs in the periphery of the ischemic region. MSCs were shown to upregulate Cx43 in HL-1 (CMs cell line) *in vitro* [96] and improve AVN conduction on AVN-blocked rats [108] through paracrine mechanisms. Thus, although MSCs are electrically unexcitable and incapable of electromechanical coupling with the host myocardium, evidences point to beneficial effects in cardiac function in the absence of evident side effects. In fact, clinical studies show no conspicuous anti-arrhythmic effect by these cells [94, 95, 109].

Skeletal myoblasts were one the first the cell types to be applied in animal and clinical studies concerning cell therapy on CVDs. This interest mainly stemmed from their capacity to proliferate, increased resistance to ischemia; and electrical excitability and the possibility of being isolated in an autologous fashion [110, 111]. However, being skeletal muscle cells, these cells lack expression of connexins upon the formation of myotubes, exhibiting minimal intercellular coupling. This characteristic precludes efficient integration of skeletal myoblasts with the myocardium and thus leading to an increased frequency of arrhythmic events, despite reported positive effects regarding other aspects [101, 112-114]. Thus, without intercellular coupling, these cells form clusters electrically isolated from the myocardium, blocking AP propagation in that region, rendering the electrical activity of these cells almost irrelevant. To surpass this limitation, some authors overexpressed Cx43 on cultured skeletal myoblasts, improving intercellular electrical coupling with CMs [115-117], which stimulated a series of *in vivo* testing [118-122]. Myocardial delivery of these cells in a cryoinjury MI murine model improved electrical coupling between skeletal myoblasts and host CMs, being the incidence of sustained arrhythmias and the ventricular arrhythmia inducibility decreased when compared to regular skeletal myoblast injection [119]. Conversely, although an amelioration of electrical coupling and improved electrical activity was observed, other studies involving rat [122] and rabbit [120] MI models reported that this coupling was insufficient to prevent arrhythmic events and that LV functional improvement was modest. This may relate to distinct AP characteristics of skeletal myoblasts which, in a cardiac environment, may also undergo downregulation of voltage-gated sodium, potassium and calcium channels [123], affecting their excitability and

function. Furthermore, as the clinical relevance of skeletal myoblast relies on Cx43 overexpression, alternative non-viral methods of gene expression should be further explored [121]. One concludes that for cells that survive and proliferate after transplantation, intercellular coupling and electrical and mechanical properties that closely mimic native CMs are mandatory to promote proper electromechanical function.

Pluripotent stem cells, which include ESCs and induced pluripotent stem cells (iPSCs), are a promising alternative due to their *in vitro* high proliferative capacity, while in an undifferentiated state, and their capacity to differentiate selectively into a great variety of cell types. These features allow generation of a great number of CMs which are immature in phenotypic and functional features. ESC-derived CMs (ESC-CMs) display immature contractile machinery and are capable of spontaneous AP generation. This inherent automaticity increases the possibility of induced arrhythmias when ESC-CMs are delivered to the myocardium. Despite that transplantation of pluripotent stem cells-derived CMs promote successful engraftment and functional improvement [124-128], few studies have thoroughly evaluated their electrically integration and/or pro-arrhythmic properties [124, 125, 128]. Shiba et al showed, in a guinea pig MI model, that hESC-derived CMs formed cell grafts with calcium transients and completely coordinated with ambulatory ECG signals, with evidences of an anti-arrhythmic effect [124, 128]. The same group applied a similar strategy in a non-human primate model of MI showing functional improvement, remuscularization and hESC-CM calcium transients completely coordinated with ambulatory ECG signals. Despite these encouraging results, all transplanted animals suffered premature ventricular contractions and ventricular tachycardias [125]. These opposing results could be explained by the disparity in the heart rate of guinea pigs and macaques. High heart rates, typical of small animal models, could mask the ESC-derived CM automaticity by surpassing their AP generation frequency. In contrast, in both large animal models and humans, the automaticity of these cells can be revealed due to slower basal heart rates [125]. Thus, although these cells show a phenotype which closely mimics CMs, their immature state can hinder its clinical applicability. Additionally, note that

pluripotent stem cells have other hurdles to surpass such as immunogenicity (especially regarding ESCs), tumorigenesis by teratoma formation or use of viral vectors (mainly in iPSCs), low cell survival and ethical concerns.

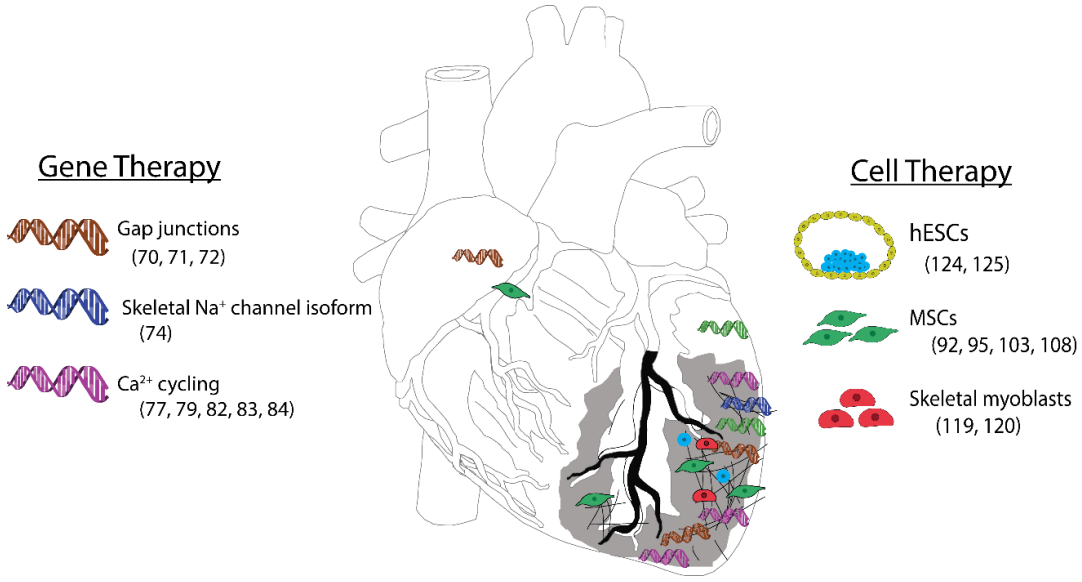

Figure 5 - Scheme representing the discussed gene and cell delivery strategies for altering cardiac conduction, along with the delivery sites. A diseased heart with reduced electrical integrity is represented. Icons positioned on the gray region are indicative of studies involving MI animal models. The cell sources and gene therapies strategies are represented on the side columns

In conclusion, an ideal cell capable of adequate cardiac electrical integrity, while improving cardiac function and tissue remodeling, is yet to be described. Regardless, one must reflect on novel therapies on different perspectives: 1) does a certain cell allow sufficient improvement in cardiac function and tissue remodeling that compensates for their pro-arrhythmic potential upon transplantation?; 2) should we focus on cellular genetic manipulation to approximate their function and phenotype to native CMs?; 3) can different aspects be improved using, for instance, tissue engineering which involves combinatorial and integrative approaches?

3.5.2. Potential of Electrical Cues to Improve Cardiac Tissue Engineering Strategies

Cardiac tissue engineering strategically combines cells, scaffolds and signaling factors to restore cardiac function and/or improve cardiac repair, which can be achieved through different approaches, such as: 1) improving therapies based on cell injection by providing a vehicles to cells and 2) allowing the formation of cardiac tissue constructs *in vitro*

for subsequent implantation (reviewed elsewhere [19, 20, 129]). Although cardiac tissue engineering resulted in promising results, particular in cell survival and engraftment *in vivo*, some limitations still remain. For instance, cardiac tissue constructs, despite exhibiting synchronous contractions, spontaneous beating can be observed (mainly with pluripotent stem cells) which, as was already discussed can have pro-arrhythmic effects. In order to solve this issue, culture conditions have been successively improved by providing biochemical, mechanical and electrical cues that closely mimic the native myocardial microenvironment.

The role of external electrical stimulation has been tested *in vitro* on cultured cardiac cells [130-133]. For instance, Radisic *et al.* conducted a pioneer work showing that, upon 8 days of *in vitro* electrical stimulation, cultured neonatal CMs exhibited increased alignment, intercellular coupling, ultrastructural organization and amplitude of synchronous contractions, concomitant with improved contractile and electrophysiological proficiency [130].

Scaffolds or constructs containing conductive components have been explored to originate constructs that mimic the myocardial environment and support functional cardiac cells and even their electromechanical integration following transplantation and/or that promote electrical integrity of the heart by acting directly on native CMs. The most explored materials are: i) gold-based materials, such as gold nanowires (AuNWs) and gold nanoparticles which exhibit great biocompatibility, low toxicity and, importantly, high electrical conductivity [134]; ii) carbon-based materials, mainly carbon nanotubes (CNTs) due to their high surface area, high chemical stability, high mechanical strength and conductivity; iii) intrinsically electroconductive polymers; and, more recently, iv) silicon-based approaches. Table 1 summarizes representative studies, some of which will be discussed.

3.5.2.1. Gold-based materials

In a pioneer study, Dvir *et al.* integrated AuNWs in the pore walls of macroporous alginate scaffolds. Neonatal CMs were cultured on AuNWs scaffolds during 3 days without electrical stimulation followed by 5 days of electrical stimulation. While alginate-only scaffolds resulted in the formation of small cell aggregates within the pores, Au-NW scaffolds showed

thick and aligned cardiac cell constructs. Furthermore, CMs in these scaffolds exhibited Ca^{2+} transients, synchronous contraction and higher amounts of α-sarcomeric actinin and Cx43 [135].

Aiming to mimic the native cardiac ECM fibrous organization, gold nanoparticles deposited on fibrous decellularized pig omental matrices promoted Cx43 rearrangement between adjacent neonatal CMs organized in elongated, aligned and striated cell constructs with stronger contraction forces [136].

To assure proper alignment and electrical coupling a cardiac patch should also be mechanically compatible with the myocardial tissue. Myocardial stiffness in humans is approximately 10 kPa and 500 kPa at the beginning and end of diastole, respectively [137]. Of note, the majority of studies with gold-based materials summarized in Table 1 report a scaffold's stiffness out of this range (Table 1). Recently, this issue has been addressed through incorporation of AuNWs into biodegradable polyurethane porous scaffolds with an elasticity of 200 to 240 kPa [138]. Electrical stimulation improved H9C2 rat CMs spreading and alignment on the conductive scaffolds however, Cx43 expression was unaffected [139].

3.5.2.2. Carbon-based materials

Initial studies showed that neonatal CMs cultured on the top of CNTs on glass substrates presented higher metabolic activity, proliferation rates and displayed larger domains of syncytial beating. Importantly, whole cell patch clamp recording showed that CMs cultured on CNTs for 3 days exhibited more negative membrane resting potential than controls, evidencing increased CM maturation [140]. The improved maturation of CMs on CNTs was further related with more abundant Cx43 gap junctions and alterations on gene expression [141].

These 2D approaches advanced to the use of carbon-based 3D ECM-like scaffolds such as scaffold comprising poly(glycerol sebacate):gelatin aligned electrospun nanofiber embedded with CNTs. Neonatal CMs cultured on CNT-containing scaffolds days had higher viability, metabolic activity, increased Cx43 levels, became more aligned and displayed higher

beating rates and lower excitation threshold than CNT-free counterparts [142]. An independent study showed that CMs cultured on CNT scaffolds augmented conduction velocity, reduced AP duration and displayed preferential localization of Cx43 at cell–cell junctions. Of note, potential cytotoxic effects of CNTs were demonstrated at high concentrations (175 ppm) [143]. In 2014, CNT-based composite cardiac patch were for the first time tested *in vivo*. CNT-gelatin scaffolds seeded with neonatal CMs were implanted on the lesion site of rats 14 days after MI. Following 4 weeks of implantation, the boundary between the scaffold and scar tissue was unclear and CNT-seeded CMs presented upregulated levels of Cx43, $Na_V1.5$ and N-cadherin (typical of intercalated discs). Interestingly, a portion of CNT-seeded CMs migrated to the scar tissue, along with CNTs. The scaffold also contained host-derived cells such as CMs, smooth muscle cells, and $CD68^+$ macrophages, showing evidences that the scaffold integrated with the host cardiac tissue. Heart function assessment showed that ejection fraction and fractional shortening were significantly improved [144]. Despite the aforementioned beneficial effect of CMs in CNTs, electromechanical coupling with native counterparts and electrophysiological influence is yet to be demonstrated.

Although the majority of the described studies show improved intercellular electrical coupling induced by carbon-based materials, the molecular mechanisms that trigger these effects are still not well understood. A recent report further demonstrated that CNT-collagen seeded CMs induced intercalated disc gap junctions assembly via β1-integrin/FAK/ERK/MEF-2c and GATA4 signaling pathway [145]. Of note, it remained unclear if CNT-collagen observed effects could be attributed to mechanical and/or to electrical cues.

3.5.2.3. Conductive polymers-based materials

The two main studied polymers are polyaniline (PANI) and polypyrrole (PPy). Some authors explored the capability of PANI-based materials to promote functional proficiency and electrical coupling of CMs [146, 147]. Baheiraei *et al.* explored the properties of porous scaffolds composed of polycaprolactone (PCL) and a biodegradable polyurethane polymer containing aniline pentamers. This strategy aimed to harness the electroconductive properties

of the aniline pentamers while trying to surpass the low biodegradability and poor mechanical properties of PANI. Conductive scaffolds promoted neonatal CMs adhesion, growth and higher expression of genes involved in contraction and cytoskeleton alignment when compared with the control groups. Nevertheless, Cx43 expression levels were not significantly altered [147].

Regarding PPy-based materials, CMs were cultured on electrospun nanofibers consisting in blend of doped PPy, polycaprolactone and gelatin onto glass coverslips. Overall, increasing the concentration of PPy (0-30%) increased tensile modulus: 15% PPy presented better conductivity, mechanical properties and biodegradability with seeded CMs displaying enhanced performance considering cell attachment, proliferation, interaction, and expression of cardiac-specific proteins [148]. More recently, Spearman *et al.* produced films comprising interpenetrating networks of PPy and polycaprolactone. HL-1 atrial myocytes seeded on these films remained viable, became more elongated, presented higher levels of Cx43 and increased calcium transient propagation velocity and spontaneous electrical activity frequency values [149].

Table 1 – Experimental results demonstrating the potential of conductive materials on cardiac tissue engineering.

Material	Refs.	Scaffold	Elastic Modulus (kPa)/ Conductivity (S/m)	Cell Source	Main Results
Gold	[135]	AuNW-incorporated alginate scaffolds	~3.5/n.a.	Neonatal CMs	Thick and aligned cell constructs; ↑ α-SA and Cx43; synchronous contractions
	[154]	AuNP-deposited PCL fibers	~60x10^3/n.a.	Neonatal CMs	Elongated, aligned and striated cell constructs; ↑ contraction rate and force
	[139]	AuNP-incorporated biodegradable PU scaffolds	~200-240/n.a.	H9C2 rat CMs	Improved cell spreading and alignment; ↑ Nkx2.5, ANF, NPPB expression
	[155]	AuNP-deposited PCL/gelatin scaffolds	n.a./n.a.	Neonatal CMs	CMs with elongated shape, conspicuous striation and higher aspect ratio; ↑ contraction amplitudes and rates
	[136]	AuNP-deposited decellularized pig omental matrices	~12.5x10^3/n.a.	Neonatal CMs	Elongated, aligned and striated cell constructs; Cx43 staining localized between adjacent CMs; ↑ contraction amplitude, calcium transient propagation velocity; ↓ excitation threshold
	[156]	AuNP-deposited thiol-HEMA/HEMA scaffolds	~600-1600/~11-15	Neonatal CMs	CMs presented as clusters or single cells; 2-fold ↑ Cx43 protein levels
	[157]	AuNW-incorporated GelMA hydrogels	~1.3/ n.a.	Neonatal CMs	↑ cell retention and viability; highly organized sarcomeric structures; ↑ beating frequency; more synchronous, stable, and robust beating behavior; synchronized calcium transients; ↓ excitation threshold
Carbon	[142]	MWCNT-embedded PG nanofibers	~373.5/n.a.	Neonatal CMs	↑ CM alignment, metabolic activity and viability; ↑ Cx43 staining
	[140, 141]	MWCNT solution coating a glass substrate	n.a./n.a.	Neonatal CMs	↑ metabolic activity; more negative membrane resting potential; ↑ αMHC, SERCA2a, Cx43; ↓ ANF
	[158]	Chitosan:CNTs composite scaffolds	~28.1/~0.25 (hydrated)	Neonatal CMs	↑ CM alignment and metabolic activity; ↑ TnI, SERCA2a, GATA4, αMHC, Cx43, βMHC and ANF expression
	[143]	SWCNT-incorporated gelatin-chitosan hydrogels	~19.3 (175 ppm)/n.a.	Neonatal CMs	Concentration-dependent cytotoxicity; more developed sarcomeres; ↑ α-SA protein levels; intercellular Cx43 stainings; ↑ beating rates and conduction velocity; ↓ AP duration
	[159]	CNT-embedded GelMA hydrogels	~20-54/n.a.	Neonatal CMs	Aligned, interconnected CMs; developed sarcomeres; attenuation of heptanol-induced intercellular coupling inhibition

	[160, 161]	PLGA:CNFs composite substrates	n.a./~$5x10^{-4}$ – $7x10^{-3}$	Human CMs, rat ECs & NIH/3T3 rat fibroblasts	↑ CM density; ↓ ECs and fibroblast growth
	[145]	SWCNT/collagen solution coating a glass substrate	n.a./ ~$1.90x10^{-8}$ – $1.77x10^{-3}$	Neonatal CMs	Marked striation and organized sarcomeres; functional beating syncytium; ↑TnI, Cx43, N-cadherin, plakophilin2 and plakoglobin expression; well-developed intercalated disc junctions; ↑ β1-integrin, FAK, p-ERK, MEF-2c and GATA4
	[144]	SWCNT-incorporated gelatin hydrogels	n.a. (shear modulus:~ 20-400 Pa)/ ~$5x10^{-5}$	Neonatal CMs	In vitro: aligned cell constructs; organized sarcomeres; ↑ α-SA and Cx43 levels; spontaneous electrical activity; In vivo (MI rats): ↑ Cx43, Na$_v$1.5 and N-cadherin protein levels; unclear scaffold/scar boundary; presence of host-derived smooth-muscle cells and $CD68^+$ macrophages; ↑ ejection fraction and fractional shortening
Conductive polymers	[147]	PCL/PU blend scaffolds containing aniline pentamers	~$1.3x10^3$/~10^{-4}-10^4	Neonatal CMs	↑ TnT, Cx43, actinin-α-4
	[146]	Nanofibrous 2D meshes of HCl-doped PANI/PLGA blend	~$91.7x10^3$/~0.31	Neonatal CMs	Isolated cell clusters; spontaneous beating activity; ↑ TnI, Cx43 expression; intercellular Cx43 localization
	[148]	PPy/PCL/gelatin blend nanofibers on glass substrate	~$16.8x10^3$/~$1.3x10^{-3}$	Rabbit CMs	↑ α-SA, TnT and Cx43; increasing PPy proportion disrupted mechanical properties and slowed CM growth
	[151]	Injectable PPy-grafted chitosan hydrogel	~2/~0.02	Neonatal CMs	In vitro: ↑ Ca^{2+} transients velocity; In vivo (MI rats): QRS interval duration similar to healthy; ↑ transverse and border zone/scar region conduction velocities; ↑ ejection fraction, dP/dt max and min, preload recruitable stroke work;
	[149]	Films of interpenetrating PPy and PCL networks	~$9.3x10^5$/~0.10	HL-1 murine atrial myocytes	↑ proportion of cells with peripheral Cx43 expression;↑ Ca^{2+} transients velocity and spontaneous electrical activity frequency
Silicon	[152, 153]	SiNW-incorporated cardiac cell spheroids	n.a./150-500	Neonatal CMs or hiPSC-derived CMs	Improved intercellular coupling (e.g. ↑ Cx43 and N-cadherin); improved contractile machinery development; ↑ β-MHC/α-MHC ratio; ↓ spontaneous beating frequency

n.a. – non-available; αMHC, alpha myosin heavy chain; α-SA, alpha-sarcomeric actinin; βMHC, beta myosin heavy chain; ANF, atrial natriuretic factor; AuNP, gold nanoparticle; AuNW, gold nanowire; CM, cardiomyocyte; CNT, carbon nanotube; CNF, carbon nanofibers; Cx43, connexin-43; EC, endothelial cell; ERK, extracellular-signal-regulated kinase; ESC, embryonic stem cell; FAK, focal adhesion kinase; GelMA, gelatin methacrylate; HEMA, hydroxyethylmethacrylate; hiPSCs, human induced pluripotent stem cells; MEF-2c, myocyte-specific enhancer factor 2C; MHC, myosin heavy chain; MI, myocardial infarction; MWCNT, multi-walled carbon nanotube; NPPB, natriuretic peptide precursor B; PANI, polyaniline; PCL, polycaprolactone; PECAM1, platelet endothelial cell adhesion molecule 1; PLGA, polylactic-co-glycolic acid; PPy, polypyrrole; PU, polyurethane; SERCA2a, sarcoplasmic reticulum Ca^{2+} ATPase 2a; SiNW, silicon nanowire; SWCNT, single-walled carbon nanotube; TnI, troponin I; TnT, troponin T

Similarly to the other conductive materials, *in vivo* studies involving electroconductive polymers are scarce, being the few existent dedicated to cell-free injectable PPy-based hydrogels rather than tissue engineered cardiac patches [150, 151]. Notwithstanding, a recent study addressed the effect of an injectable hydrogel composed of PPy-grafted chitosan, on cardiac function and AP propagation in a rat MI model. The hydrogel was administered to the infarcted LV 1 week after MI. Eight weeks after injection the treated group showed improved LV function and QRS interval duration of PPy/chitosan-injected heart was similar to that of healthy animals [151].

3.5.2.4. Silicon-based approaches

Recently, when incorporated in spheroids comprising of neonatal rat CMs or human iPScs-derived CMs, silicon nanowires were shown to enhance contractility and synchronization and increase expression of α-sarcomeric actinin and Cx43 [152, 153]. Furthermore, silicon nanowires and electrical stimulation had a synergistic effect on hiPSC-derived CMs spheroids which presented more developed sarcomeric apparatus, improved intercellular coupling, higher degree of maturation and reduced spontaneous beating frequency [152].

Overall, conductive scaffolds showed promising results as potentiate the formation of aligned, striated and synchronously contracting CMs, exhibiting increased calcium transients and AP propagation velocities and higher contractility forces (Table 1). Additionally, upregulation of CM maturation-associated genes and/or functional proficiency was also observed (Table 1). Constructs were often beating spontaneously, underlining that electrical cues were not sufficient to obtain full maturation. Notwithstanding, it is conceivable that full maturation could only be obtained upon implantation. In line with this, some authors appear to consider an increase in beating frequency as a positive outcome however it could be associated with increased automaticity and, thus, a pro-arrhythmic tendency upon implantation. It should also be noted the lack of *in vivo* studies involving conductive materials. In order to ascertain whether these materials have clinical applicability in a near-future, *in vivo*

studies with thorough electrophysiological assessments in larger animal models (*e.g.* pig) are warranted. Apart from their potential for altering *in vivo* electrical integrity, other essential issues such as biocompatibility, concentration-dependent toxicity (especially for CNTs) and poor mechanical properties (mainly for electroconductive polymers) should also be evaluated.

3.6. Final Remarks

The reported progresses show the relevance of considering cardiac electrical integrity as a central aim of innovative therapies. Promising results stemmed from both gene and cell therapies that aimed to restore a defective electrical conduction system. In a CVDs involving extensive loss of CMs, as is the case of MI, an efficient therapy must rely not only in CMs replacement but also in restoring myocardial electrical integrity and/or arrhythmogenicity. Hence, conductive biomaterials coupled or not with external electrical stimulation may enhanced the outcome of conventional tissue engineering strategies by promoting cell-biomaterial-myocardium electromechanical integration. Future studies exploring combinatory therapies to promote electrical integrity and CMs replacement in clinically relevant *in vivo* models and further dissection of the underlying mechanisms, are warranted (**Figure 6**).

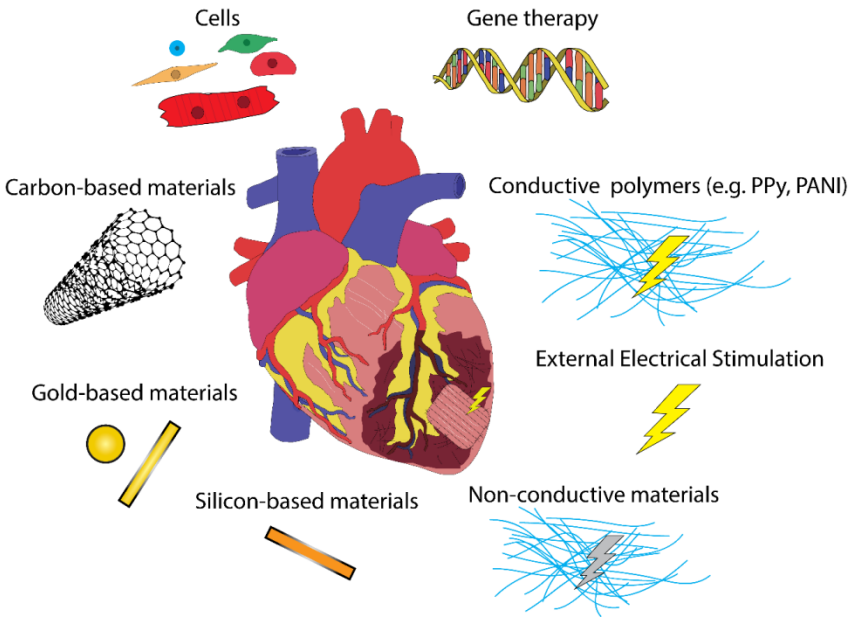

Figure 6 - Summary of discussed approaches with great potential to restore electrical integrity, and that are amenable to be combined as a electromechanical integrated biomaterial-based patch.

4. PRELIMINARY RESULTS

Apart from the mentioned studies addressing potential of electrical cues in the form of conductive materials, the role of external electrical stimulation alone has also been tested *in vitro* on cultured cardiac cells, with promising results [130-133]. For instance, Radisic *et al.* conducted a pioneer work in which it has been shown that, upon 8 days of in vitro electrical stimulation, cultured neonatal CMs exhibited increased alignment, intercellular coupling, ultrastructural organization and amplitude of synchronous contractions, concomitant with an improvement of contractile and electrophysiological proficiency [130]. In that sense, in the context of a cardiac tissue engineering applications, it would be of interest to further evaluate the effect of adequate *in vivo* electrical stimulation. Currently, that would imply the use of external electrical stimulation, which is impractical. Piezoelectric materials could comprise a future solution for this issue, as discussed below.

A given material is considered piezoelectric when it exhibits an electric polarization (and a resultant electrical activity) upon mechanical stress (direct effect) or vice-versa (converse effect). Furthermore, in order to exhibit piezoelectricity, the molecular structure of a given material must present a certain anisotropy [162].

Although most common applications for piezoelectric materials are related to electronics and sensors, biomedical applications have been encouraged for these materials due to their inherent potential to provide electrical stimuli in the absence of an external electrical source by, for instance, harnessing body movements, added to the fact that some biological tissues naturally exhibit piezoelectric properties (e.g. bone, tendons) [163-165]. Particularly for tissue engineering approaches, most studies have been focusing on bone and neural tissue engineering, which are out of the scope of the herein work and are reviewed elsewhere [166, 167]. Nevertheless, it is worth mentioning that the most commonly used piezoelectric materials on these studies are the lead zirconate titanate (a piezoceramic) and polyvinylidene fluoride (PVDF) and its co-polymers (a piezoelectric polymer) [166].

Since the heart exhibits robust cyclic movements, the implantation of these materials on an injured myocardium holds great potential as could be possible to obtain a sustainable electrical activity, induced by native mechanical stimuli, with a consequent improvement of electromechanical integration and cardiac function. Nevertheless, studies applying piezoelectric materials on cardiac tissue engineering are scarce [168]. In fact, to our knowledge, up to this point, only one *in vitro* study has been published in that line. CMs derived from mouse embryonic stem cells were cultured on a scaffold composed of aligned poly(vinylidene fluoride–trifluoroethylene) (PVDF-TrFE) co-polymer piezoelectric fibers [168]. The formed cell constructs became striated and were aligned with the fibers, while presenting spontaneous synchronous contractions throughout the scaffold. Furthermore, cardiac troponin and alpha myosin heavy chain protein levels were increased when compared with 2D culture dish controls. However, the former had Cx43 significantly decreased protein levels, suggesting a reduction in intercellular coupling. Regarding electrophysiological parameters, although the cells cultured on the piezoelectric scaffolds exhibited increased calcium transient amplitude, calcium fractional release and responsiveness to adrenergic stimulation, they also presented a longer calcium transient duration, which can be associated with an impaired ability of calcium reuptake [168].

Moreover, under the scope of a research line in the laboratory of Dr. Lino Ferreira (Biocant/CNC), neonatal rat CMs were cultured on materials comprising PCL thin-films, over which PVDF-TrFE piezoelectric fibers were electrospun. Briefly, results showed that these piezoelectric materials sustained CM viability, promoted their alignment and contractility *in vitro* for at least 12 days (Figure 7), induced an upregulation of relevant ionic channel subunits, such as alpha 1C (Cav1.2), and 1D (Cav1.3) subunits of L-type Ca^{2+} channels, Nav1.5, Kv7.1 and Kv11.1 (hERG) (Figure 8), and increased expression of functional Cx43 while improving calcium handling (Figure 9) (unpublished data).

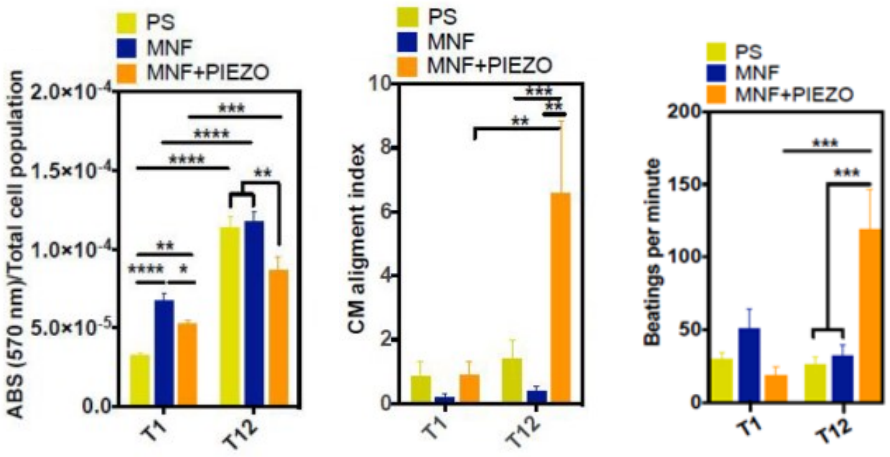

Figure 7 - Piezoeletric fibers-containing materials allow CM viability, alignment and increase beating frequency. (A) – viability as assessed by MTT assay; (B) – Cardiomyocyte alignment index; (C) – CM beating frequency when cultured on films PS – Polysterene; MNF – magnetic nanofilm..

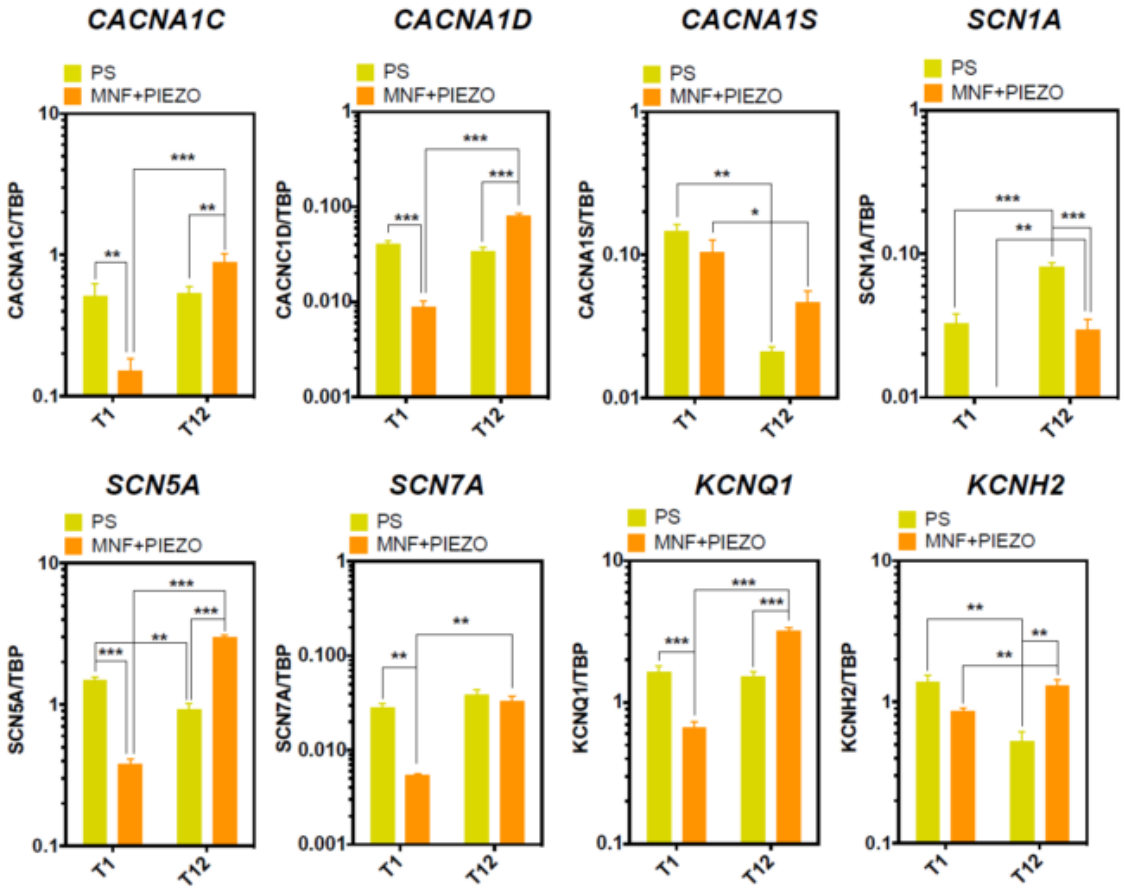

Figure 8 - Cellular expression of ion channels as assessed by quantitative RT PCR. . Cells cultured on PS or MNF+PIEZO at day 1 and day 12 were used for these analyses. Target genes include: voltage gated Ca2+ channel subunits Cav1.1 (CACNA1S), Cav1.2 (CACNA1C), Cav1.3 (CACNA1D), voltage gated Na+ channel subunits Nav1.1 (SCN1A), Nav1.5 (SCN5A), Nax (SCN7A), voltage gated K+ channel subunits Kv7.1 (KCNQ1), Kv11.1 (KCNH2). Target genes were normalized against TBP gene expression. Results are Average ± SEM, n=4. *Denotes statistical significance: *P<0.05, **P<0.01, ***P<0.001. PS – Polysterene; MNF – magnetic nanofilm.

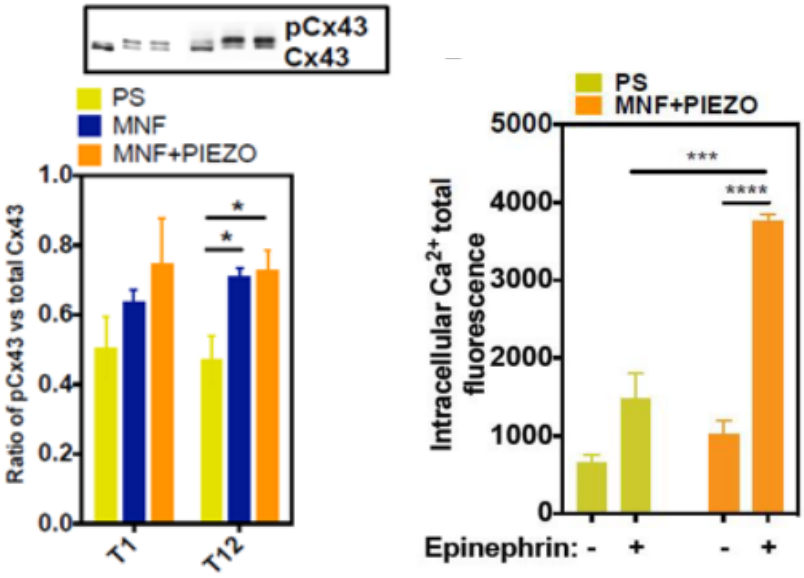

Figure 9 - Piezoelectric fiber-based materials increase the proportion of function Cx43 and improves calcium handling. (A) Ratio of phosphorylated versus total Cx43, at day 1 and 12 of culture (n = 3, 3 replicas at minimum). (B) Normalized fluorescence signal in cardiac cells cultured in PS and MNF+PIEZO, in the absence and presence of epinephrine. Fluorescence intensity values in each experiment were normalized by the minimum background intensity registered during that recording.

The promising results obtained in the aforementioned work motivated the assessment of the therapeutic effect of piezoelectric-containing thin film materials on an animal model of heart failure. In line with this, the work of the herein Master thesis emerged from this motivation and, thus PCL films deposited with piezoelectric PVDF-trFE fibers were applied in a murine model of MI.

5. AIMS

Although a tissue engineering approach with piezoelectric materials is yet to be tested *in vivo*, these materials have been already tested *in vivo* in the heart in the context of other applications [169-171]. Recently, Dagdeviren *et al.* produced thin-film flexible lead zirconate titanate-based mechanical energy harvester circuit incorporated in a polyimide layer and connected to both a rectifier and a 3.2 V rechargeable battery. Upon suturing of these films, *in vivo*, on the epicardium of healthy swine, ovine and bovine hearts, the authors observed that, although the efficiency of the mechanical to electrical energy conversion was around 2%, the energy induced by the heart movements on the piezoelectric film was sufficient to recharge the battery, upon both open and closed chest assessments. Furthermore, it was also verified that by stacking multiple layers of these films would allow this system to support the power consumption of an electronic pacemaker device [170]. Thus, this proof-of-concept study shows that it is possible to obtain significant amounts of energy by harnessing heart movements through piezoelectric materials, which further underlines the need to explore these systems on cardiac tissue engineering approaches. These results, in combination with the ones obtained in the preliminary work outlined above strongly encouraged the testing of the therapeutic potential of the piezoelectric materials on an *in vivo* MI model.

Thus, the main aim of work of the herein Master thesis was to **evaluate the therapeutic potential of piezoelectric fibers-coated thin films for the treatment of MI.** For that purpose, PCL thin films containing deposited PVDF-TrFE piezoelectric fibers were implanted (as patches) in the epicardium of in adult murine model of MI, in order to assess if said materials induced some kind of response (beneficial or detrimental). Depending on the observed response, one can reflect on the potential of using these materials as, for instance, tissue engineering scaffolds or in combination with other therapies. PCL-thin films containing deposited PCL fibers were used as control.

Hence, the detailed specific aims of the herein MSc thesis were:

- To optimize the method of surgical patch fixation to the heart of on adult C57BL/6 mice immediately after MI;
- To characterize the functional impact of the Piezo patch on cardiac function 30 days following MI by echocardiography and electrocardiography
- Determine the impact of Piezo patch on the extent of cardiac remodeling and infarct size 30 days after MI
- Evaluate the local response to the patch by histological analysis and detection of relevant proteins (CD45, alpha-smooth muscle actin (α-SMA) and Cx43) by immunofluorescence.

6. MATERIALS AND METHODS

6.1. Animals, Ethics And Regulation

Adult female C57BL/6 mice aged 8 to 10 weeks (Charles River) were used in this work. All the animal experimental procedures were approved by the i3S (Instituto de Investigação e Inovação em Saúde) Animal Ethics Committee, and by the Direção-Geral de Alimentação e Veterinária (DGAV). These procedures are in conformity with the European Directive 2010/63/EU [172]. Humane endpoints were considered according to OECD Guidance Document on the Recognition, Assessment, and Use of Clinical Signs as Humane End points for Experimental Animals Used in Safety Evaluation (2000) [173].

6.2. Patches

Although the production of the used patches was not performed in the herein work, the patch production methodology and their characterization are briefly described, for contextualization purposes.

Two types of patches were used: 1) the control patches, 400 nm-thick 20 mg/mL polycaprolactone (PCL) films coated with aligned PCL fibers, and that will be referred as “PCL patches” from this point on; and 2) the test patches, 400 nm-thick 20 mg/mL PCL films coated with aligned fibers composed of a piezoelectric copolymer, the poly(vinylidene fluoride–trifluoroethylene) (PVDF-TrFE), that will be herein referred as “Piezo patches”.

PCL films were obtained by spin-coating in combination with a sacrificial layer approach. The sacrificial layer was obtained by spin-coating a water-soluble polymer, the polyvinyl alcohol (PVA) (1% w/v, in water; 1 ml; Mw = 25.000, 88% hydrolysed; Polysciences, Inc, over a silicon wafer (400 µm thick, 2 x 2.5 cm; Primewafers) at 4000 rpm for 20 seconds (Spincoat G3P- 8, Pi-Kem). Furthermore, a PCL solution (20 mg/mL in chloroform; Mw=80000, Aldrich) was spin-coated, with the same parameters, over the sacrificial layer. This sacrificial layer strategy allows the PCL films to detach from the silicon wafers only upon contact with an

aqueous solution. PCL films on their own exhibit an elastic modulus of 0.06 ± 0.04 MPa (assessed by traction test).

The deposition of aligned piezoelectric and PCL fibers was performed by electrospinning. The silicon substrates deposited with PVA and PCL were fixed in a rotating collector for the deposition of aligned fibers. Relatively to the piezoelectric fibers, a solution of PVDF (70:30 w; Solvay) dissolved in methylethylketone (Labor Spirit) was electrospun (voltage: 10-12 kV; polymer solution concentration: 20% w/v; tip to collector distance: 12 cm; injection rate: 2 mL/h; relative humidity: 40-50% at room temperature (RT); collector's rotation speed: 2000 rpm; collection time: 4 min.). Fibers with a diameter of 1.24 ± 0.13 μm were obtained. Piezo patches exhibit an elastic modulus of 5.08 ± 0.82 MPa. Concerning PCL fibers, a PCL solution (25% w/v, Aldrich) dissolved in Formic Acid/Acetic Acid (60/40) was electrospun using the same parameters as for the piezoelectric fibers except for the tip to collector distance (approximately 13 cm) and voltage: 23 kV.

6.3. Surgical Induction Of Myocardial Infarction And Patch Fixation Procedure

MI was experimentally induced by means of permanent ligation of the Left Anterior Descending (LAD) coronary artery, as previously described [174], with slight alterations. Firstly, buprenorphine (0.08 mg/kg; Bupaq; Richter Pharma) was administered intraperitoneally (ip) for analgesia purposes. Mice were then anesthetized by ip injection of a solution of ketamine (75 mg/kg, Clorketam; Vétoquinol) and medetomidine (1 mg/kg, Sededorm; ProdivetZN) and subsequently hydrated, via subcutaneous injection, with 1 mL of a Ringer's lactate solution (B. Braun). Animals were mechanically ventilated with a small-animal respirator (Minivent 845; Harvard Apparatus) coupled to an endotracheal tube. With the support of a stereomicroscope (Olympus SZX 10; Olympus), mice were submitted to a left thoracotomy on the third intercostal space, exposing the heart. The pericardial sac was gently disrupted and the first portion of the LAD artery (a pulsating bright red vessel positioned close to the left atrium) was ligated by passing a non-absorbable 7/0 suture (Silkam; B. Braun) under the artery and then knotting, permanently occluding the vessel.

Patches were immersed beforehand in a 1% Penicillin/Streptomycin (P/S) solution (100 U/ml Penicillin and 100 µg/ml Streptomycin, Labclinics) to facilitate their detachment from the silicon substrates, while avoiding bacterial contamination. Prior to surgery, the patches were detached from the substrates, using forceps and fine scissors, and placed over a PBS solution in a Petri dish. Immediately following LAD artery ligation, the infarcted area of the LV was further exposed. Subsequently, the floating patches were placed on the extremity of a biopsy punch (Ø – 4.0 mm) (BPP-40F; kai medical), positioning the fiber-containing side of the patch outwards. In parallel, a two-component fibrin glue (F007; zedira GmbH), extracted from porcine plasma, was prepared in an hydrophobic surface (Parafilm M®) by mixing 20 µL of component 1 (fibrinogen concentrate, 49-55 mg/mL) with 1 µL of component 2 (thrombin, 18-20 NIH units/mL) in order to initiate polymerization and hydrogel/glue formation. Subsequently, patches were quickly immersed in the fibrin glue and, using the biopsy punch as a support, the patches were fixed by establishing contact with the epicardium of the exposed infarcted myocardium, aiming to orient the Piezo patch fibers in an oblique manner. To promote patch adhesion, the fibrin glue was allowed to polymerize for 20 seconds while the patches were pressed against the epicardium. During that period, gauze was applied in the edges of the intercostal incision to reduce fibrin glue spillage into the thoracic cavity. Thereafter, the biopsy punch was detached from the patch, and the unattached borders of the patch were removed with fine scissors.

Intercostal and skin incisions were closed by an absorbable 6.0 suture (Safil, B. Braun) and surgical staples, respectively. Anesthesia was reversed by ip injection of atipamezole (5 mg/kg, Revertor; Virbac). Analgesia and fluid therapy were performed by ip administration of buprenorphine (0.08 mg/kg; Bupaq; Richter Pharma) and subcutaneous injection of 1 mL of a Ringer's lactate solution (B. Braun), respectively. This procedure was repeated every 12 hours up to 72 hours after surgery or until full recovery.

6.4. Functional Characterization

6.4.1. Echocardiography

At 30 days post-MI, animals were subjected to transthoracic echocardiography by using the VEVO® 2100 system (Visual Sonics) coupled to a 40-MHz probe. Anesthesia was induced by placing the animals in an induction chamber filled with 5% isoflurane (IsoVet®, Braun) until loss of body posture and paw withdrawal reflex were confirmed. Thereafter, mice were transferred to a warm platform (at 37ºC) and placed in the left lateral decubitus position. Anesthesia state was maintained using a face mask (1.5% isoflurane) and, in order to measure heart rate (HR) and respiratory rate, their paws were placed over sensors that were in contact with an electroconductive gel, while body temperature was monitored by means of a rectal probe. Two-dimensional (2D) images were acquired of both short-axis (SAX) and parasternal long-axis (PSLAX) views. In SAX view, these were required to properly position the Motion-mode (M-mode) cursor so that the dimensions of the LV cavity and LV walls (at systole and diastole) could be measured. PSLAX view images allowed to determine cardiac output (CO), *i.e.* the volume of blood pumped every minute, by measuring the diameter of the ascending aorta (by positioning the M-mode cursor at the level of the aortic walls) and the blood flow through this vessel by resorting to the Pulsed Wave Doppler (PW Doppler) mode.

Several parameters were determined from the performed measurements. The LV internal diameter during diastole ($LVID_d$) and systole ($LVID_s$), obtained in SAX view in M-mode, were used to calculate the fractional shortening (FS) (*i.e.* the fraction of any diastolic dimension that is lost in systole):

$$FS(\%) = \frac{LVID_d - LVID_s}{LVID_d} \times 100 \quad (Eq. 1)$$

and the LV volume during diastole ($LVVOL_d$) or systole ($LVVOL_s$) using the Tiecholz formula:

$$LVVOL_{d/s} = \frac{7}{2.4 + LVID_{d/s}} \quad (Eq. 2)$$

that, in turn, were required to calculate the ejection fraction (EF) (*i.e.* the fraction of the blood pumped from the heart at each heartbeat):

$$EF\ (\%) = \frac{LVVOL_d - LVVOL_s}{LVVOL_d} \times 100. \ (Eq.3)$$

Furthermore, $LVID_d$, LV posterior wall thickness (LVPW), and LV anterior wall thickness (LVAW) (measured in SAX view) were used to estimate LV mass:

$$LV\ mass = 0.8 \times [1.053 \times ([IVS\ (or\ LVAW) + LVID_d + LVPW]^3 - LVID_d^3)]. \ (Eq.4)$$

The ascending aorta diameter, or LV outflow tract diameter (LVOT), and the velocity-time integral of the aortic flow (VTI) (measured in PW Doppler mode), allowed the calculation of the stroke volume (SV) (*i.e.* the volume of blood pumped at each heartbeat):

$$SV = 0.785 \times VTI \times LVOT^2 \ (Eq.5)$$

that, in turn, in combination with the HR, was required to determine the CO:

$$CO = SV \times HR. \ (Eq.6)$$

Epicardial areas in systole and diastole ($EPIarea_s$ and $EPIarea_d$, respectively), and endocardial areas in systole and diastole ($ENDOarea_s$ and $ENDOarea_d$) were measured in the SAX view images, being the latter two used to calculate the endocardial fractional area change (EndoFAC):

$$EndoFAC(\%) = \frac{ENDOarea_d - ENDOarea_s}{ENDOarea_d} \times 100. \ (Eq.7)$$

6.4.2. Electrocardiography

Electrophysiological parameters were assessed at 30 days post-MI by means of surface ECGs. Firstly, mice were anesthetized as described for echocardiography. Then, animals were placed in supine position in a stable platform. ECG signals were obtained using a data acquisition hardware (PowerLab 8/35; ADInstruments) coupled to a signal amplifier (Animal Bio Amp; ADInstruments) and ECG electrodes, with the support of the LabChart 8

software (ADInstruments). The equivalent of a lead II configuration was used to obtain the ECG signals.

Using an ECG analysis module, several parameters were measured: RR Interval, HR, PR Interval, P Duration, QRS Interval, QT Interval, JT Interval, T-peak to T-end interval, the amplitudes of P, Q, R, S and T waves and the ST segment height. Furthermore, QT corrected for the HR (QTc) was calculated through the Bazett's formula:

$$QTc = \frac{QT}{\sqrt{RR\ Interval}}. \quad (Eq. 8)$$

6.5. Histological Procedures And Immunohistochemistry

At 0, 2, 3, 7 and 30 days after surgery, animals were deeply anesthetized by ip injection of solution of ketamine (75 mg/kg, Clorketam; Vétoquinol) and medetomidine (1 mg/kg, Sededorm; ProdivetZN). After 4M potassium chloride (Sigma-Aldrich) injection, diastole-arrested hearts were harvested and washed in PBS. Macroscopic photographs of the hearts were obtained using a stereomicroscope (Olympus SZX 10; Olympus) coupled to a camera (Olympus DP21; Olympus).

Hearts were fixed in 10% (v/v) neutral buffered formalin (Prolabo; VWR International) for approximately 16 hours at RT. Prior to paraffin embedding, hearts were submitted to an automated histological processing in a paraffin tissue processor (Microm STP 120-2; Thermo Scientific) in which the samples are immersed in the following solutions, for a total of 12 hours: phosphate buffered saline (PBS), crescent series of alcohols (from 70% to absolute) (Aga), Clear Rite 3® (Thermo Scientific) and paraffin (Histoplast Paraffin; Thermo Scientific) at 56ºC. Following histological processing, hearts were embedded in paraffin blocks in a modular paraffin embedding system (Microm EC-1/2; Thermo Scientific).

Paraffin-embedded hearts were sectioned transversally (microtome RM2255; Leica) from the apex to the base accordingly to [175]. In order to achieve a representative sampling of the LV, 3 µm-thick sections were obtained from equidistant regions (300 µm) of the LV (in a

total of, approximately, 15 sections per heart). In order to assess the presence of the patches at early timepoints (0 to 7 days after surgery) and to perform morphometric analysis/infarct size quantification, the paraffin sections were stained with Hematoxylin-Eosin (HE) or modified Masson's Trichrome (MT), respectively. Sections were dewaxed using xylene and hydrated by a descending series of ethanol prior to both HE and MT stains. For the HE stain, paraffin sections were immersed for 5 minutes in Gill's Hematoxylin (GHS232, Sigma-Aldrich) and washed for 2 minutes with tap water. Sections were then dehydrated by an ascending series of ethanol and incubated for 2 minutes in alcoholic eosin (Leica & Thermo). MT stain was performed according to the Trichrome (Masson) Stain kit (Sigma-Aldrich), except for the following alterations: nuclei were prestained with Celestine Blue solution prior to Gill's Hematoxylin stain, followed by a 1-hour incubation in aqueous Bouin's solution (HT10132-1L, Sigma-Aldrich) in order to promote an uniform staining. Following either HE or MT stains, the sections were diafanized in xylene and mounted in Entellan® mounting medium (107960, Merck Millipore). Whole-section low-magnification images were acquired with a stereomicroscope (Olympus SZX 10; Olympus) coupled to a camera (Olympus DP21, Olympus), while high-magnification images were acquired using an optical microscope (Olympus CX31, Olympus) coupled to a camera (Olympus DP21, Olympus) or by means of a digital slide scanner (NanoZoomer 2.0-HT, Hamamatsu).

For immunostainings, sections were subjected to dewaxing and hydration. Antigen retrieval of masked epitopes, which is frequently required in formaldehyde-fixed tissues in order to allow an efficient antibody-antigen binding, was executed for some of the assessed antigens (Table 2). Then, since assessed antigens were located in the cytoplasm, heart tissue sections were permeabilized with 0.2% Triton X-100 (Sigma-Aldrich). Since we used primary antibodies that were produced in mouse, the Vector M.O.M.™ kit (BMK-2202, Vector Laboratories) was applied to block endogenous mouse immunoglobulins of the tissue, which could bind to the secondary antibodies and, ultimately, lead to unspecific stainings [176]. Sections were incubated with primary antibodies (Table 2) overnight at 4ºC, in a humidified

chamber. Thereafter, incubation with secondary antibodies (Table 3) was performed for 1 hour at room temperature (RT). Lastly, sections were mounted with Fluoroshield™ with DAPI (F6182, Sigma-Aldrich). Images were acquired with an inverted fluorescence microscope (Leica DMI 6000B FRET, Leica Microsystems) coupled to a camera (Leica DFC360 FX, Leica Microsystems).

Table 2 - List of primary antibodies used along with their respective working dilution and antigen retrieval.

Primary Antibody (Isotype)	Reference	Dilution	Antigen Retrieval
α-sarcomeric actin (Mouse IgM)	A2172, Sigma	1:500	None
α-smooth muscle actin (Mouse IgG)	A5228, Sigma	1:750	10 mM Sodium Citrate Buffer pH=6.0 (35 min. 98ºC water bath + 20 min. RT)
CD45 (Goat IgG)	AF114, R&D	1:50	10 mM Sodium Citrate Buffer pH=6.0 (35 min. 98ºC water bath + 20 min. RT)
Connexin 43 (Goat IgG)	AB0015-200, SICGEN	1:100	None

Table 3 - List of secondary antibodies used along with their respective working dilution

Secondary Antibody	Reference	Dilution
Alexa Fluor® 488 Donkey anti Goat IgG	A-11055, Thermo Fischer Scientific	1:1000
Alexa Fluor® 488 Donkey anti Mouse IgG	A-21202, Invitrogen	1:1000
Alexa Fluor® 568 Donkey anti Goat IgG	A-11057, Invitrogen	1:1000
Goat anti Mouse IgM-Texas Red	sc-2983	1:1000

6.6. Piezoelectric Fibers Orientation Scoring

Since piezoelectric materials originate electric currents in an anisotropic fashion we assessed their orientation. One representative Masson's Trichrome stained section of each 30 days post-MI (dpmi) heart of the Piezo group was selected for scoring and several high magnification images (fields with approximately 94 556 μm^2 each) were acquired along the region of the implantation site. Four fields from separate regions were selected. A total of randomly selected 100 fibers (25 per field) were scored for each heart and, in order to reduce subjectivity, the scoring was performed by two operators, each one scoring 2 fields per heart. A score was assigned for each analyzed fiber, ranging from score I (transverse orientation) to

IV (longitudinal orientation). Scoring was mainly based on length measurement: score I - directly assigned to fibers that had a clear transverse orientation or that exhibited a length inferior or equal to 0,9 μm; score II - 0,9 μm < fiber length ≤ 12 μm; score III - 12 μm < fiber length ≤ 24 μm; score IV – fiber length > 24 μm.

6.7. Measurement Of Myocardial Infarct Size And Morphometric Analysis

To determine infarct size, deposited collagen, which becomes stained blue when subjected to MT staining, was used to define the LV scarred region. The stereomicroscope-acquired low magnification images of the MT-stained histological sections were analyzed using the semiautomated software *MIQuant*, a tool previously developed by our team [177]. This software determines the percentage of ischemic LV wall by two distinct methods: area measurement [174] and midline length [178]. Additionally, scar volume was calculated as previously described [179]. First, scar volume between serial histological sections was obtained by using the formula of the volume of a truncated pyramid and then total scar volume was calculated by the sum of the latter:

$$Total\ Scar\ Volume = \sum_{i=1}^{N-1} \frac{1}{3} d\left(A_i + A_{i+1} + \sqrt{A_i \times A_{i+1}}\right) \quad (Eq. 9)$$

A_i and A_{i+1} are the infarcted areas obtained by *MIQuant* of section number *i* and the subsequent one in the series, respectively; *d* is the distance between sections (which in this case is 0.300 mm); and *N* is the number of sections analyzed. Simillarly, the data obtained from *MIQuant* concerning the midline length was used to estimate the total scar surface area at the midline position, resorting to the formula of the truncated pyramid lateral surface area:

$$Total\ Scar\ Midline\ Area = \sum_{i=1}^{N-1} \frac{M_i + M_{i+1}}{2} \sqrt{(R_i - R_{i+1})^2 + d^2} \quad (Eq. 10)$$

M_i and M_{i+1} are the midline lengths of the infarcted region obtained by *MIQuant* of the section number *i* and the subsequent one in the series, respectively; R_i and R_{i+1} are the LV radius at the midline position, assuming the midline path as a circumference; *d* is the distance

between sections which, in this case, is 0.300 mm; and *N* is the number of sections analyzed. The same calculations (volume and midline area) were performed for the total LV in order to calculate percentage of ischemic wall through these parameters. Morphometric analysis was executed by using the Image J software (NIH). LV wall thickness was determined on regions that exhibited collagen deposition in 50% or more of the wall and calculated as the average of the distance across the wall of five equidistant points of the ischemic wall. LV dilation was assessed by the lumen-area percentage, *i.e.* the ratio between the lumen area delimited by the endocardium and the total LV area. Area of myocardium within the infarcted regions was quantified. The area of the cell infiltrate surrounding the patches was calculated as the average of infiltration areas in subsequent serial sections. The volume of the inflammatory mass was calculated by applying Eq. 9.

6.8. Statistical Analysis

Values presented in text and figures are mean ± standard error of the mean (SEM). Data statistical analysis was performed with the IBM SPSS Statistics 21 software. Shapiro-Wilk's test was used to evaluate if the data displayed a normal distribution. If so, the homoscedasticity of the data was tested by Levene's test. These results defined the statistical test(s) used further. Normal distributed and homocedastic data were tested with parametric tests (independent samples t-test). Non-normal distributed and/or heterocedastic data were tested with non-parametric tests (Mann-Whitney U Test). The statistical significance level chosen for all statistical tests was $p<0.05$.

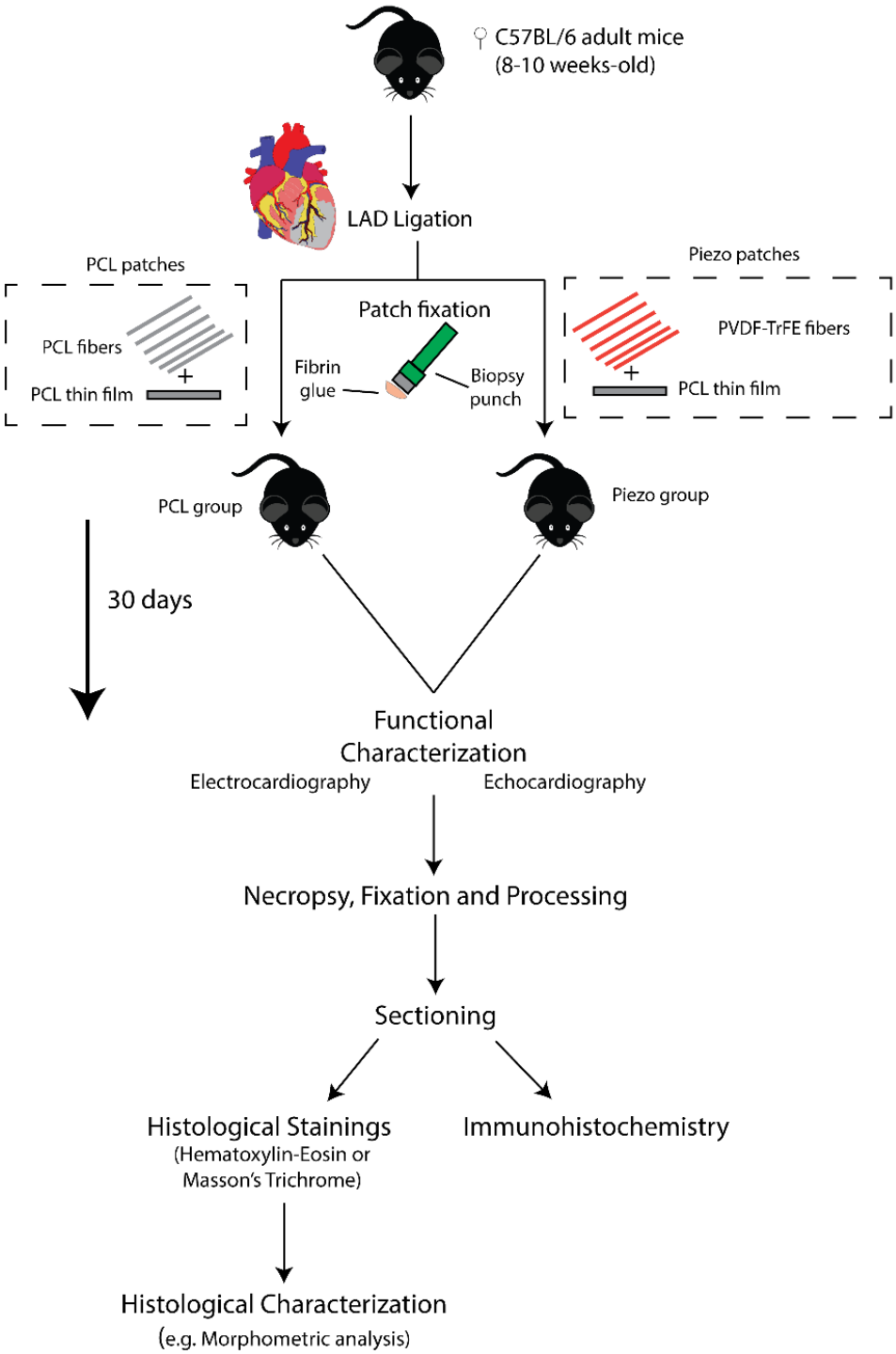

Figure 10 - Schematic representation of the main experiment methodology

7. RESULTS

7.1. Optimization And Implementation of Surgical Fixation of The Patch

Aiming to evaluate the therapeutic potential of the Piezo patches, a patch fixation procedure was implemented at our laboratory. For ethical and practical reasons, prior to its evaluation 30 dpmi in a substantial number of animals, the procedure was optimized beforehand at earlier timepoints. Hence, the following criteria had to be fulfilled and tested: 1) the patch had to remain adhered to the epicardium for several days; and 2) the patch had to be placed in a manner that allowed it to be deformed in a cyclic fashion and in synchrony with the myocardial activity; 3) the duration of the patch fixation should not extend significantly the surgical procedure.

Since patch fixation to the heart by sutures is commonly used in rat models [180-182], in the first application attempts, the Piezo patches were sutured to the epicardium (Figure 11A, B). Sutures were performed on two opposite sites, being attempted two different patch configurations: 1) a spread patch (Figure 11A); or 2) a stretched bundle patch (Figure 11B). In both situations the patch was not sufficiently stretched so, although the patch was fixed to the epicardium at the sutured sites, the remaining portion was wrinkled and was not in direct contact to the myocardium. Following this outcome, we hypothesized whether fully spread patches directly glued to the epicardium would allow a closer contact with the myocardium. To test this hypothesis, the effect of fibrin glue was assessed. Fibrin glue has been widely used as a tissue sealant in animal *in vivo* studies and clinical applications (reviewed on [183]), including in a study where a patch was successfully applied to a murine heart following MI [184]. Furthermore, in order to allow the patches to be stretched upon application, a biopsy pen was used (Figure 11C). The biopsy pen also allowed the piezo patches to be oriented since fiber orientation was visible under a stereomicroscope (Figure 11D), and provided a physical support upon patch placement (Figure 11E). This patch placement method allowed the patch to be stretched and closely adhered to the epicardium, being deformed

synchronously with the heart cycle (Figure 11F). Of note, gauze was applied in the incision border below the patch (Figure 11E) to avoid spillage of fibrin glue into the thoracic cavity, since we observed that the organs of the thoracic cavity could become severely adhered to each other if caution was not taken (not shown).

To assess whether the patches remained adhered to the epicardium after surgery, hearts were harvested in the first 24 hours following surgery (0 dpmi) for histological analysis. Macroscopic images of the harvested hearts show clearly that the patch remained adhered to the hearts at the infarcted region (below the ligation site) in both Piezo (Figure 11G, I) and PCL groups (Figure 11J, L). Furthermore, histology showed that the PVDF-TrFE fibers of the Piezo patches are visible, exhibiting a translucent appearance (Figure 11H, arrow heads), and in close contact to the myocardium. Conversely, PCL fibers were not detectable by histology (Figure 11K). Nevertheless, in both groups an acellular layer juxtaposed to the myocardium was observed under the microscope (Figure 11H, K, #), possibly fibrin glue. Having confirmed the presence of the piezoelectric fibers at the first 24 hours after surgery, we analyzed the hearts of the Piezo group at later timepoints: 2, 3 and 7 dpmi. Histological analysis revealed that the piezoelectric fibers were present at the considered timepoints in the proximity of cardiomyocytes (Figure 11M, N, O, arrow heads). Of note, at 7 dpmi piezoelectric fibers were surrounded by cells which morphologically resembled inflammatory cells Figure 11-O, *).

Following establishment of the surgical patch fixation, a proof-of-principle experiment was designed and initiated (Figure 10) to evaluate the histo-physiological impact of a 30-day Piezo patch delivery to an infarcted mouse heart. Overall the duration of the surgical procedure was ~20 minutes and patch fixation efficiency, i.e. the percentage of patches successfully applied relatively to the total of patch placement attempts, was ~78% for PCL patches and ~80% for the Piezo counterparts. Furthermore, the survival rate at 30 dpmi was 33.37% (Figure 12) and 76.64% of the deaths occurred in the first 24 hours (Figure 12).

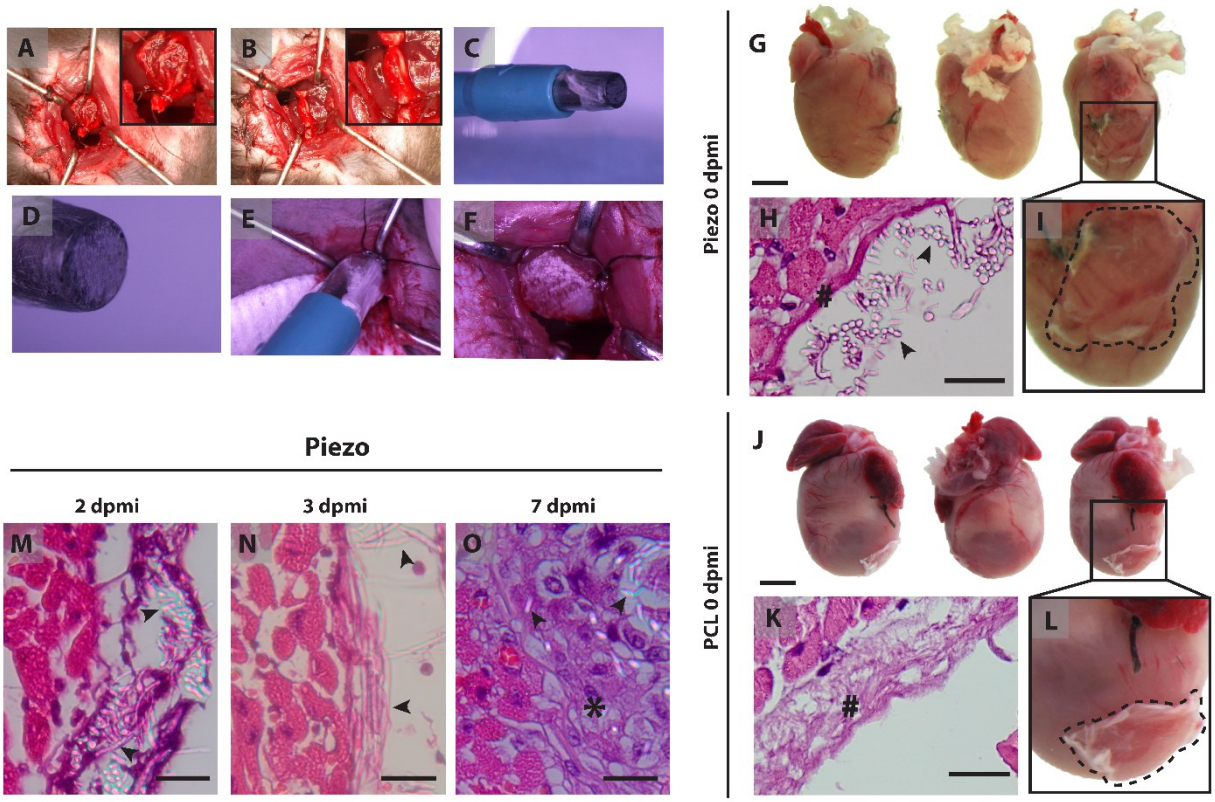

Figure 11 - Implementation and Optimization of the patch surgical fixation. (**A** and **B**) - Suture-based patch placement, including spread patch (A) and bundle (B) configurations; inset: 2x magnification of the implantation site. (**C** and **D**) - Biopsy punch showing clear fiber orientation of a Piezo patch (D). (**E** and **F**) - Patch fixation procedure with a biopsy punch and fibrin glue, while using gauze to reduce fibrin glue spillage into the thoracic cavity (E), resulted in an adhered and properly stretched patch (F). (**G**, **I**, **J** and **L**) – Macroscopic images of hearts subjected to MI and Piezo (G and I) or PCL patch delivery (J and L) revealed that patches (outlined in dashed line) remain adhered at least during the first 24 hours post-MI (0 dpmi) (n=4 for each group). Scale bars: 2 mm. (**H** and **K**) – Representative images of HE-stained sections of hearts 24 hours after Piezo (H) or PCL (K) patch fixation. Fibrin glue is visible in both groups (#) but polymeric fibers are only visible in the Piezo group (arrow heads). Scale bars: 20 µm. (**M** to **O**) Representative images of HE-stained sections of hearts 2 (M, n=2), 3 (N, n=1) and 7 days (O, n=1) after Piezo patch implantation. Fibers were visible at all timepoints (arrowheads) and a cell infiltrate around Piezo fibers was detected at 7 days (*). Scale bars: 20 µm.

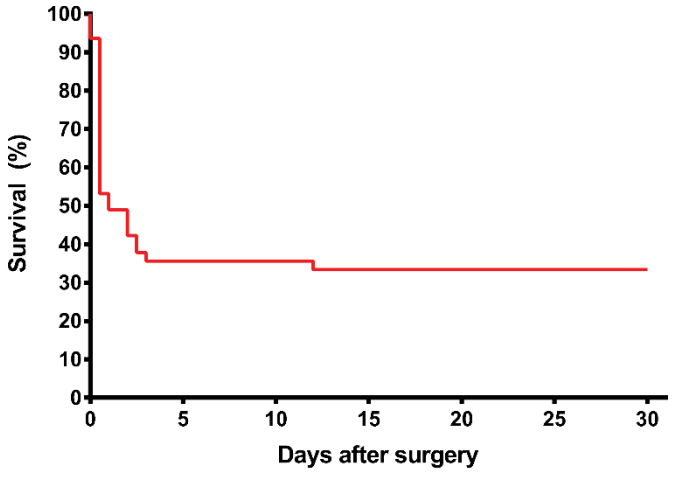

Figure 12 – Animal survival. Kaplan-Meier Survival Curve for the 30 days elapsed after patch placement procedure in both Piezo and PCL groups.

7.2. Functional Characterization

In order to assess functional proficiency, animals were subjected to transthoracic echocardiography at 30 dpmi and several parameters were determined (Table 4). Although not statistically different, most analyzed echocardiographic parameters showed a tendency for improved LV systolic function in the Piezo patch group (Figure 13A-E and Table 4). The average of left ventricular internal diameter during diastole (LVIDd) was increased over 10% in the PCL group relatively to the Piezo group (Figure 13A, B and Table 4) suggesting an aggravated LV cavity dilation in the former. Moreover, there were evidences of improved LV systolic function in the Piezo group since displayed increased fractional shortening (FS) and ejection fraction (EF) when compared to the PCL counterparts (Figure13C, D and Table 4). Interestingly, cardiac output (CO) was increased in the PCL group (Figure 13E, F and Table 4), owing both to an augmented heart rate and stroke volume (Table 4).

Table 4 – Echocardiographic parameters obtained in both Piezo and PCL groups.

Echocardiographic Parameters	**Piezo Group(mean ± SEM) n=5**	**PCL Group (mean ± SEM) n=6**
SAX LVIDd (mm)	4,392 ± 0,243	5,007 ± 0,258
SAX LVIDs (mm)	3,684 ± 0,296	4,408 ± 0,330
SAX FS (%)	16,41 ± 2,82	12,26 ± 3,20
SAX EF (%)	33,97 ± 5,28	25,55 ± 6,39
HR (bpm)	370 ± 15	411,3 ± 18,75
VTI (mm)	19,55 ± 1,93	17,79 ± 2,26
LVOT (mm)	1,314 ± 0,045	1,448 ± 0,0168
SV (µL)	26,91 ± 4,00	29,40 ± 4,00
CO (mL/min.)	9,828 ± 1,356	12,00 ± 1,634
ENDOarea;d (mm^2)	13,89 ± 1,80	19,28 ± 2,24
ENDOarea;s (mm^2)	11,23 ± 1,78	13,71 ± 2,11
EndoFAC (%)	13,10 ± 1,77	18,58 ± 2,22
SAX LV mass (mg)	122,5 ± 15,93	173,2 ± 9,80
SAX LVAWd (mm)	0,7800 ± 0,1083	0,9767± 0,0733
SAX LVPWd (mm)	0,9500 ± 0,1281	0,9617 ± 0,1319

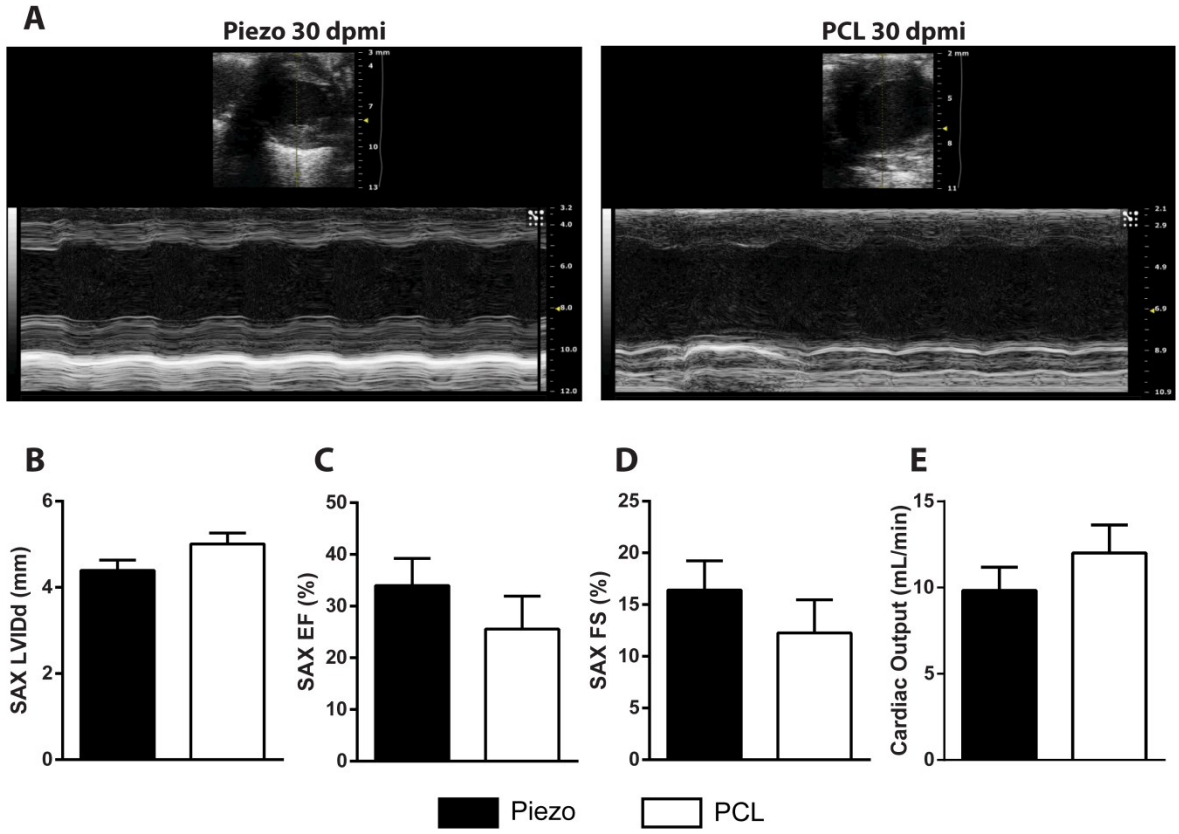

Figure 13 – Functional characterization by transthoracic echocardiography. (**A**) Representative M-mode images of SAX view of both Piezo (left) and PCL (right) groups, at 30 dpmi. (**B** to **E**) LV internal diameter during diastole (LVIDd) (B), ejection fraction (EF) (C) and fractional shortening (FS) (D) revealed functional improvements in the Piezo group although without statistical significance. Cardiac output (CO) was increased in the PCL group (E). Values are mean±SEM. n(Piezo)=5, n(PCL)=6.

The effect of the Piezo patches on cardiac electrical conduction was assessed by surface ECGs. ECG morphology of the PCL group was clearly more disrupted than in the Piezo group (Figure 14A). Table 5 summarizes the obtained electrophysiological parameters. Notably, the QRS complex of the Piezo group was narrower than in the PCL group (Figure 14B and Table 5), suggesting an improvement in ventricular electrical activation on the former. Strikingly, the PCL group exhibited markedly prolonged JT and Tpeak to Tend intervals relatively to Piezo counterpart, with the latter parameter being statistically different between groups ($p<0,05$). Both of these parameters highly indicate that the Piezo group has a more efficient ventricular repolarization. As expected, the values of said parameters culminated in a decreased QTc interval in the Piezo group when compared to the PCL counterpart (Figure 14E and Table 5). Piezo group also showed an almost neutral Q amplitude, which contrasted to the

abnormally increased negative value observed in the PCL group, and a significantly increased R amplitude (Figure 14A, F and G and Table 5), Collectively, these results strongly suggest that the Piezo group has a decreased risk of ventricular arrhythmias, associated with improved ventricular electrical integrity.

Table 5 - ECG parameters obtained in both Piezo and PCL groups

ECG Parameters	Piezo Group (mean ± SEM) n=5	PCL Group (mean ± SEM) n=6
RR Interval (ms)	129,1 ± 7,7	118,7 ± 2,5
HR (bpm)	472,3 ± 25,0	508,4 ± 10,5
QRS Interval (ms)	9,637 ± 0,869	13,75 ± 2,15
JT Interval	7,783 ± 2,881	31,20 ± 10,80
Tpeak to Tend Interval (ms)[1]	4,343 ± 1,409	16,000 ± 4,579
QT Interval (ms)[1]	17,73 ± 3,91	45,31 ± 12,33
QTc Interval (ms)[1]	50,05 ± 10,55	131,20 ± 34,23
ST height	-0,06316 ± 0,02085	0,02130 ± 0,09218
P duration	25,90 ± 12,22	23,90 ± 5,13
P amplitude	0,05285 ± 0,04558	0,08919 ± 0,02811
Q amplitude[2]	0,02613 ± 0,03697	-0,5002 ± 0,1495
R amplitude[1]	0,8580 ± 0,08783	0,5172 ± 0,1136
S amplitude	-0,3963 ± 0,09222	-0,3210 ± 0,1289
T amplitude	0,1334 ± 0,06453	0,04487 ± 0,02423

1 – p<0.05;2 – p<0.01

7.3. Cardiac Tissue Response and Remodeling

Having the animals been functionally characterized 30 dpmi, heart were harvested and processed for histological analysis. Firstly, the presence of the patch and the tissue response originated from their implantation was assessed. In both experimental groups, an extensive cellular infiltrate was observed in the implantation site (Figure 15A-C, F-H, *), similar to what was observed 7 dpmi in the Piezo group (Figure 11O, *). Interestingly, blood vessels (Figure 15K) and, apparently, multinuclear cells were detected within the cell mass (Figure 15K, arrow head).The area occupied by this cellular infiltrates was increased in the Piezo group (area: 0,8275 ± 0,205 mm^2, volume: 1,817 ± 0,553 mm^3; n=5), relatively to the PCL group (area: 0,5243 ± 0,107 mm^2, volume: 0,7613 ± 0,154 mm^3; n=6) (Figure 15D,E). Furthermore, note that the cells from the patch region were not in direct contact with the myocardium, being the

interface composed of collagen fibers (Figure 15C and H, #). Polymer-based fibers, only visible in Piezo group, were intermingled with the cellular infiltrate at a density of 2922 ± 136 fibers/mm^2 and were not in direct contact with cardiomyocytes (Figure 15C, inset, arrow heads). Most piezoelectric fibers showed a nearly-transverse orientation (Figure 15I) and, as observed at early timepoints, fibers were translucent (Figure 15J-L).

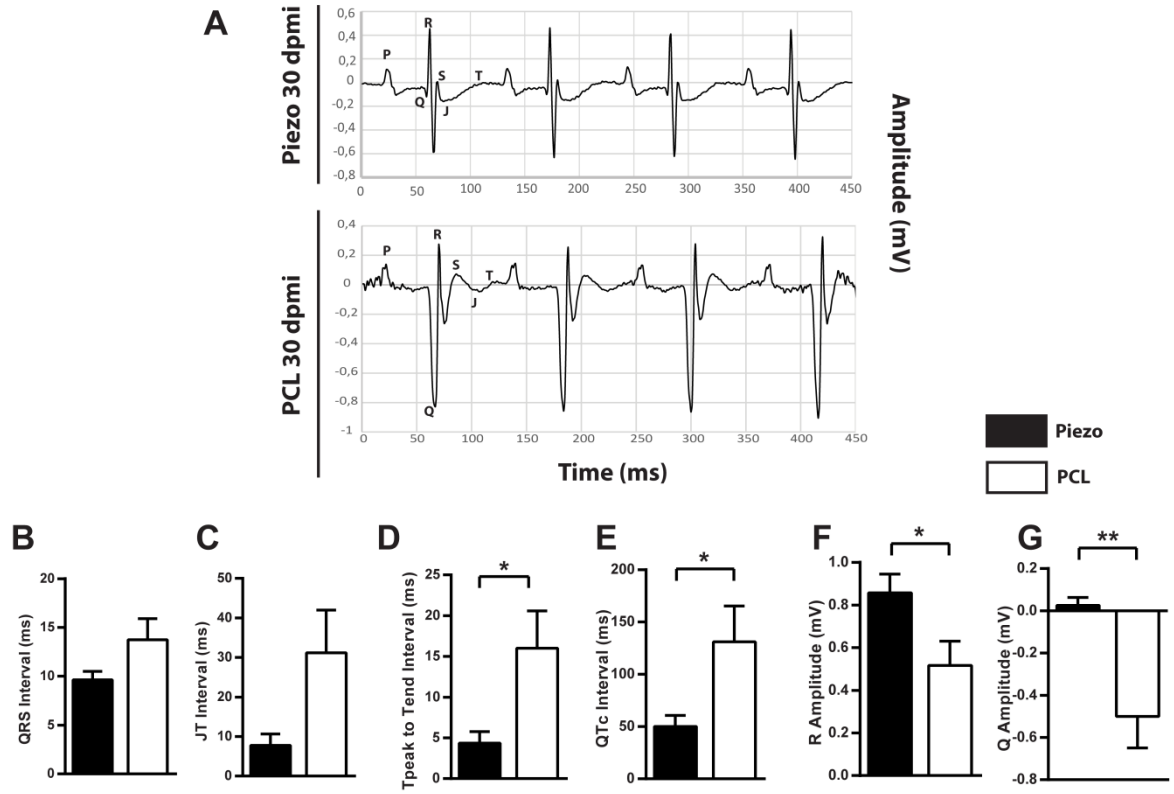

Figure 14 – Functional characterization by electrocardiography. (**A**) Representative ECG signal samples of Piezo (top) and PCL (bottom) groups. J point and P, Q, R and S waves are indicated in the first cycle. A clear disruption in the QRS complex is observed in t in the PCL group. (**B** to **G**) QRS interval and JT interval show clear tendencies to be increased in the PCL group, while QTc interval, Tpeak to Tend interval, R and Q amplitudes revealed statistically significant improvements in cardiac conduction on the Piezo group. Values are presented as mean ± SEM**.** n(Piezo)=5, n(PCL)=6. *p<0,05; **p<0,01.

To assess whether the Piezo patches had an effect on cardiac remodeling, *i.e.* in LV wall thinning and non-contractile collagen-rich scar tissue formation, morphometric analysis of representative LV histological sections was performed in both groups (Figure 16). Infarct size, as assessed by infarct area (29,95 ± 4,04 % in the Piezo group *vs* 32,69 ± 4,06 % in the PCL group; n=5 and n=6, respectively), volume (21,70 ± 1,79 % in the Piezo group *vs* 22,26 ± 2,10

% in the PCL group; n=5 and n=6, respectively), midline length (36,32 ± 4,11 % in the Piezo group vs 40,46 ± 4,83 % in the PCL group; n=5 and n=6, respectively) and midline area (36,95 ± 4,50 % in the Piezo group vs 44,02 ± 7,07 % in the PCL group; n=5 and n=6, respectively), was similar in both groups (Figure 16B). Furthermore, although no statistical differences were found on the LV free wall thinning (596,5 ± 54,42 μm in the Piezo group vs 541,9 ± 46,04 μm in the PCL group; n=5 and n=6, respectively) (Figure 16C) and LV chamber dilation (24,95 ± 2,93 % in the Piezo group vs 27,27 ± 3,57 % in the PCL group; n=5 and n=6, respectively) across groups (Figure 16D), PCL group displayed a small tendency for aggravated remodeling. Interestingly, the PCL exhibited extended regions of myocardial tissue within the infarcted zone (7,784 ± 1,915 % in the Piezo group vs 9,266 ± 0,8146 % in the PCL group; n=5 and n=6, respectively) (Figure 16E), however the degree of viability and contractility of this tissue was not determined .

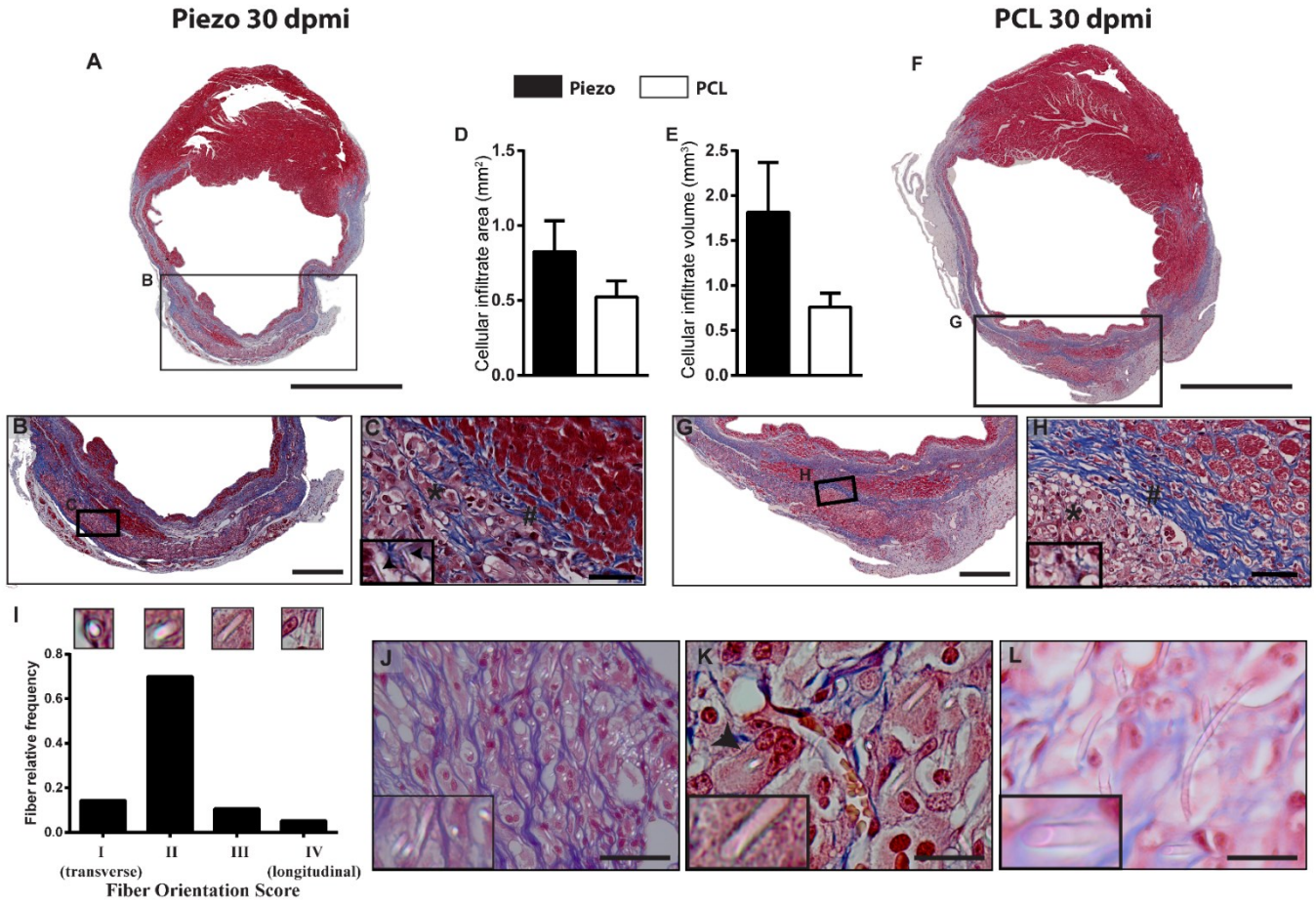

Figure 15 – Tissue response to patch implantation. (**A** to **H**) - High-resolution whole-section images of representative Masson's Trichrome stained sections of hearts at 30 dpmi of both Piezo (A and B) and PCL (F and G) revealed the presence of an cell extensive cell infiltrate at the implantation site, mainly composed of cells with a macrophage-like morphology (C and H, *), that is separated from the myocardium by collagen fibers (blue colored) (C and H, #). Polymeric fibers are only visible in the Piezo group (C, arrow heads). The extent of the cellular infiltrate appears to be increased in both area (D) and volume (E) on the Piezo group. Scale bars: A and F – 2 mm, B and G - 500 µm, C and H – 50 µm. (**I**) Histogram representing the scoring of the orientation of piezoelectric fibers relative to the sectioning cut showing a clear tendency for transversal orientation. (**J** to **L**) – Piezoelectric fibers show a translucent appearance and are often surrounded by macrophage-like multinucleated cells (arrow head) and in the vicinity of perfused vessels (K). Scale bars: J – 50 µm, K and L - 20 µm. Values are presented as mean ± SEM. n(Piezo)=5, n(PCL)=6

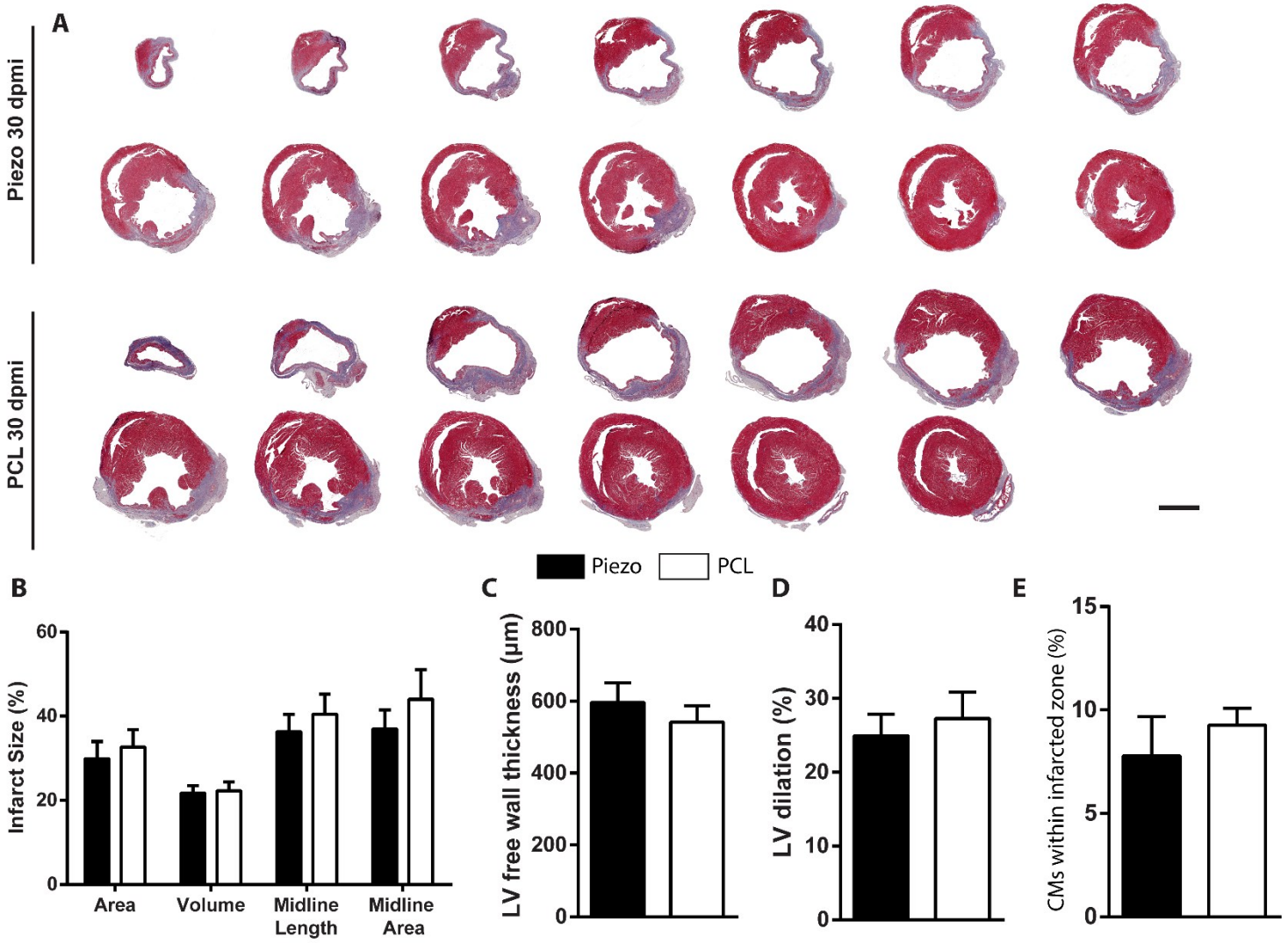

Figure 16 - – Effect of the Piezo patch on cardiac remodeling. (**A**) Representative Masson's Trichrome-stained histological sections of the LV from the apex (top left) to the base (bottom right) of Piezo (top) and PCL (bottom) groups at 30 dpmi. Scar tissue is clearly visible in blue, contrasting with the red-stained myocardium. Scale bar: 2 mm. (**B** to **E**) Infarct size (calculated by infarct area, infarct volume, midline length and midline area) (B), LV free wall thickness (C) and LV cavity dilation (D) showed slight tendencies in favor of the Piezo group, although the PCL group present increased proportion of CMs within the scar tissue (E). Values are presented as mean ± SEM. n(Piezo)=5, n(PCL)=6.

7.4. Protein Expression at The Patch-Myocardium Interface

In order to further characterize the tissue response to the patch, immunofluorescence was performed. Considering that the histological characterization revealed the presence of an extensive cell infiltrate on the implantation site and surrounding piezoelectric fibers (in the Piezo group), we explored if this was part of an inflammatory reaction to the patch by assessing the presence of hematopoietic cells (that, except for mature erythrocytes, express CD45, a membrane glycoprotein). Additionally, the expression of α-smooth muscle actin (αSMA), expressed in smooth muscle cells and in myofibroblasts, was assessed at the patch-myocardium interface. In both groups, the cell infiltrate at the implantation site was rich in CD45-expressing cells (Figure 17), when compared to adjacent scar and myocardial tissues (Figure 17B and D). Moreover, cells surrounding the piezoelectric fibers Figure 17A-C) were also $CD45^+$. Of note, these $CD45^+$ cells were big and multinucleated (Figure 17C, arrow heads), contrasting to small-sized $CD45^+$ cells found in the myocardial border zone and scar region (Figure 17B). These aspects, in combination with histological observations (Figure 15), are indicative of macrophages and foreign body giant cells, which result from macrophage fusion in the context of foreign body reaction to a biomaterial. Additionally, these big and often multinucleated $CD45^+$ cells were less abundant in the PCL group in which mainly small, round $CD45^+$ were observed Figure 17D). Furthermore, αSMA-expressing cells sparsely distributed (apart from the blood vessel counterparts which were also present in this tissue) were detected in the vicinity of piezoelectric fibers (Figure 17C, arrows), suggesting the presence of myofibroblasts.

Considering the marked improvement on cardiac conduction of the Piezo group, Cx43 expression pattern was evaluated in both experimental groups, in combination with the alpha-sarcomeric actin (α-SA) (a marker of sarcomeres which was used to detect CMs) to assess the localization of gap junctions in CMs (Figure 18). No relevant differences were detected in the expression levels or localization of Cx43 expression across groups (Figure 18) as, in both conditions, Cx43 expression pattern appeared equally disrupted in CMs of the peri-infarct zone (Figure 18B and E) when compared to CMs of the remote myocardium (Figure 18C and F)

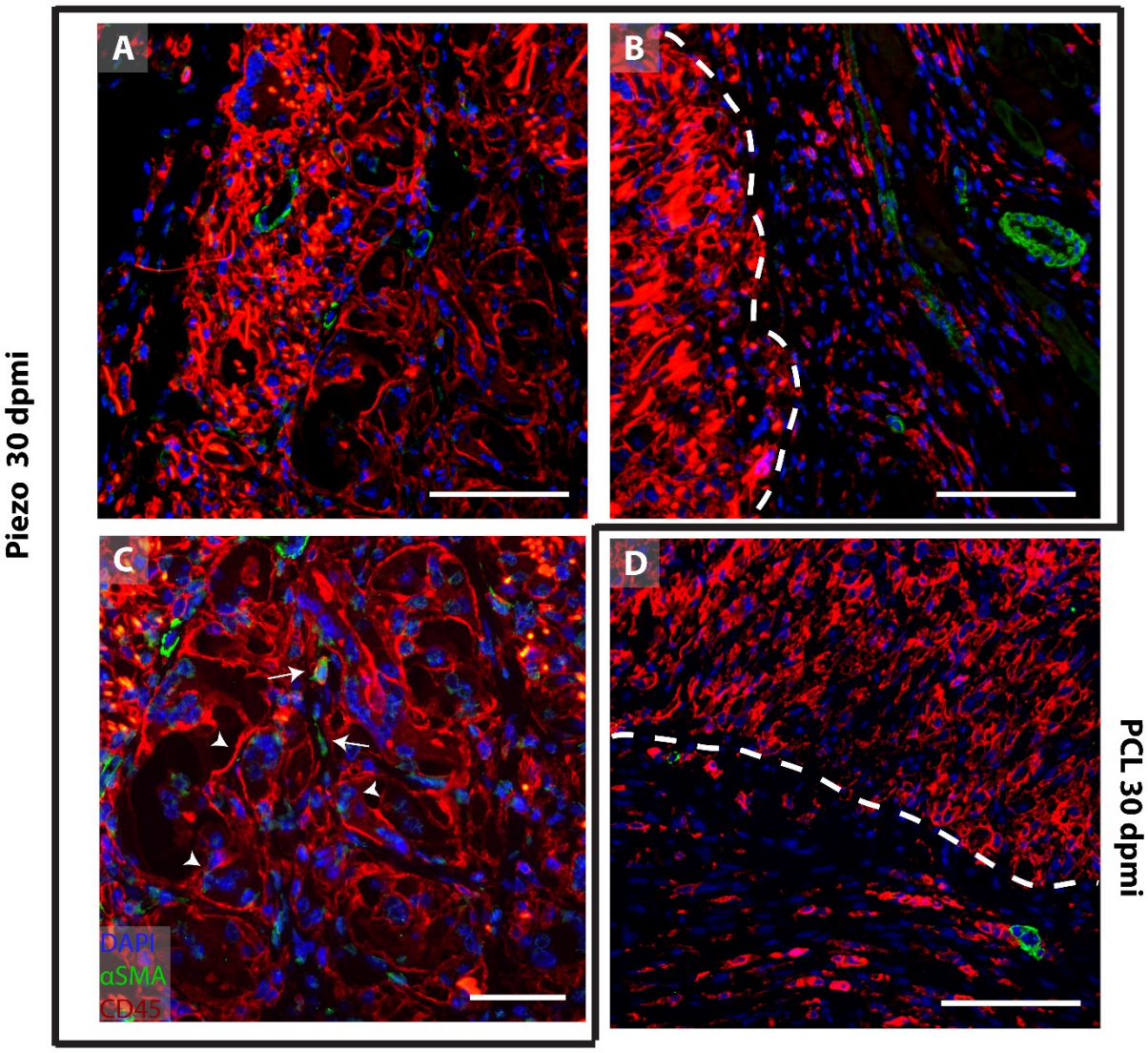

Figure 17 – Inflammatory response on the patch-myocardial interface. Representative images of the Piezo (**A** to **C**) and PCL (**D**) at the patch-myocardium interface following immunofluorescence for αSMA (green) and CD45 (red). Piezoelectric fibers are highly autofluorescent and appear in bright orange-red (A, B and C). CD45-expressing cells are abundant in the cell infiltrate surrounding the fibers, which contrasts with the adjacent myocardium in which the CD45+ cells are sparsely found. Large, multinucleated $CD45^{+}$ cells were common within the cell mass (C, arrowheads). Sparsely distributed αSMA^{+} cells were present mainly in the cell mass of the Piezo group (C, arrows). $CD45^{+}$ cells of the PCL group were smaller and rarely multinucleated (D). Dashed lines: interface between the patch region and the scar or myocardial tissue. Nuclei stained in blue (DAPI) Scale bars: A, B and D – 100 μm; C – 50 μm. αSMA - alpha-smooth muscle actin.

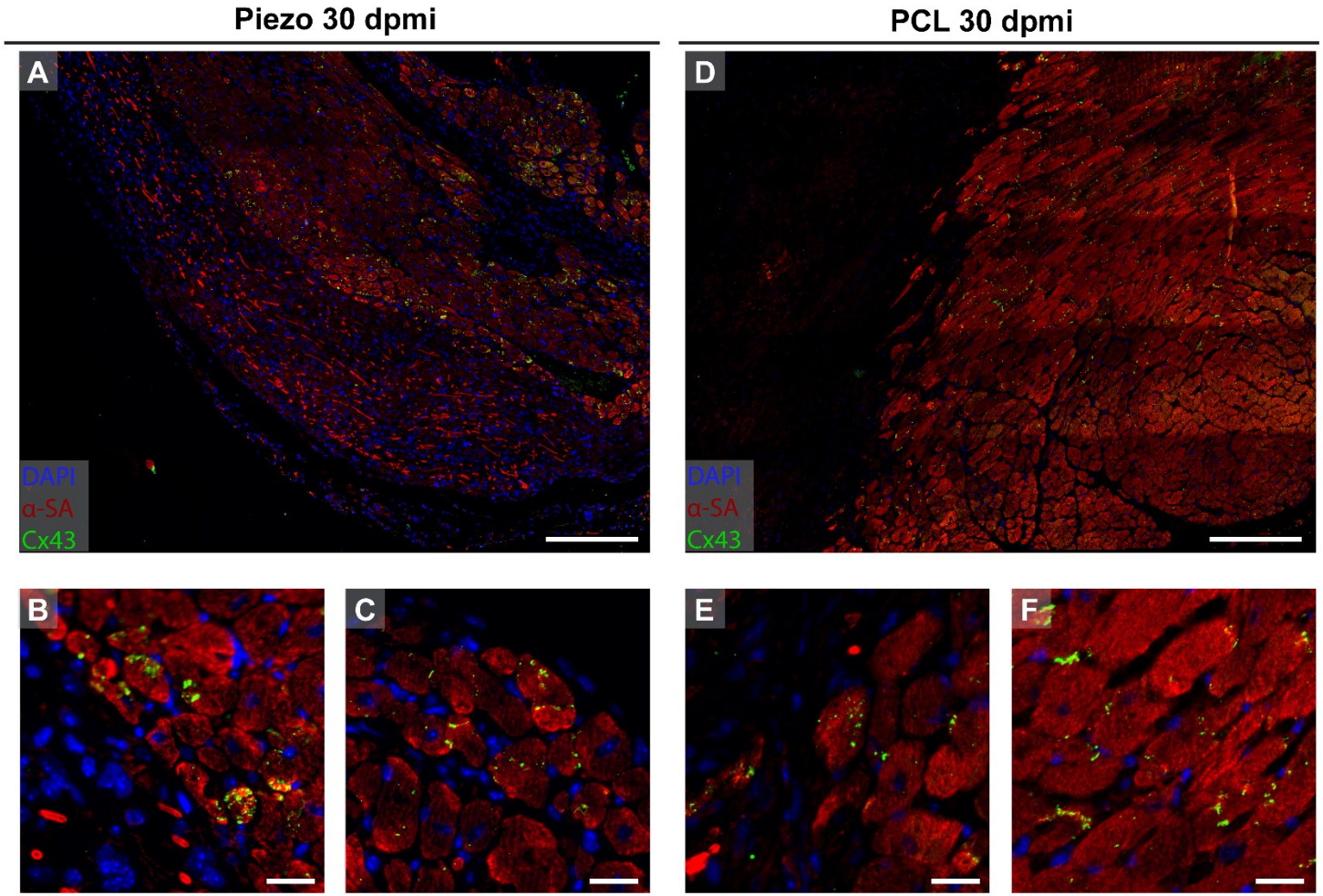

Figure 18– Effect of the Piezo patch on intercellular coupling. Representative images of Piezo (**A** to **C**) and PCL (**D** and **F**) groups, following immunofluorescence for Cx43 (green) and α-SA (red). Although, intercellular coupling appeared slightly disrupted in peri-infarct and near the patch (B and E) when compared to remote myocardial regions (C and F), no apparent differences were detected between experimental groups. Nuclei stained in blue (DAPI). Scale bars: A and D – 200 μm; B, C, E and F – 20 μm. α-SA - alpha-sarcomeric actin, Cx43 – connexin 43.

8. DISCUSSION

CVDs are the leading cause of death in the industrialized world, being estimated that they are cause of approximately 17,4 million deaths per year, with an expected increase up to 23,6 million by the year 2030 [1]. These conditions are frequently associated with cardiac electrical disruption and the onset of arrhythmias [6] that, in turn, can be fatal. Considering the several drawbacks of the current gold-standard therapies for cardiac failure (*e.g.* heart transplant) and aiming to restoring cardiac electrical integrity (*e.g.* electronic pacemakers, implantable cardioverter devices) it is of paramount relevance to develop novel therapies that allow full restoration of cardiac function, by acting on cardiac tissue remodeling, contractility and electrical conduction capabilities. Although novel approaches involving cell therapy, injectable hydrogels or biomaterial-based cardiac patches (with or without cells) have been emerging, these are mainly focused on reducing the detrimental effects of fibrosis upon CVDs (reviewed on [19, 20]) rather than focusing on restoring cardiac electrical integrity.

In the herein study, we aimed to test the in vivo effect, in a murine model of MI, of a patch comprising a film composed of PCL, a biocompatible and biodegradable polymer extensively used in biomedical applications [185-189] (including cardiovascular ones [190, 191]), with electrospuned PVDF-TrFE fibers with piezoelectric properties. Since piezoelectric materials accumulate electric charges upon mechanical deformation [192] we hypothesized that successive deformation cycles induced by the cardiac cycle would induce charge accumulation on the piezoelectric fibers, provoking the formation of electrical currents in synchrony with the heart rate and, ultimately, restore cardiac electrical conduction on a disease scenario. In vivo testing of these patches was prompted by preliminary in vitro work that showed that these Piezo patches sustain neonatal rat CM contractility for at least 12 days and induced an increased expression of functional Cx43 and relevant ionic channels on these cells (unpublished data, please see Preliminary Results) Additionally, these materials resulted in improved calcium cycling and induction of a more mature, aligned morphology (unpublished data). Herein, the *in vivo* effect was compared with a control group involving the use of PCL films with deposited PCL fibers.

In order to evaluate the *in vivo* effect of the Piezo patches we first implemented the patch surgical fixation in our laboratory (Figure 11). Although suturing methods have been commonly applied to fix patches to the epicardium of rat [180-182, 193], this approach was not efficient in our setting. On one hand, the delicate and flexible structure of the patch impaired handling and smooth perforation of the suture needle, extending significantly the surgery duration (not shown). And, on other hand, although the patches remained fixed to the heart during surgery with both spread and bundle configuration, the films were not in close contact with the epicardium and were not stretched, which is an essential prerequisite to allow the patch to properly suffer heart cycle-induced deformations and, ultimately, allow electrical current induction. Nevertheless, this issue was solved by resorting to a biopsy pen and porcine fibrin glue, being fibrin glue commonly used in several biomedical applications [183]. However, it should be referred that fibrin glue should be used with caution, as it could lead to severe adhesion between the organs [194]. Using this method, Piezo and PCL patches remained attached the heart at early time points despite the elevated heart rate of mice (~400 BPM), suggesting the feasibility of this patch placement method. Following establishment of the patch fixation method, a proof-of-principle experiment was initiated in which the patch effect were observed at 30 days post MI. The experimental survival rate was reduced (~33, 37%) when compared to mice uniquely subjected to MI [174, 195]. However this survival is in accordance with other models established at our laboratory, namely, cell intramyocardial injection after MI. Moreover, considering that more than 70% of the deaths occurred during the first 24 hours, this high mortality appears to be caused by the procedure itself rather than by patch-related effects. Indeed, the patch fixation is an invasive procedure that increases the duration of an open-chest surgery, which is a key parameter influencing animal survival [196].

Histological analysis at 30 days post-MI showed that piezoelectric fibers were abundant in the fixation site, with a similar aspect to early timepoint, thus showing that the patch persisted throughout the experiment and without any detectable fiber degradation. Conversely, the PCL fibers were not even observed at the first 24 hours, despite clear macroscopic evidences that the patch was yet in place. Whether this fact is due to much reduced fiber dimensions or due to degradation caused

by fixation and/or histological processing, it is unknown. Nevertheless, the fact that in both experimental groups, an extensive cell infiltrate of mainly $CD45^+$ cells was visible at the implantation site (Figure 15 and Figure 17), supports the hypothesis that both patches remained adhered to the epicardium originating an exacerbated extra-cardiac inflammatory response. The cell infiltrate appeared surrounded by a fibrous capsule, being collagen fibers present at the interface between the infiltrate and the myocardium. In the Piezo group, this response likely evolved to a foreign body reaction as fibers were surrounded by $CD45^+$ multinucleated cells (resembling foreign body giant cells, which originate from macrophage fusion), capillaries (typical of the granulation tissue), collagen fibers and the presence of sparsely distributed α-SMA^+ cells which could possibly be myofibroblasts, which are commonly present on wound healing scenarios [197]. This type of tissue response was also obtained by others, where, for instance, a PCL fiber-based scaffold was sutured in the epicardium of a MI rat model [193]. The presence of giant multinucleated cells was less apparent in the PCL group, possibly due to the absence of fibers with substantial dimension. These results question the biocompatibility of the Piezo patches, as an exacerbated inflammatory reaction followed by a foreign body reaction could have detrimental effects on the cardiac function and attenuate the putative effects of the piezoelectric fibers, due to their foreign body reaction-induced isolation. Thus, one should evaluate the pros and cons of having non-degradable (at least for 30 days) piezoelectric fibers, which, on one hand, induce a foreign body reaction response but, on the other hand, only exhibit piezoelectric properties in an intact state. Notwithstanding, novel strategies to avoid biomaterial-related foreign body reaction are emerging [198, 199] and that could render the Piezo patches more biocompatible. Additionally, should be mentioned that this massive inflammatory response may not be uniquely originated from the patches themselves but, probably, by the invasive patch placement procedure and due to the application of fibrin glue. The latter comprises a component of the provisional matrix which it is formed early in the response to biomaterials and that modulates the subsequent inflammatory cell accumulation and, consequently, the extent of the inflammatory response [197].

In order to assess the *in vivo* effect of the Piezo patches, mice were functionally characterized by echocardiography (Figure 13) and ECG (Figure 14) at 30 dpmi. ECG assessment showed

statistically relevant differences, in favor of the Piezo group, on several parameters associated with ventricular conduction and the depolarization/repolarization processes (QTc interval, Tpeak to Tend interval, R amplitude and Q amplitudes), with the QRS interval and JT interval revealing clear tendencies. Decreased QTc, Tpeak to Tend and JT intervals indicate that the depolarization and/or repolarization is occurring more rapidly and efficiently [200-202]. Increased R amplitude suggests that the Piezo group exhibits a more uniform and concordant depolarization process since the ECG signal results from the sum of the several electrical signals originating from different points of the myocardium. These results not only point for a restoration of cardiac electrical integrity but also suggest that the Piezo group is less amenable to suffer ventricular arrhythmias [200-204]. However, this electrical conduction restoration did not reflect on significant improvements on systolic function, as assessed by transthoracic echocardiography. Nevertheless, the Piezo group presented tendencies to have improved fractional shortening and ejection fraction, while exhibiting a less dilated LV chamber. Curiously, the PCL group presented an increased (not statistical significant) cardiac output. The latter result might not necessarily imply improved cardiac function, since for equal ejection fractions, greatly dilated LV would present an increased cardiac output. The reasons behind the observed discrepancy between the echocardiography and the ECG results are unknown. However, it can be hypothesized that the piezoelectric fibers could have caused a more direct and rapid improvement on ventricular electrical conduction, while their impact on LV contractility and systolic function could be more progressive, causing relevant differences to be revealed only at later timepoints. This could be due to an effect similar to that of the primary electrical remodeling that can be defined as changes in the electrophysiological parameters of the heart that occur as a consequence of alterations in the natural order of electrical activation of the heart [205]. These alterations can induce, for instance, alterations in mechanical strain of the myocardium and, ultimately, alter its contraction patterns [205-208]. Furthermore, histological characterization showed no significant differences concerning infarct size and morphometric parameters (*e.g* LV free wall thickness), although LV dilation showed a tendency that corroborates with the echocardiographic findings (Figure 16).

Despite the fact that the piezoelectric fibers became physically isolated from the myocardium due to the foreign body reaction, a significant improvement of the cardiac electrical conduction was observed. It can be hypothesized that the charge accumulation that occurs on the piezoelectric fibers upon mechanical deformation could generate an electrical field with a sufficient range to electrically stimulate viable CMs in the periphery. In an attempt to maximize this putative effect of the fibers on the peripheral myocardial tissue, the Piezo patches were oriented in an oblique fashion upon its surgical placement so that most of the piezoelectric fibers would become parallel to the myocardial fibers [170, 209]. And, in fact, fiber orientation scoring revealed a clear tendency for the piezoelectric fibers to be oriented accordingly (Figure 15). However, even assuming that the fibers generated electrical fields with an almost optimal orientation, the exact mechanism through which these electrical stimuli induce improvements on ventricular conduction is unknown. We hypothesized that the Piezo patches could increase the amount of CMs near the implantation site that would, consequently, facilitate electrical conduction. However, histology revealed that the PCL group exhibited a higher proportion of CM islets within the infarcted zone Figure 16), disproving the hypothesis. In an attempt to unveil the mechanism, intercellular coupling was evaluated by analyzing the expression pattern of Cx43 (Figure 18), since it was observed an increase of functional Cx43 in the preliminary *in vitro* work involving these patches (unpublished data). However, no notable differences were detected between experimental groups. As it was observed in the preliminary *in vitro* work, the improvement of cardiac conduction could alternatively be explained by improved Ca^{2+} handling and/or increased expression of genes encoding for ionic channels subunits, such as alpha 1C (Cav1.2), and 1D (Cav1.3) subunits of L-type Ca^{2+} channels, Nav1.5, Kv7.1 and voltage-activated potassium channels (Kv11.1) (hERG), however the expression of said genes were not assessed in the herein work. It is known that cells react to changes on the biophysical properties of the surrounding microenvironment, which include electrical cues. Alterations on the surrounding electrical properties can instigate the occurrence of phenomena that can be transduced to biochemical signals, such as, for example: changes in membrane electrical charge, bound or release of ions from proteins, ion channel clustering in certain sites of the cell membrane and the activation of complex voltage-sensitive enzymes such as the

voltage-sensitive phosphatases (VSPs), which contain a voltage-sensitive domain that alters its conformation depending on the surrounding electrical field and that, by being attached to cytoplasmic phosphatase, it acts by dephosphorylating phosphoinositide phosphates (PIPs) that, in turn, can intervene in signaling pathways and alter cell phenotype and function [210-215].

To the best of our knowledge, previous studies that applied piezoelectric materials on the cardiovascular system have been only focusing on evaluating the beneficial effect of these materials on *in vitro* studies [216], being *in vivo* studies directed to energy harvesting by harnessing the movements originated from the cardiac cycle [217], which underline the novelty of the herein work.

Despite no significant improvement on systolic function was observed, the results showed a marked ameliorating on electrical conduction. Although more thorough assessments should be performed on the present animal model, the results encourages one to scale-up this putative therapy for larger animal models and, eventually, for clinical application. However, note that larger animals and humans exhibit slower heart rates which, without an adequate scale-up, could hinder the electrical activity of the piezoelectric fibers. Since most novel therapies have been focusing on improving systolic function, LV remodeling and neovascularization (with promising results) (reviewed on [19, 20]), rather than acting on cardiac conduction, therapeutic potential of the Piezo patches could be more efficiently harnessed if applied as a complementary therapy to the former, rather than being applied in an isolated manner. Additionally, in order to be successfully applied in a clinical environment, a more sterile and *off-the-shelf* formulation in association with less invasive patch placement procedure is advised. Moreover, considering the *in vitro* effect on CM maturation and intercellular coupling, the Piezo patches could be seeded with clinically relevant cells (*e.g.* iPSC or ESC-derived immature CMs) in a cardiac tissue engineering approach, promoting both ventricular conduction and, possibly, improved cell engraftment onto the native myocardium.

9. CONCLUSIONS

The main goal of the herein work was to assess the therapeutic potential of biomaterial-based patches composed of PCL films and piezoelectric fibers on a murine model of MI. The successfully implanted patches triggered an exacerbated inflammatory response with characteristics which were typical of a foreign body reaction with piezoelectric fibers remaining detectable at 30 days after MI/patch implantation. Although ameliorations on systolic function and cardiac remodeling were not statistically significant (when compared to PCL-only controls), animals implanted with the Piezo patches exhibited improved cardiac conduction with evidences of having a reduced susceptibility to suffer ventricular arrhythmia events. These results support the therapeutic potential of Piezo patches, in particular, to restore electrical integrity restoration in heart failure scenarios. Moreover, herein *in vivo* results together with the previous biocompatibility studies (please see Preliminary Results) further anticipate the use of Piezo patches as conductive scaffolds for cardiac tissue engineering applications.

10. FUTURE PERSPECTIVES

Despite the obtained evidences that Piezo patches demonstrate potential to improve outcome of MI, some methodological approaches may be improved and other parameters evaluated.

To minimize the *in vivo* inflammatory response to the patch and avoid the observed foreign body response to Piezo patches, novel approaches such as biocompatible material coatings can be applied [198]. Moreover, alternatively to the use of the porcine fibrin glue, which is commercially available for research purposes, it should be considered the use of thrombin and fibrinogen isolated from murine plasma (as it is performed in humans for clinical applications). In line with this, as the putative foreign body cells were identified uniquely by their morphology and CD45 expression, the expression of, for instance, macrophage-related markers (*e.g.* CD68 [218]) are worth exploring. Moreover, it would be of interest to assess the composition of the macrophage compartment relatively to the M1 vs M2 phenotypes, since the latter exhibit anti-inflammatory properties [197, 218].

Regarding functional characterization, both echocardiographic and electrophysiological assessments should be performed on later timepoints in order to access the long-term effect of the Piezo patches. Relatively to the methodology, the analysis of electrophysiological parameters could be further insightful. For instance, surface ECGs should be measured at several timepoints or an ambulatory ECG monitoring system, allowing the analysis of isolated arrhythmic events which cannot be detected in a short time window [219]. Moreover, it would be useful to perform intracardiac electrograms for a more local electrophysiological assessment [75, 220] and/or Langerdoff perfusion system-associated *ex vivo* optical mapping [70, 151, 221] to understand whether Piezo patches affect conduction velocity and AP propagation of the myocardial tissue located near the infarcted zone. In addition, arrhythmia inducibility could be tested by means of, for instance, programmed electrical stimulation [74, 77].

In order to assess the mechanism through which the Piezo patches exert their beneficial effect, the transcriptional profile and protein expression of the CMs adjacent to the Piezo patches should be further explored by means of quantitative PCR and Western blot, respectively. This would

allow the assessment of not only the expression of the connexins and ionic channels (such as the ones that became overexpressed in the preliminary *in vitro* work) but also to assess if certain signaling pathways are altered in these CMs. For instance it would be interesting to explore alterations on the β1-integrin/ FAK/ERK/MEF-2c and GATA4 signaling pathway which influences Cx43 expression and that became altered in an *in vitro* study in that a conductive CNT-based material was used [145]. It would also be of interest to study the signaling pathways that could be influenced by VSP-mediated activity [210-215].

11. REFERENCES

[1] Mozaffarian D, Benjamin EJ, Go AS, Arnett DK, Blaha MJ, Cushman M, et al. Heart Disease and Stroke Statistics-2016 Update: A Report From the American Heart Association. Circulation. 2016;133:e38-60.

[2] Mendis S PP, Norrving B. Global Atlas on Cardiovascular Disease Prevention and Control. World Health Organization. Geneva 2011.

[3] Wong ND. Epidemiological studies of CHD and the evolution of preventive cardiology. Nat Rev Cardiol. 2014;11:276-89.

[4] WHO - Cardiovascular Diseases (CVDs) Fact Sheet, 2015. Available from: http://www.who.int/mediacentre/factsheets/fs317/en/.

.[5] WHO - The top 10 causes of death Fact Sheet, 2014. Available from: http://www.who.int/mediacentre/factsheets/fs310/en/

[6] Kleber AG, Rudy Y. Basic mechanisms of cardiac impulse propagation and associated arrhythmias. Physiological reviews. 2004;84:431-88.

[7] Lip GY, Heinzel FR, Gaita F, Juanatey JR, Le Heuzey JY, Potpara T, et al. European Heart Rhythm Association/Heart Failure Association joint consensus document on arrhythmias in heart failure, endorsed by the Heart Rhythm Society and the Asia Pacific Heart Rhythm Society. European journal of heart failure. 2015;17:848-74.

[8] Thygesen K, Alpert JS, Jaffe AS, Simoons ML, Chaitman BR, White HD. Third universal definition of myocardial infarction. Nat Rev Cardiol. 2012;9:620-33.

[9] Lusis AJ. Atherosclerosis. Nature. 2000;407:233-41.

[10] Jhund PS, McMurray JJV. Heart Failure After Acute Myocardial Infarction. Circulation. 2008;118:2019.

[11] Minicucci MF, Azevedo PS, Polegato BF, Paiva SA, Zornoff LA. Heart failure after myocardial infarction: clinical implications and treatment. Clinical cardiology. 2011;34:410-4.

[12] Vasan RS, Levy D. Defining Diastolic Heart Failure. Circulation. 2000;101:2118.

[13] Cohn JN, Ferrari R, Sharpe N. Cardiac remodeling--concepts and clinical implications: a consensus paper from an international forum on cardiac remodeling. Behalf of an International Forum on Cardiac Remodeling. Journal of the American College of Cardiology. 2000;35:569-82.

[14] Yang F, Liu YH, Yang XP, Xu J, Kapke A, Carretero OA. Myocardial infarction and cardiac remodelling in mice. Experimental physiology. 2002;87:547-55.

[15] Sutton MGSJ, Sharpe N. Left Ventricular Remodeling After Myocardial Infarction. Circulation. 2000;101:2981.

[16] Vunjak-Novakovic G, Tandon N, Godier A, Maidhof R, Marsano A, Martens TP, et al. Challenges in cardiac tissue engineering. Tissue engineering Part B, Reviews. 2010;16:169-87.

[17] Cleutjens JP, Kandala JC, Guarda E, Guntaka RV, Weber KT. Regulation of collagen degradation in the rat myocardium after infarction. J Mol Cell Cardiol. 1995;27:1281-92.

[18] Bergmann O, Bhardwaj RD, Bernard S, Zdunek S, Barnabé-Heider F, Walsh S, et al. Evidence for cardiomyocyte renewal in humans. Science (New York, NY). 2009;324:98-102.

[19] Hirt MN, Hansen A, Eschenhagen T. Cardiac tissue engineering: state of the art. Circulation research. 2014;114:354-67.

[20] Alrefai MT, Murali D, Paul A, Ridwan KM, Connell JM, Shum-Tim D. Cardiac tissue engineering and regeneration using cell-based therapy. Stem Cells and Cloning : Advances and Applications. 2015;8:81-101.

[21] Hall JE. Cardiac Muscle; The Heart as a Pump and Function of the Heart Valves. Guyton and Hall Textbook of Medical Physiology - 13th edition. Philadelphia, PA, USA: Elsevier Health Sciences; 2016. p. 109-22.

[22] Hall JE. Rhythmical Excitation of the Heart. Guyton and Hall Textbook of Medical Physiology - 13th edition. Philadelphia, PA, USA: Elsevier Health Sciences; 2016. p. 123-9.

[23] Shimada T, Kawazato H, Yasuda A, Ono N, Sueda K. Cytoarchitecture and intercalated disks of the working myocardium and the conduction system in the mammalian heart. Anat Rec A Discov Mol Cell Evol Biol. 2004;280:940-51.

[24] Miyamoto T, Zhang L, Sekiguchi A, Hadama T, Shimada T. Structural differences in the cytoarchitecture and intercalated discs between the working myocardium and conduction system in the human heart. Heart Vessels. 2002;16:232-40.

[25] Mezzano V, Pellman J, Sheikh F. Cell junctions in the specialized conduction system of the heart. Cell Commun Adhes. 2014;21:149-59.

[26] Blank AC, van Veen TA, Jonsson MK, Zelen JS, Strengers JL, de Boer TP, et al. Rewiring the heart: stem cell therapy to restore normal cardiac excitability and conduction. Curr Stem Cell Res Ther. 2009;4:23-33.

[27] Veerman CC, Wilde AA, Lodder EM. The cardiac sodium channel gene SCN5A and its gene product NaV1.5: Role in physiology and pathophysiology. Gene. 2015;573:177-87.

[28] Thiriet M. Cardiomyocytes. Tissue Functioning and Remodeling in the Circulatory and Ventilatory Systems. NY, USA: Springer-Verlag; 2013. p. 189-269.

[29] Amin AS, Tan HL, Wilde AA. Cardiac ion channels in health and disease. Heart rhythm : the official journal of the Heart Rhythm Society. 2010;7:117-26.

[30] Nerbonne JM. Molecular basis of functional voltage-gated K+ channel diversity in the mammalian myocardium. J Physiol. 2000;525 Pt 2:285-98.

[31] Weiss S, Oz S, Benmocha A, Dascal N. Regulation of Cardiac L-Type Ca2+ Channel CaV1.2 Via the β-Adrenergic-cAMP-Protein Kinase A Pathway: Old Dogmas, Advances, and New Uncertainties. Circulation research. 2013;113:617-31.

[32] Robinson RB, Siegelbaum SA. Hyperpolarization-activated cation currents: from molecules to physiological function. Annu Rev Physiol. 2003;65:453-80.

[33] Baruscotti M, Robinson RB. Electrophysiology and pacemaker function of the developing sinoatrial node. American journal of physiology Heart and circulatory physiology. 2007;293:H2613-23.

[34] Diaz ME, Graham HK, O'Neill S C, Trafford AW, Eisner DA. The control of sarcoplasmic reticulum Ca content in cardiac muscle. Cell Calcium. 2005;38:391-6.

[35] Lehman W, Galinska-Rakoczy A, Hatch V, Tobacman LS, Craig R. Structural basis for the activation of muscle contraction by troponin and tropomyosin. J Mol Biol. 2009;388:673-81.

[36] Wehrens XHT, Marks AR. Novel therapeutic approaches for heart failure by normalizing calcium cycling. Nat Rev Drug Discov. 2004;3:565-74.

[37] Lakatta EG, Maltsev VA, Vinogradova TM. A coupled SYSTEM of intracellular Ca2+ clocks and surface membrane voltage clocks controls the timekeeping mechanism of the heart's pacemaker. Circulation research. 2010;106:659-73.

[38] Lakatta EG, DiFrancesco D. What keeps us ticking: a funny current, a calcium clock, or both? J Mol Cell Cardiol. 2009;47:157-70.

[39] Oshima A. Structure and closure of connexin gap junction channels. FEBS Letters. 2014;588:1230-7.

[40] Kanter HL, Saffitz JE, Beyer EC. Cardiac myocytes express multiple gap junction proteins. Circulation research. 1992;70:438-44.

[41] Jansen JA, van Veen TAB, de Bakker JMT, van Rijen HVM. Cardiac connexins and impulse propagation. Journal of Molecular and Cellular Cardiology. 2010;48:76-82.

[42] van Kempen MJ, Fromaget C, Gros D, Moorman AF, Lamers WH. Spatial distribution of connexin43, the major cardiac gap junction protein, in the developing and adult rat heart. Circulation research. 1991;68:1638-51.

[43] Davis LM, Kanter HL, Beyer EC, Saffitz JE. Distinct gap junction protein phenotypes in cardiac tissues with disparate conduction properties. Journal of the American College of Cardiology. 1994;24:1124-32.

[44] Severs NJ, Bruce AF, Dupont E, Rothery S. Remodelling of gap junctions and connexin expression in diseased myocardium. Cardiovascular Research. 2008;80:9-19.

[45] Gourdie RG, Severs NJ, Green CR, Rothery S, Germroth P, Thompson RP. The spatial distribution and relative abundance of gap-junctional connexin40 and connexin43 correlate to functional properties of components of the cardiac atrioventricular conduction system. J Cell Sci. 1993;105 (Pt 4):985-91.

[46] Kanter HL, Laing JG, Beau SL, Beyer EC, Saffitz JE. Distinct patterns of connexin expression in canine Purkinje fibers and ventricular muscle. Circulation research. 1993;72:1124-31.

[47] Temple IP, Inada S, Dobrzynski H, Boyett MR. Connexins and the atrioventricular node. Heart rhythm : the official journal of the Heart Rhythm Society. 2013;10:297-304.

[48] Coppen SR, Severs NJ, Gourdie RG. Connexin45 (alpha 6) expression delineates an extended conduction system in the embryonic and mature rodent heart. Dev Genet. 1999;24:82-90.

[49] Veenstra RD, Wang HZ, Westphale EM, Beyer EC. Multiple connexins confer distinct regulatory and conductance properties of gap junctions in developing heart. Circulation research. 1992;71:1277-83.

[50] Boyett MR, Inada S, Yoo S, Li J, Liu J, Tellez J, et al. Connexins in the sinoatrial and atrioventricular nodes. Adv Cardiol. 2006;42:175-97.

[51] Veenstra RD. Size and selectivity of gap junction channels formed from different connexins. J Bioenerg Biomembr. 1996;28:327-37.

[52] Beblo DA, Wang HZ, Beyer EC, Westphale EM, Veenstra RD. Unique conductance, gating, and selective permeability properties of gap junction channels formed by connexin40. Circulation research. 1995;77:813-22.

[53] Greener ID, Monfredi O, Inada S, Chandler NJ, Tellez JO, Atkinson A, et al. Molecular architecture of the human specialised atrioventricular conduction axis. J Mol Cell Cardiol. 2011;50:642-51.

[54] Davis LM, Rodefeld ME, Green K, Beyer EC, Saffitz JE. Gap junction protein phenotypes of the human heart and conduction system. Journal of cardiovascular electrophysiology. 1995;6:813-22.

[55] Veeraraghavan R, Poelzing S, Gourdie RG. Intercellular electrical communication in the heart: a new, active role for the intercalated disk. Cell Commun Adhes. 2014;21:161-7.

[56] Veeraraghavan R, Gourdie RG, Poelzing S. Mechanisms of cardiac conduction: a history of revisions. American journal of physiology Heart and circulatory physiology. 2014;306:H619-27.

[57] Motloch LJ, Akar FG. Gene therapy to restore electrophysiological function in heart failure. Expert opinion on biological therapy. 2015;15:803-17.

[58] Hall JE. Cardiac Arrhythmias and Their Electrocardiographic Interpretation. Guyton and Hall Textbook of Medical Physiology - 13th edition. Philadelphia, PA, USA: Elsevier Health Sciences; 2016. p. 155-66.

[59] Coronel R, Wilders R, Verkerk AO, Wiegerinck RF, Benoist D, Bernus O. Electrophysiological changes in heart failure and their implications for arrhythmogenesis. Biochimica et biophysica acta. 2013;1832:2432-41.

[60] Tomaselli GF, Marban E. Electrophysiological remodeling in hypertrophy and heart failure. Cardiovasc Res. 1999;42:270-83.

[61] Schmidt U, Hajjar RJ, Helm PA, Kim CS, Doye AA, Gwathmey JK. Contribution of Abnormal Sarcoplasmic Reticulum ATPase Activity to Systolic and Diastolic Dysfunction in Human Heart Failure. Journal of Molecular and Cellular Cardiology. 1998;30:1929-37.

[62] Hasenfuss G, Reinecke H, Studer R, Meyer M, Pieske B, Holtz J, et al. Relation between myocardial function and expression of sarcoplasmic reticulum Ca(2+)-ATPase in failing and nonfailing human myocardium. Circulation research. 1994;75:434-42.

[63] Thomas SP, Kucera JP, Bircher-Lehmann L, Rudy Y, Saffitz JE, Kléber AG. Impulse Propagation in Synthetic Strands of Neonatal Cardiac Myocytes With Genetically Reduced Levels of Connexin43. Circulation research. 2003;92:1209-16.

[64] Ai X, Pogwizd SM. Connexin 43 downregulation and dephosphorylation in nonischemic heart failure is associated with enhanced colocalized protein phosphatase type 2A. Circulation research. 2005;96:54-63.

[65] Gaztañaga L, Marchlinski FE, Betensky BP. Mechanisms of Cardiac Arrhythmias. Revista Española de Cardiología (English Version). 2012;65:174-85.

[66] Echt DS, Liebson PR, Mitchell LB, Peters RW, Obias-Manno D, Barker AH, et al. Mortality and morbidity in patients receiving encainide, flecainide, or placebo. The Cardiac Arrhythmia Suppression Trial. The New England journal of medicine. 1991;324:781-8.

[67] Waldo AL, Camm AJ, deRuyter H, Friedman PL, MacNeil DJ, Pauls JF, et al. Effect of d-sotalol on mortality in patients with left ventricular dysfunction after recent and remote myocardial infarction. The SWORD Investigators. Survival With Oral d-Sotalol. Lancet (London, England). 1996;348:7-12.

[68] Bostwick JM, Sola CL. An updated review of implantable cardioverter/defibrillators, induced anxiety, and quality of life. The Psychiatric clinics of North America. 2007;30:677-88.

[69] Betts TR. Atrioventricular junction ablation and pacemaker implant for atrial fibrillation: still a valid treatment in appropriately selected patients. Europace : European pacing, arrhythmias, and cardiac electrophysiology : journal of the working groups on cardiac pacing, arrhythmias, and cardiac cellular electrophysiology of the European Society of Cardiology. 2008;10:425-32.

[70] Greener ID, Sasano T, Wan X, Igarashi T, Strom M, Rosenbaum DS, et al. Connexin43 gene transfer reduces ventricular tachycardia susceptibility after myocardial infarction. Journal of the American College of Cardiology. 2012;60:1103-10.

[71] Igarashi T, Finet JE, Takeuchi A, Fujino Y, Strom M, Greener ID, et al. Connexin gene transfer preserves conduction velocity and prevents atrial fibrillation. Circulation. 2012;125:216-25.

[72] Boink GJ, Lau DH, Shlapakova IN, Sosunov EA, Anyukhovsky EP, Driessen HE, et al. SkM1 and Cx32 improve conduction in canine myocardial infarcts yet only SkM1 is antiarrhythmic. Cardiovasc Res. 2012;94:450-9.

[73] Protas L, Dun W, Jia Z, Lu J, Bucchi A, Kumari S, et al. Expression of skeletal but not cardiac Na(+) channel isoform preserves normal conduction in a depolarized cardiac syncytium. Cardiovascular Research. 2009;81:528-35.

[74] Lau DH, Clausen C, Sosunov EA, Shlapakova IN, Anyukhovsky EP, Danilo P, Jr., et al. Epicardial border zone overexpression of skeletal muscle sodium channel SkM1 normalizes activation, preserves conduction, and suppresses ventricular arrhythmia: an in silico, in vivo, in vitro study. Circulation. 2009;119:19-27.

[75] Coronel R, Lau DH, Sosunov EA, Janse MJ, Danilo P, Jr., Anyukhovsky EP, et al. Cardiac expression of skeletal muscle sodium channels increases longitudinal conduction velocity in the canine 1-week myocardial infarction. Heart rhythm : the official journal of the Heart Rhythm Society. 2010;7:1104-10.

[76] Miyamoto MI, del Monte F, Schmidt U, DiSalvo TS, Kang ZB, Matsui T, et al. Adenoviral gene transfer of SERCA2a improves left-ventricular function in aortic-banded rats in transition to heart failure. Proceedings of the National Academy of Sciences of the United States of America. 2000;97:793-8.

[77] Lyon AR, Bannister ML, Collins T, Pearce E, Sepehripour AH, Dubb SS, et al. SERCA2a gene transfer decreases sarcoplasmic reticulum calcium leak and reduces ventricular arrhythmias in a model of chronic heart failure. Circulation Arrhythmia and electrophysiology. 2011;4:362-72.

[78] Cutler MJ, Wan X, Plummer BN, Liu H, Deschenes I, Laurita KR, et al. Targeted sarcoplasmic reticulum Ca2+ ATPase 2a gene delivery to restore electrical stability in the failing heart. Circulation. 2012;126:2095-104.

[79] Jaski BE, Jessup ML, Mancini DM, Cappola TP, Pauly DF, Greenberg B, et al. Calcium Upregulation by Percutaneous Administration of Gene Therapy in Cardiac Disease (CUPID Trial), a First-in-Human Phase 1/2 Clinical Trial. Journal of cardiac failure. 2009;15:171-81.

[80] Jessup M, Greenberg B, Mancini D, Cappola T, Pauly DF, Jaski B, et al. Calcium Upregulation by Percutaneous Administration of Gene Therapy in Cardiac Disease (CUPID): a phase 2 trial of intracoronary gene therapy of sarcoplasmic reticulum Ca2+-ATPase in patients with advanced heart failure. Circulation. 2011;124:304-13.

[81] Zsebo K, Yaroshinsky A, Rudy JJ, Wagner K, Greenberg B, Jessup M, et al. Long-term effects of AAV1/SERCA2a gene transfer in patients with severe heart failure: analysis of recurrent cardiovascular events and mortality. Circulation research. 2014;114:101-8.

[82] Prunier F, Kawase Y, Gianni D, Scapin C, Danik SB, Ellinor PT, et al. Prevention of ventricular arrhythmias with sarcoplasmic reticulum Ca2+ ATPase pump overexpression in a porcine model of ischemia reperfusion. Circulation. 2008;118:614-24.

[83] del Monte F, Lebeche D, Guerrero JL, Tsuji T, Doye AA, Gwathmey JK, et al. Abrogation of ventricular arrhythmias in a model of ischemia and reperfusion by targeting myocardial calcium cycling. Proceedings of the National Academy of Sciences of the United States of America. 2004;101:5622-7.

[84] Kanno S, Kovacs A, Yamada KA, Saffitz JE. Connexin43 as a determinant of myocardial infarct size following coronary occlusion in mice. Journal of the American College of Cardiology. 2003;41:681-6.

[85] Sanganalmath SK, Bolli R. Cell therapy for heart failure: a comprehensive overview of experimental and clinical studies, current challenges, and future directions. Circulation research. 2013;113:810-34.

[86] Santos Nascimento D, Mosqueira D, Sousa LM, Teixeira M, Filipe M, Resende TP, et al. Human umbilical cord tissue-derived mesenchymal stromal cells attenuate remodeling after myocardial infarction by proangiogenic, antiapoptotic, and endogenous cell-activation mechanisms. Stem cell research & therapy. 2014;5:5.

[87] Tang J, Xie Q, Pan G, Wang J, Wang M. Mesenchymal stem cells participate in angiogenesis and improve heart function in rat model of myocardial ischemia with reperfusion. European journal of cardio-thoracic surgery : official journal of the European Association for Cardio-thoracic Surgery. 2006;30:353-61.

[88] Mathiasen AB, Qayyum AA, Jorgensen E, Helqvist S, Fischer-Nielsen A, Kofoed KF, et al. Bone marrow-derived mesenchymal stromal cell treatment in patients with severe ischaemic heart failure: a randomized placebo-controlled trial (MSC-HF trial). European heart journal. 2015;36:1744-53.

[89] Garikipati VN, Jadhav S, Pal L, Prakash P, Dikshit M, Nityanand S. Mesenchymal stem cells from fetal heart attenuate myocardial injury after infarction: an in vivo serial pinhole gated SPECT-CT study in rats. PloS one. 2014;9:e100982.

[90] He J, Teng X, Yu Y, Huang H, Ye W, Ding Y, et al. Injection of Sca-1+/CD45+/CD31+ mouse bone mesenchymal stromal-like cells improves cardiac function in a mouse myocardial infarct model. Differentiation; research in biological diversity. 2013;86:57-64.

[91] Jeevanantham V, Afzal MR, Zuba-Surma EK, Dawn B. Clinical trials of cardiac repair with adult bone marrow- derived cells. Methods in molecular biology (Clifton, NJ). 2013;1036:179-205.

[92] Price MJ, Chou CC, Frantzen M, Miyamoto T, Kar S, Lee S, et al. Intravenous mesenchymal stem cell therapy early after reperfused acute myocardial infarction improves left ventricular function and alters electrophysiologic properties. International journal of cardiology. 2006;111:231-9.

[93] Kim SK, Pak HN, Park JH, Fang YF, Kim GI, Park YD, et al. Cardiac cell therapy with mesenchymal stem cell induces cardiac nerve sprouting, angiogenesis, and reduced connexin43-positive gap junctions, but concomitant electrical pacing increases connexin43-positive gap junctions in canine heart. Cardiology in the young. 2010;20:308-17.

[94] Chen SL, Fang WW, Qian J, Ye F, Liu YH, Shan SJ, et al. Improvement of cardiac function after transplantation of autologous bone marrow mesenchymal stem cells in patients with acute myocardial infarction. Chinese medical journal. 2004;117:1443-8.

[95] Katritsis DG, Sotiropoulou P, Giazitzoglou E, Karvouni E, Papamichail M. Electrophysiological effects of intracoronary transplantation of autologous mesenchymal and endothelial progenitor cells. Europace : European pacing, arrhythmias, and cardiac electrophysiology : journal of the working groups on cardiac pacing, arrhythmias, and cardiac cellular electrophysiology of the European Society of Cardiology. 2007;9:167-71.

[96] Mureli S, Gans CP, Bare DJ, Geenen DL, Kumar NM, Banach K. Mesenchymal stem cells improve cardiac conduction by upregulation of connexin 43 through paracrine signaling. American journal of physiology Heart and circulatory physiology. 2013;304:H600-9.

[97] Wang D, Zhang F, Shen W, Chen M, Yang B, Zhang Y, et al. Mesenchymal stem cell injection ameliorates the inducibility of ventricular arrhythmias after myocardial infarction in rats. International journal of cardiology. 2011;152:314-20.

[98] Wei F, Wang TZ, Zhang J, Yuan ZY, Tian HY, Ni YJ, et al. Mesenchymal stem cells neither fully acquire the electrophysiological properties of mature cardiomyocytes nor promote ventricular arrhythmias in infarcted rats. Basic research in cardiology. 2012;107:274.

[99] Chang MG, Tung L, Sekar RB, Chang CY, Cysyk J, Dong P, et al. Proarrhythmic potential of mesenchymal stem cell transplantation revealed in an in vitro coculture model. Circulation. 2006;113:1832-41.

[100] Askar SF, Ramkisoensing AA, Atsma DE, Schalij MJ, de Vries AA, Pijnappels DA. Engraftment patterns of human adult mesenchymal stem cells expose electrotonic and paracrine proarrhythmic mechanisms in myocardial cell cultures. Circulation Arrhythmia and electrophysiology. 2013;6:380-91.

[101] Mills WR, Mal N, Kiedrowski MJ, Unger R, Forudi F, Popovic ZB, et al. Stem cell therapy enhances electrical viability in myocardial infarction. J Mol Cell Cardiol. 2007;42:304-14.

[102] Fukushima S, Varela-Carver A, Coppen SR, Yamahara K, Felkin LE, Lee J, et al. Direct intramyocardial but not intracoronary injection of bone marrow cells induces ventricular arrhythmias in a rat chronic ischemic heart failure model. Circulation. 2007;115:2254-61.

[103] Pak HN, Qayyum M, Kim DT, Hamabe A, Miyauchi Y, Lill MC, et al. Mesenchymal stem cell injection induces cardiac nerve sprouting and increased tenascin expression in a Swine model of myocardial infarction. Journal of cardiovascular electrophysiology. 2003;14:841-8.

[104] Pijnappels DA, Schalij MJ, van Tuyn J, Ypey DL, de Vries AA, van der Wall EE, et al. Progressive increase in conduction velocity across human mesenchymal stem cells is mediated by enhanced electrical coupling. Cardiovasc Res. 2006;72:282-91.

[105] Beeres SLMA, Atsma DE, van der Laarse A, Pijnappels DA, van Tuyn J, Fibbe WE, et al. Human Adult Bone Marrow Mesenchymal Stem Cells Repair Experimental Conduction Block in Rat Cardiomyocyte Cultures. Journal of the American College of Cardiology. 2005;46:1943-52.

[106] Vasquez C, Benamer N, Morley GE. The cardiac fibroblast: functional and electrophysiological considerations in healthy and diseased hearts. Journal of cardiovascular pharmacology. 2011;57:380-8.

[107] Goshima K, Tonomura Y. Synchronized beating of embryonic mouse myocardial cells mediated by FL cells in monolayer culture. Experimental Cell Research. 1969;56:387-92.

[108] Yokokawa M, Ohnishi S, Ishibashi-Ueda H, Obata H, Otani K, Miyahara Y, et al. Transplantation of mesenchymal stem cells improves atrioventricular conduction in a rat model of complete atrioventricular block. Cell transplantation. 2008;17:1145-55.

[109] Hare JM, Traverse JH, Henry TD, Dib N, Strumpf RK, Schulman SP, et al. A randomized, double-blind, placebo-controlled, dose-escalation study of intravenous adult human mesenchymal stem cells (prochymal) after acute myocardial infarction. Journal of the American College of Cardiology. 2009;54:2277-86.

[110] Menasche P. Skeletal myoblasts as a therapeutic agent. Progress in cardiovascular diseases. 2007;50:7-17.

[111] Durrani S, Konoplyannikov M, Ashraf M, Haider KH. Skeletal myoblasts for cardiac repair. Regenerative medicine. 2010;5:919-32.

[112] Menasche P, Alfieri O, Janssens S, McKenna W, Reichenspurner H, Trinquart L, et al. The Myoblast Autologous Grafting in Ischemic Cardiomyopathy (MAGIC) trial: first randomized placebo-controlled study of myoblast transplantation. Circulation. 2008;117:1189-200.

[113] Leobon B, Garcin I, Menasche P, Vilquin JT, Audinat E, Charpak S. Myoblasts transplanted into rat infarcted myocardium are functionally isolated from their host. Proceedings of the National Academy of Sciences of the United States of America. 2003;100:7808-11.

[114] Fernandes S, Amirault JC, Lande G, Nguyen JM, Forest V, Bignolais O, et al. Autologous myoblast transplantation after myocardial infarction increases the inducibility of ventricular arrhythmias. Cardiovasc Res. 2006;69:348-58.

[115] Suzuki K, Brand NJ, Allen S, Khan MA, Farrell AO, Murtuza B, et al. Overexpression of connexin 43 in skeletal myoblasts: Relevance to cell transplantation to the heart. The Journal of thoracic and cardiovascular surgery. 2001;122:759-66.

[116] Abraham MR, Henrikson CA, Tung L, Chang MG, Aon M, Xue T, et al. Antiarrhythmic engineering of skeletal myoblasts for cardiac transplantation. Circulation research. 2005;97:159-67.

[117] Tolmachov O, Ma YL, Themis M, Patel P, Spohr H, Macleod KT, et al. Overexpression of connexin 43 using a retroviral vector improves electrical coupling of skeletal myoblasts with cardiac myocytes in vitro. BMC cardiovascular disorders. 2006;6:25.

[118] Choi YH, Stamm C, Hammer PE, Kwaku KF, Marler JJ, Friehs I, et al. Cardiac conduction through engineered tissue. The American journal of pathology. 2006;169:72-85.

[119] Roell W, Lewalter T, Sasse P, Tallini YN, Choi BR, Breitbach M, et al. Engraftment of connexin 43-expressing cells prevents post-infarct arrhythmia. Nature. 2007;450:819-24.

[120] Antanaviciute I, Ereminiene E, Vysockas V, Rackauskas M, Skipskis V, Rysevaite K, et al. Exogenous connexin43-expressing autologous skeletal myoblasts ameliorate mechanical function and electrical activity of the rabbit heart after experimental infarction. International journal of experimental pathology. 2015;96:42-53.

[121] Kolanowski TJ, Rozwadowska N, Malcher A, Szymczyk E, Kasprzak JD, Mietkiewski T, et al. In vitro and in vivo characteristics of connexin 43-modified human skeletal myoblasts as candidates for prospective stem cell therapy for the failing heart. International journal of cardiology. 2014;173:55-64.

[122] Fernandes S, van Rijen HV, Forest V, Evain S, Leblond AL, Merot J, et al. Cardiac cell therapy: overexpression of connexin43 in skeletal myoblasts and prevention of ventricular arrhythmias. Journal of cellular and molecular medicine. 2009;13:3703-12.

[123] Ott HC, Berjukow S, Marksteiner R, Margreiter E, Bock G, Laufer G, et al. On the fate of skeletal myoblasts in a cardiac environment: down-regulation of voltage-gated ion channels. J Physiol. 2004;558:793-805.

[124] Shiba Y, Fernandes S, Zhu WZ, Filice D, Muskheli V, Kim J, et al. Human ES-cell-derived cardiomyocytes electrically couple and suppress arrhythmias in injured hearts. Nature. 2012;489:322-5.

[125] Chong JJ, Yang X, Don CW, Minami E, Liu YW, Weyers JJ, et al. Human embryonic-stem-cell-derived cardiomyocytes regenerate non-human primate hearts. Nature. 2014;510:273-7.

[126] Ye J, Gaur M, Zhang Y, Sievers RE, Woods BJ, Aurigui J, et al. Treatment with hESC-Derived Myocardial Precursors Improves Cardiac Function after a Myocardial Infarction. PloS one. 2015;10:e0131123.

[127] Mauritz C, Martens A, Rojas SV, Schnick T, Rathert C, Schecker N, et al. Induced pluripotent stem cell (iPSC)-derived Flk-1 progenitor cells engraft, differentiate, and improve heart function in a mouse model of acute myocardial infarction. European heart journal. 2011;32:2634-41.

[128] Shiba Y, Filice D, Fernandes S, Minami E, Dupras SK, Biber BV, et al. Electrical Integration of Human Embryonic Stem Cell-Derived Cardiomyocytes in a Guinea Pig Chronic Infarct Model. Journal of cardiovascular pharmacology and therapeutics. 2014;19:368-81.

[129] Reis LA, Chiu LL, Feric N, Fu L, Radisic M. Biomaterials in myocardial tissue engineering. Journal of tissue engineering and regenerative medicine. 2016;10:11-28.

[130] Radisic M, Park H, Shing H, Consi T, Schoen FJ, Langer R, et al. Functional assembly of engineered myocardium by electrical stimulation of cardiac myocytes cultured on scaffolds. Proceedings of the National Academy of Sciences of the United States of America. 2004;101:18129-34.

[131] Au HT, Cheng I, Chowdhury MF, Radisic M. Interactive effects of surface topography and pulsatile electrical field stimulation on orientation and elongation of fibroblasts and cardiomyocytes. Biomaterials. 2007;28:4277-93.

[132] Miklas JW, Nunes SS, Sofla A, Reis LA, Pahnke A, Xiao Y, et al. Bioreactor for modulation of cardiac microtissue phenotype by combined static stretch and electrical stimulation. Biofabrication. 2014;6:024113.

[133] Nunes SS, Miklas JW, Liu J, Aschar-Sobbi R, Xiao Y, Zhang B, et al. Biowire: a platform for maturation of human pluripotent stem cell-derived cardiomyocytes. Nature methods. 2013;10:781-7.

[134] Shah M, Badwaik VD, Dakshinamurthy R. Biological applications of gold nanoparticles. J Nanosci Nanotechnol. 2014;14:344-62.

[135] Dvir T, Timko BP, Brigham MD, Naik SR, Karajanagi SS, Levy O, et al. Nanowired three-dimensional cardiac patches. Nature nanotechnology. 2011;6:720-5.

[136] Shevach M, Fleischer S, Shapira A, Dvir T. Gold nanoparticle-decellularized matrix hybrids for cardiac tissue engineering. Nano letters. 2014;14:5792-6.

[137] Chen Q-Z, Bismarck A, Hansen U, Junaid S, Tran MQ, Harding SE, et al. Characterisation of a soft elastomer poly(glycerol sebacate) designed to match the mechanical properties of myocardial tissue. Biomaterials. 2008;29:47-57.

[138] Ganji Y, Kasra M, Salahshour Kordestani S, Bagheri Hariri M. Synthesis and characterization of gold nanotube/nanowire-polyurethane composite based on castor oil and polyethylene glycol. Materials science & engineering C, Materials for biological applications. 2014;42:341-9.

[139] Ganji Y, Li Q, Quabius ES, Böttner M, Selhuber-Unkel C, Kasra M. Cardiomyocyte behavior on biodegradable polyurethane/gold nanocomposite scaffolds under electrical stimulation. Materials Science and Engineering: C. 2016;59:10-8.

[140] Martinelli V, Cellot G, Toma FM, Long CS, Caldwell JH, Zentilin L, et al. Carbon Nanotubes Promote Growth and Spontaneous Electrical Activity in Cultured Cardiac Myocytes. Nano letters. 2012;12:1831-8.

[141] Martinelli V, Cellot G, Toma FM, Long CS, Caldwell JH, Zentilin L, et al. Carbon Nanotubes Instruct Physiological Growth and Functionally Mature Syncytia: Nongenetic Engineering of Cardiac Myocytes. ACS Nano. 2013;7:5746-56.

[142] Kharaziha M, Shin SR, Nikkhah M, Topkaya SN, Masoumi N, Annabi N, et al. Tough and flexible CNT-polymeric hybrid scaffolds for engineering cardiac constructs. Biomaterials. 2014;35:7346-54.

[143] Pok S, Vitale F, Eichmann SL, Benavides OM, Pasquali M, Jacot JG. Biocompatible Carbon Nanotube–Chitosan Scaffold Matching the Electrical Conductivity of the Heart. ACS Nano. 2014;8:9822-32.

[144] Zhou J, Chen J, Sun H, Qiu X, Mou Y, Liu Z, et al. Engineering the heart: evaluation of conductive nanomaterials for improving implant integration and cardiac function. Scientific reports. 2014;4:3733.

[145] Sun H, Lu S, Jiang XX, Li X, Li H, Lin Q, et al. Carbon nanotubes enhance intercalated disc assembly in cardiac myocytes via the beta1-integrin-mediated signaling pathway. Biomaterials. 2015;55:84-95.

[146] Hsiao CW, Bai MY, Chang Y, Chung MF, Lee TY, Wu CT, et al. Electrical coupling of isolated cardiomyocyte clusters grown on aligned conductive nanofibrous meshes for their synchronized beating. Biomaterials. 2013;34:1063-72.

[147] Baheiraei N, Yeganeh H, Ai J, Gharibi R, Ebrahimi-Barough S, Azami M, et al. Preparation of a porous conductive scaffold from aniline pentamer-modified polyurethane/PCL blend for cardiac tissue engineering. Journal of biomedical materials research Part A. 2015;103:3179-87.

[148] Kai D, Prabhakaran MP, Jin G, Ramakrishna S. Polypyrrole-contained electrospun conductive nanofibrous membranes for cardiac tissue engineering. Journal of biomedical materials research Part A. 2011;99:376-85.

[149] Spearman BS, Hodge AJ, Porter JL, Hardy JG, Davis ZD, Xu T, et al. Conductive interpenetrating networks of polypyrrole and polycaprolactone encourage electrophysiological development of cardiac cells. Acta biomaterialia. 2015;28:109-20.

[150] Mihardja SS, Sievers RE, Lee RJ. The effect of polypyrrole on arteriogenesis in an acute rat infarct model. Biomaterials. 2008;29:4205-10.

[151] Mihic A, Cui Z, Wu J, Vlacic G, Miyagi Y, Li SH, et al. A Conductive Polymer Hydrogel Supports Cell Electrical Signaling and Improves Cardiac Function After Implantation into Myocardial Infarct. Circulation. 2015;132:772-84.

[152] Richards DJ, Tan Y, Coyle R, Li Y, Xu R, Yeung N, et al. Nanowires and Electrical Stimulation Synergistically Improve Functions of hiPSC Cardiac Spheroids. Nano letters. 2016;16:4670-8.

[153] Tan Y, Richards D, Xu R, Stewart-Clark S, Mani SK, Borg TK, et al. Silicon nanowire-induced maturation of cardiomyocytes derived from human induced pluripotent stem cells. Nano letters. 2015;15:2765-72.

[154] Fleischer S, Shevach M, Feiner R, Dvir T. Coiled fiber scaffolds embedded with gold nanoparticles improve the performance of engineered cardiac tissues. Nanoscale. 2014;6:9410-4.

[155] Shevach M, Maoz BM, Feiner R, Shapira A, Dvir T. Nanoengineering gold particle composite fibers for cardiac tissue engineering. Journal of Materials Chemistry B. 2013;1:5210-7.

[156] You JO, Rafat M, Ye GJ, Auguste DT. Nanoengineering the heart: conductive scaffolds enhance connexin 43 expression. Nano letters. 2011;11:3643-8.

[157] Navaei A, Saini H, Christenson W, Sullivan RT, Ros R, Nikkhah M. Gold nanorod-incorporated gelatin-based conductive hydrogels for engineering cardiac tissue constructs. Acta biomaterialia. 2016;41:133-46.

[158] Martins AM, Eng G, Caridade SG, Mano JF, Reis RL, Vunjak-Novakovic G. Electrically Conductive Chitosan/Carbon Scaffolds for Cardiac Tissue Engineering. Biomacromolecules. 2014;15:635-43.

[159] Shin SR, Jung SM, Zalabany M, Kim K, Zorlutuna P, Kim Sb, et al. Carbon-Nanotube-Embedded Hydrogel Sheets for Engineering Cardiac Constructs and Bioactuators. ACS Nano. 2013;7:2369-80.

[160] Stout DA, Basu B, Webster TJ. Poly(lactic-co-glycolic acid): carbon nanofiber composites for myocardial tissue engineering applications. Acta biomaterialia. 2011;7:3101-12.

[161] Stout DA, Raimondo E, Marostica G, Webster TJ. Growth characteristics of different heart cells on novel nanopatch substrate during electrical stimulation. Bio-medical materials and engineering. 2014;24:2101-7.

[162] Cady WG. Piezoelectricity: an introduction to the theory and applications of electromechancial phenomena in crystals: McGraw-Hill Book Company, inc.; 1946.

[163] Shamos MH, Lavine LS. Piezoelectricity as a Fundamental Property of Biological Tissues. Nature. 1967;213:267-9.

[164] Minary-Jolandan M, Yu MF. Nanoscale characterization of isolated individual type I collagen fibrils: polarization and piezoelectricity. Nanotechnology. 2009;20:085706.

[165] Williams WS, Breger L. Piezoelectricity in tendon and bone. Journal of Biomechanics. 1975;8:407-13.

[166] Rajabi AH, Jaffe M, Arinzeh TL. Piezoelectric materials for tissue regeneration: A review. Acta biomaterialia. 2015;24:12-23.

[167] Ribeiro C, Sencadas V, Correia DM, Lanceros-Mendez S. Piezoelectric polymers as biomaterials for tissue engineering applications. Colloids and surfaces B, Biointerfaces. 2015;136:46-55.

[168] Hitscherich P, Wu S, Gordan R, Xie LH, Arinzeh T, Lee EJ. The effect of piezoelectric PVDF-TrFE scaffolds on stem cell derived cardiovascular cells. Biotechnology and bioengineering. 2015.

[169] Ruhparwar A, Piontek P, Ungerer M, Ghodsizad A, Partovi S, Foroughi J, et al. Electrically contractile polymers augment right ventricular output in the heart. Artificial organs. 2014;38:1034-9.

[170] Dagdeviren C, Yang BD, Su Y, Tran PL, Joe P, Anderson E, et al. Conformal piezoelectric energy harvesting and storage from motions of the heart, lung, and diaphragm. Proceedings of the National Academy of Sciences. 2014;111:1927-32.

[171] Lu B, Chen Y, Ou D, Chen H, Diao L, Zhang W, et al. Ultra-flexible Piezoelectric Devices Integrated with Heart to Harvest the Biomechanical Energy. Scientific reports. 2015;5:16065.

[172] Directive 2010/63/EU of the European Parliament and of the Council of 22 September 2010 on the protection of animals used for scientific purposes.(http://eur-lex.europa.eu/legal-content/EN/TXT/PDF/?uri=CELEX:32010L0063).

[173] Guidance document on the recognition, assessment and use of clinical signs as human endpoints for experimental animals used in safety evaluation. (http://www.oecd-ilibrary.org/environment/guidance-document-on-the-recognition-assessment-and-use-of-clinical-signs-as-human-endpoints-for-experimental-animals-used-in-safety-evaluation_9789264078376-en).

[174] Michael LH, Entman ML, Hartley CJ, Youker KA, Zhu J, Hall SR, et al. Myocardial ischemia and reperfusion: a murine model. The American journal of physiology. 1995;269:H2147-54.

[175] Valente M, Araujo A, Esteves T, Laundos TL, Freire AG, Quelhas P, et al. Optimized Heart Sampling and Systematic Evaluation of Cardiac Therapies in Mouse Models of Ischemic Injury: Assessment of Cardiac Remodeling and Semi-Automated Quantification of Myocardial Infarct Size. Current protocols in mouse biology. 2015;5:359-91.

[176] Lu QL, Partridge TA. A new blocking method for application of murine monoclonal antibody to mouse tissue sections. The journal of histochemistry and cytochemistry : official journal of the Histochemistry Society. 1998;46:977-84.

[177] Nascimento DS, Valente M, Esteves T, de Pina Mde F, Guedes JG, Freire A, et al. MIQuant--semi-automation of infarct size assessment in models of cardiac ischemic injury. PloS one. 2011;6:e25045.

[178] Takagawa J, Zhang Y, Wong ML, Sievers RE, Kapasi NK, Wang Y, et al. Myocardial infarct size measurement in the mouse chronic infarction model: comparison of area- and length-based approaches. Journal of applied physiology (Bethesda, Md : 1985). 2007;102:2104-11.

[179] D'Uva G, Aharonov A, Lauriola M, Kain D, Yahalom-Ronen Y, Carvalho S, et al. ERBB2 triggers mammalian heart regeneration by promoting cardiomyocyte dedifferentiation and proliferation. Nature cell biology. 2015;17:627-38.

[180] Fujimoto KL, Tobita K, Merryman WD, Guan J, Momoi N, Stolz DB, et al. An elastic, biodegradable cardiac patch induces contractile smooth muscle and improves cardiac remodeling and function in subacute myocardial infarction. Journal of the American College of Cardiology. 2007;49:2292-300.

[181] Wendel JS, Ye L, Tao R, Zhang J, Zhang J, Kamp TJ, et al. Functional Effects of a Tissue-Engineered Cardiac Patch From Human Induced Pluripotent Stem Cell-Derived Cardiomyocytes in a Rat Infarct Model. Stem cells translational medicine. 2015;4:1324-32.

[182] Amir G, Miller L, Shachar M, Feinberg MS, Holbova R, Cohen S, et al. Evaluation of a peritoneal-generated cardiac patch in a rat model of heterotopic heart transplantation. Cell transplantation. 2009;18:275-82.

[183] Spotnitz WD. Fibrin Sealant: The Only Approved Hemostat, Sealant, and Adhesive-a Laboratory and Clinical Perspective. ISRN surgery. 2014;2014:203943.

[184] Melhem M, Jensen T, Reinkensmeyer L, Knapp L, Flewellyn J, Schook L. A Hydrogel Construct and Fibrin-based Glue Approach to Deliver Therapeutics in a Murine Myocardial Infarction Model. Journal of visualized experiments : JoVE. 2015:e52562.

[185] Entekhabi E, Haghbin Nazarpak M, Moztarzadeh F, Sadeghi A. Design and manufacture of neural tissue engineering scaffolds using hyaluronic acid and polycaprolactone nanofibers with controlled porosity. Materials science & engineering C, Materials for biological applications. 2016;69:380-7.

[186] Gunatillake P, Mayadunne R, Adhikari R. Recent developments in biodegradable synthetic polymers. Biotechnology annual review. 2006;12:301-47.

[187] Yun YP, Lee JY, Jeong WJ, Park K, Kim HJ, Song JJ. Improving Osteogenesis Activity on BMP-2-Immobilized PCL Fibers Modified by the gamma-Ray Irradiation Technique. 2015;2015:302820.

[188] Goncalves EM, Oliveira FJ, Silva RF, Neto MA, Fernandes MH, Amaral M, et al. Three-dimensional printed PCL-hydroxyapatite scaffolds filled with CNTs for bone cell growth stimulation. Journal of biomedical materials research Part B, Applied biomaterials. 2016;104:1210-9.

[189] Woodruff MA, Hutmacher DW. The return of a forgotten polymer—Polycaprolactone in the 21st century. Progress in Polymer Science. 2010;35:1217-56.

[190] Tallawi M, Rosellini E, Barbani N, Cascone MG, Rai R, Saint-Pierre G, et al. Strategies for the chemical and biological functionalization of scaffolds for cardiac tissue engineering: a review. Journal of the Royal Society, Interface / the Royal Society. 2015;12:20150254.

[191] Shin M, Ishii O, Sueda T, Vacanti JP. Contractile cardiac grafts using a novel nanofibrous mesh. Biomaterials. 2004;25:3717-23.

[192] Kochervinskii VV. Piezoelectricity in crystallizing ferroelectric polymers: Poly(vinylidene fluoride) and its copolymers (A review). Crystallography Reports. 2003;48:649-75.

[193] Castellano D, Blanes M, Marco B, Cerrada I, Ruiz-Saurí A, Pelacho B, et al. A Comparison of Electrospun Polymers Reveals Poly(3-Hydroxybutyrate) Fiber as a Superior Scaffold for Cardiac Repair. Stem Cells and Development. 2014;23:1479-90.

[194] Krieger KH, Isom OW. Blood Conservation in Cardiac Surgery: Springer New York; 2012.

[195] Gao E, Lei YH, Shang X, Huang ZM, Zuo L, Boucher M, et al. A novel and efficient model of coronary artery ligation and myocardial infarction in the mouse. Circulation research. 2010;107:1445-53.

[196] Gao E, Lei YH, Shang X, Huang ZM, Zuo L, Boucher M, ;A Novel and Efficient Model of Coronary Artery Ligation and Myocardial Infarction in the Mouse. Circulation research. 2010;107:1445.

[197] Anderson JM, Rodriguez A, Chang DT. FOREIGN BODY REACTION TO BIOMATERIALS. Seminars in immunology. 2008;20:86-100.

[198] Morais JM, Papadimitrakopoulos F, Burgess DJ. Biomaterials/tissue interactions: possible solutions to overcome foreign body response. The AAPS journal. 2010;12:188-96.

[199] Wang Y, Papadimitrakopoulos F, Burgess DJ. Polymeric "smart" coatings to prevent foreign body response to implantable biosensors. Journal of controlled release : official journal of the Controlled Release Society. 2013;169:341-7.

[200] Crow RS, Hannan PJ, Folsom AR. Prognostic Significance of Corrected QT and Corrected JT Interval for Incident Coronary Heart Disease in a General Population Sample Stratified by Presence or Absence of Wide QRS Complex. Circulation. 2003;108:1985.

[201] Niemeijer MN, van den Berg ME, Deckers JW, Franco OH, Hofman A, Kors JA, et al. Consistency of heart rate-QTc prolongation consistency and sudden cardiac death: The Rotterdam Study. Heart rhythm : the official journal of the Heart Rhythm Society. 2015;12:2078-85.

[202] Morin DP, Saad MN, Shams OF, Owen JS, Xue JQ, Abi-Samra FM, et al. Relationships between the T-peak to T-end interval, ventricular tachyarrhythmia, and death in left ventricular systolic dysfunction. Europace : European pacing, arrhythmias, and cardiac electrophysiology : journal of the working groups on cardiac pacing, arrhythmias, and cardiac cellular electrophysiology of the European Society of Cardiology. 2012;14:1172.

[203] Panikkath R, Reinier K, Uy-Evanado A, Teodorescu C, Hattenhauer J, Mariani R, et al. Prolonged Tpeak-to-tend interval on the resting ECG is associated with increased risk of sudden cardiac death. Circulation Arrhythmia and electrophysiology. 2011;4:441-7.

[204] Teodorescu C, Reinier K, Uy-Evanado A, Navarro J, Mariani R, Gunson K, et al. Prolonged QRS duration on the resting ECG is associated with sudden death risk in coronary disease, independent of prolonged ventricular repolarization. Heart rhythm : the official journal of the Heart Rhythm Society. 2011;8:1562-7.

[205] Cutler MJ, Jeyaraj D, Rosenbaum DS. Cardiac electrical remodeling in health and disease. Trends in pharmacological sciences. 2011;32:174-80.

[206] Jeyaraj D, Wilson LD, Zhong J, Flask C, Saffitz JE, Deschenes I, et al. Mechanoelectrical feedback as novel mechanism of cardiac electrical remodeling. Circulation. 2007;115:3145-55.

[207] Tops LF, Schalij MJ, Bax JJ. The effects of right ventricular apical pacing on ventricular function and dyssynchrony implications for therapy. Journal of the American College of Cardiology. 2009;54:764-76.

[208] Prinzen FW, Hunter WC, Wyman BT, McVeigh ER. Mapping of regional myocardial strain and work during ventricular pacing: experimental study using magnetic resonance imaging tagging. Journal of the American College of Cardiology. 1999;33:1735-42.

[209] Buckberg G, Hoffman JI, Mahajan A, Saleh S, Coghlan C. Cardiac mechanics revisited: the relationship of cardiac architecture to ventricular function. Circulation. 2008;118:2571-87.

[210] Hobiger K, Friedrich T. Voltage sensitive phosphatases: emerging kinship to protein tyrosine phosphatases from structure-function research. Frontiers in Pharmacology. 2015;6:20.

[211] Thavandiran N, Nunes SS, Xiao Y, Radisic M. Topological and electrical control of cardiac differentiation and assembly. Stem cell research & therapy. 2013;4:14.

[212] Funk RH, Monsees T, Ozkucur N. Electromagnetic effects - From cell biology to medicine. Progress in histochemistry and cytochemistry. 2009;43:177-264.

[213] Horn R. Electrifying phosphatases. Science's STKE : signal transduction knowledge environment. 2005;2005:pe50.

[214] Murata Y, Iwasaki H, Sasaki M, Inaba K, Okamura Y. Phosphoinositide phosphatase activity coupled to an intrinsic voltage sensor. Nature. 2005;435:1239-43.

[215] Halaszovich CR, Leitner MG, Mavrantoni A, Le A, Frezza L, Feuer A, et al. A human phospholipid phosphatase activated by a transmembrane control module. Journal of Lipid Research. 2012;53:2266-74.

[216] Hitscherich P, Wu S, Gordan R, Xie LH, Arinzeh T, Lee EJ. The effect of PVDF-TrFE scaffolds on stem cell derived cardiovascular cells. Biotechnology and bioengineering. 2016;113:1577-85.

[217] Dagdeviren C, Yang BD, Su Y, Tran PL, Joe P, Anderson E, et al. Conformal piezoelectric energy harvesting and storage from motions of the heart, lung, and diaphragm. Proceedings of the National Academy of Sciences of the United States of America. 2014;111:1927-32.

[218] Murray PJ, Wynn TA. Protective and pathogenic functions of macrophage subsets. Nat Rev Immunol. 2011;11:723-37.

[219] McCauley MD, Wehrens XH. Ambulatory ECG recording in mice. Journal of visualized experiments : JoVE. 2010.

[220] Berul CI, McConnell BK, Wakimoto H, Moskowitz IPG, Maguire CT, Semsarian C, et al. Ventricular Arrhythmia Vulnerability in Cardiomyopathic Mice With Homozygous Mutant Myosin-Binding Protein C Gene. Circulation. 2001;104:2734.

[221] Xue T, Cho HC, Akar FG, Tsang SY, Jones SP, Marban E, et al. Functional integration of electrically active cardiac derivatives from genetically engineered human embryonic stem cells with quiescent recipient ventricular cardiomyocytes: insights into the development of cell-based pacemakers. Circulation. 2005;111:11-20.